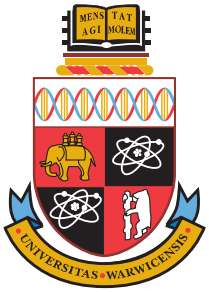

Linear dichroism spectroscopy and biophysics of an amyloid protein

by

Stephen R. Norton

Thesis

Submitted to the University of Warwick

for the degree of

Doctor of Philosophy

Supervisors: Prof. Alison Rodger and Dr. Teresa Pinheiro

MOAC Doctoral Training Centre

September 2015

THE UNIVERSITY OF WARWICK

For my Nan.

Contents

List of Figures

List of Tables

Abbreviations

Aβ	amyloid-β
AD	Alzheimer's Disease
AFM	Atomic force microscopy
αHL	α-haemolysin
αS	α-synuclein
BSE	Bovine spongiform encephalopathy
CD	Circular dichroism
DiO	3,3′-dioctadecyloxocarbocyanine perchlorate
DLS	Dynamic light scattering
DPH	1,6-Diphenyl-1,3,5-hexatriene
DPPC	1,2-dipalmitoyl-sn-glycero-3-phosphocholine
EDTA	Ethylenediaminetetraacetic acid
ESI-MS	Electrospray ionisation mass spectrometry
GM1	Monosialoganglioside
GST	Glutathione S-transferase
IPTG	Isopropyl β-D-1-thiogalactopyranoside
LB	Lysogeny broth
LD	Linear dichroism
MOPS	3-(N-morpholino)propanesulfonic acid
MPTP	1-methyl-4-phenyl-1,2,3,6-tetrahydropyridine
MWCO	Molecular weight cut off
PA	Phosphate
PAGE	Polyacrylamide gel electrophoresis

PBS	Phosphate-buffered saline
PC	Phosphocholine
PD	Parkinson's Disease
PE	Phosphoethanolamine
PFP	Pore-forming protein
PG	Phosphoglycerol
PI	Phosphoinositol
PMSF	Phenylmethylsulfonyl fluoride
POPA	1-palmitoyl-2-oleoyl-sn-glycero-3-phosphate (sodium salt)
POPC	1-palmitoyl-2-oleoyl-sn-glycero-3-phosphocholine
POPE	1-palmitoyl-2-oleoyl-sn-glycero-3-phosphoethanolamine
POPG	1-palmitoyl-2-oleoyl-sn-glycero-3-phospho-(1′-rac-glycerol) (sodium salt)
POPI	1-palmitoyl-2-oleoyl-sn-glycero-3-phosphoinositol (ammonium salt)
POPS	1-palmitoyl-2-oleoyl-sn-glycero-3-phospho-L-serine (sodium salt)
PrP	prion protein
PS	Phosphoserine
ROS	Reactive oxygen species
SDS	Sodium dodecyl sulphate
SM1	Sphingomyelin
TB	Terrific broth
TEM	Transmission electron microscopy
TEMED	N,N,N′,N′-tetramethylethane-1,2-diamine
TES	N-[Tris(hydroxymethyl)methyl]-2-aminoethanesulfonic acid
ThT	Thioflavin T
vCJD	Creutzfeldt-Jakob Disease
WT	Wild type

Acknowledgements

Scientific research never happens in isolation, and I have benefitted from many opportunities and much experience during my time at Warwick. First, I must thank the EPSRC for funding my project, and to the MOAC CDT for hosting me. My work in the School of Life Sciences owes much to the kind gift of a plasmid from Prof Benson (Lancaster University), and of *E. coli* from Dr Walker. Advice from Kelly and from Dr Sanghera turned this biomedical scientist into a biochemist. I owe thanks to the rest of the C010 lab for all their loaning of chemicals, tips on using instruments, and seemingly infinite knowledge and experience. In the Department of Chemistry, the Biophysical Chemistry Group turned me from a biochemist into a biophysicist. Dr Chmel has been so generous with his time, and his knowledge, that I owe much of my success to him. Of course, this work would not have been possible without my supervisors. The experience of Alison and Teresa has made this project fulfilling and fascinating.

Working as part of a cohort made my MSc and PhD much more enjoyable, and gave me somewhere to turn whenever I hit stumbling blocks. The support of all members of the MOAC community (Drs Richards, Sheldon, Broughton, Montgomery, and Harrison in particular) was invaluable for their friendship, advice, and help with LaTeX. Finally, the support of my family and friends has helped me through the tougher times including the passing of my Nan – a sufferer of Parkinson's Disease. I know she would have been proud to see me gain this degree. I also owe thanks to my friends from Lancaster University and from home who have been there when I have needed to escape the Warwick bubble and get back to normality. Without Andy, Matt, Hannah and Liz I would not have started this journey, and without Muriel and Adam I wouldn't have finished it.

Declarations

The work presented in this document is original. All work, except where stated in the text, was carried out by the author of this thesis. The thesis has not been submitted for a degree at another university.

Abstract

Though Parkinson's Disease is known to be caused by cell death in one region of the brain, and though the protein α-synuclein is known to be associated with it, the causes are still poorly understood. It has not yet been shown how α-synuclein may cause cells to die, with research focusing on the range of structures the protein is able to adopt. The classic amyloid fibrils are currently believed to be non-toxic, but smaller, soluble oligomers appear to be the toxic species. Key to toxicity and to the normal function of α-synucein (also unknown to-date) appear to be the ability of the protein to bind to lipids, as toxicity may be due to oligomers forming pores in cells, and the normal function of the protein may be in vesicle transport.

The work presented in this thesis represents a collection of studies, across several disciplines, that test aspects of the behaviour of α-synuclein. Circular dichroism and fluorescence data presented here show that the protein interacts with the lipid POPS in a concentration-dependent manner. Linear dichroism was an important and complementary technique to these, but required some method refinement and sample preparation improvement. This work is presented in this thesis, alongside experimental and theoretical studies into the behaviour of lipid vesicles in Couette flow. It was shown that certain lipids perform better in Couette flow, particularly the mixture of POPC and POPS. This informed the linear dichroism studies, and enabled experiments suggesting that oligomers of α-synuclein may insert across the membrane of vesicles. If confirmed, this would support the amyloid pore theory of α-synuclein toxicity.

Chapter 1

Introduction

Amyloid proteins are thought to be responsible for several neurodegenerative diseases, yet the mechanisms by which these diseases are caused are poorly understood. In this thesis, work is presented that aims to understand the mechanism of one such protein, α-synuclein, by applying spectroscopic techniques in several experimental configurations. It was also apparent that one of the key techniques, linear dichroism, was not optimised for the experiments carried out here. Work is presented on improving the usability of the technique, and the quality of data generated in this way.

1.1 Amyloid proteins and disease

In neurodegenerative amyloid diseases, three proteins are considered especially important: α-synuclein (αS), amyloid-β (Aβ), and prion protein (PrP). These proteins, however, are found in both healthy and diseased individuals, making understanding their biology both interesting and extremely important. Neurodegeneration is caused by the death of neurones in various regions of the brain, so a major therapeutic target is the prevention of cell death. Therefore, much research is aimed at understanding the cause of cell death; a process still not fully understood.

Prusiner was able to show in the early 1980s that prions could be linked to scrapie (a sheep form of prion disease), and this knowledge soon led to the understanding that other

diseases (*e.g.* bovine spongiform encephalopathy (BSE) and variant Creutzfeldt-Jakob Disease (vCJD)) were also due to prion toxicity (Prusiner, 1982). Amyloid-β was known to be a major component in so-called amyloid plaques in Alzheimer's Disease (AD) patients, as was the insolubility of these protein aggregates (Selkoe *et al.*, 1982), leading to the hypothesis that disease was cause by amyloid protein fibrils. Since fibrils of α-synuclein were found in the Lewy Bodies of Parkinson's Disease (PD) patients, this theory seemed to solve the question of why neurodegeneration occurred.

Recently, however, the focus of the field has been shifted away from the large insoluble aggregates of amyloid proteins to smaller, soluble oligomers. These species are now believed to be more able to exert toxic effects on neurones, and may be the true causative agent of disease (Selkoe, 2008; Simoneau *et al.*, 2007). Oligomerisation was known to occur, and to be differently regulated for different mutants of the proteins, but was previously thought to be simply an intermediate step to fibril formation (fibrillogenesis) (Lotharius & Brundin, 2002).

It has been possible in the last decade to hypothesise on what caused cell death, even before oligomers were known to be the likely culprit. Oxidative stress is a damage mechanism suggested for a number of degenerative processes, ageing and neurodegeneration being among them. In PD, Lotharius and Brundin discussed a model of cell death by oxidative stress. Cellular metabolism of dopamine generates reactive oxygen species (ROS) such as superoxide anions ($O_2^{\cdot -}$), dopamine-quinone species ($SQ^{\cdot}$), and hydroxyl radicals ($OH^{\cdot}$). The authors suggest that when the dopaminergic neurones are damaged by a trigger of oxidative stress, an excess of dopamine is able to enter their cytoplasm. Cytoplasmic dopamine would then be metabolised to ROS, which causes further damage to the cell, eventually forcing it onto the apoptosis pathway. The region of the brain in which most dopinanergic neurones are found is the *substantia nigra*, the region that suffers degeneration in PD. If one accepts that α-synuclein has a role in transporting vesicles containing dopamine (unproven but often suggested), one can easily deduce how damage

to the protein would lead to disruption to the dopamine supply, and whatever further damage that would cause (Bellucci *et al.*, 2012). Figure 1.1 presents a schematic of this pathway to damage. Since the Lotharius and Brundin review, other evidence has come to light implicating α-synuclein in other forms of damage: malfunction of homeostasis, nitric damage, and neuroinflammation to name a few (Lotharius & Brundin, 2002; Jellinger, 2012).

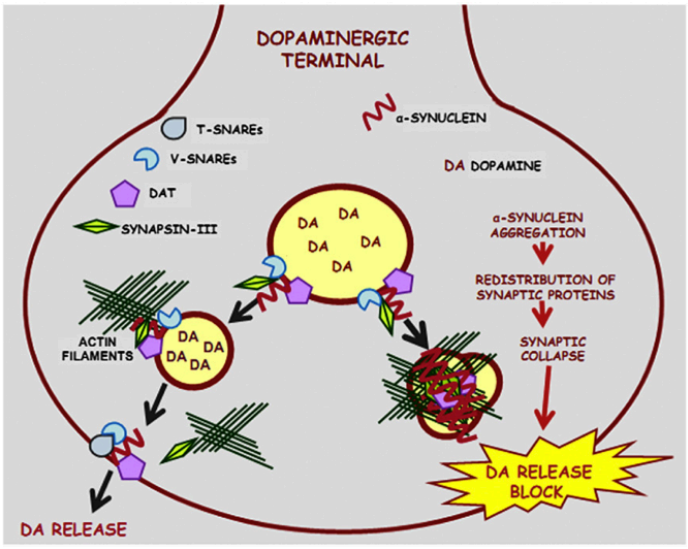

Figure 1.1: Image reproduced from Bellucci *et al.*, 2012 showing how α-synuclein may disrupt the pathways associated with dopamine (DA), and therefore lead to damage in the cell.

Whether it is oligomer, or fibril, or some as yet unknown form of the protein that causes disease, it is clear that the native proteins are not harmful, but in fact may be important in various pathways, such as the putative role of PrP in neuroprotection against several insults (Roucou *et al.*, 2004). As with many diseases, a genetic link was sought. The symptoms of Parkinson's Disease can be caused by environmental factors (*e.g.* the toxin MPTP, now used in animal models of PD), but a small number of cases have a genetic link. Knockout mice have been bred that lack the gene for α-synuclein, but they do not show PD symptoms (Kurz *et al.*, 2010). Instead, only curious neurochemical changes were observed.

These include effects such as fewer synaptic vesicles in knockout mice, especially in the so-called reserve pool of vesicles recruited during high-frequency stimulation. Recent work using mice deficient in α-synuclein showed that glyoxylase I expression was up-regulated, and the animals exhibited glycation stress. These data suggest that α-synuclein may be a key regulator of glucose metabolism in the brain, and may have a role in vesicle transport to or from the reserve pool (Lotharius & Brundin, 2002; Kurz *et al.*, 2010).

Five mutations in α-synuclein have been found to cause PD symptoms: Ala30Pro, Ala53Thr, Glu46Lys, His50Gln and Gly51Asp (A30P, A53T, E46K, H50Q, and G51D) (Conway *et al.*, 1998; Warner & Schapira, 2003; Zhu *et al.*, 2003; Choi *et al.*, 2004; Zarranz *et al.*, 2004; Appel-Cresswell *et al.*, 2013; Fares *et al.*, 2014). With this information, transgenic mice have been developed, and with these lines researchers have had further success in producing PD-like symptoms. Lines that overexpress A53T mutant α-synuclein have been variously shown to lose motor neurones and develop Lewy Body-like inclusions, though these traits are not universal amongst the mouse lines (Lotharius & Brundin, 2002). A30P, A53T, and E46K constructs, when expressed in mice or *in vitro*, have been shown to form fibrillar structures, such as those found in Lewy Bodies of PD patients. Figure 1.2, reproduced from Choi *et al.*, demonstrates morphological differences in fibrils formed by the different α-synuclein mutants, shown by taking electron microscopy (EM) images of the protein after incubation.

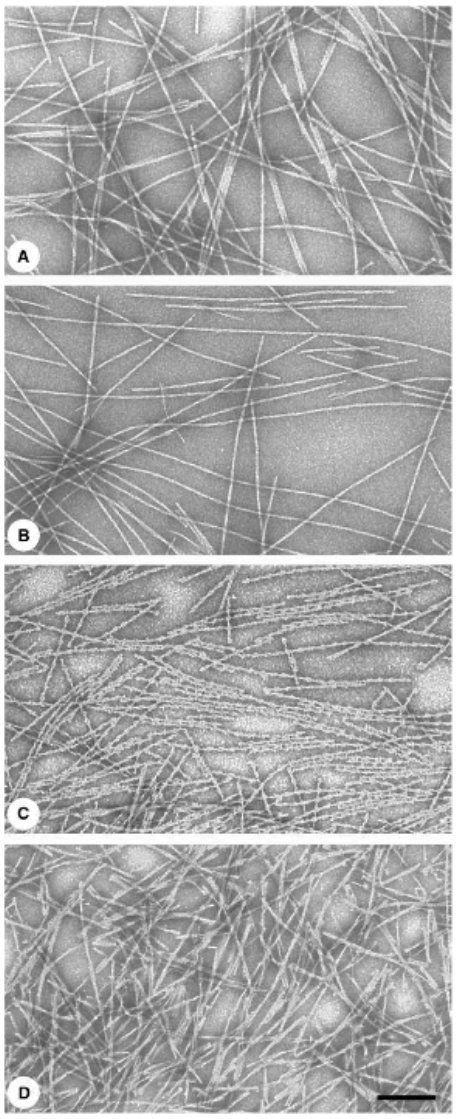

Figure 1.2: Electron micrographs of the filaments formed by forms of alpha-synuclein. (A) - wild type, (B) - A30P, (C) - E46K, (D) - A53T (Choi *et al.*, 2004).

At the time of publication of the Choi *et al.* study, E46K was a recently found α-synuclein mutant, and its properties were not yet understood. The authors here chose to probe some characteristics of E46K, in the hope of revealing some routes to pathogenesis (Choi *et al.*, 2004). One key study determined that fibrillation of WT α-synuclein was much less efficient than for all three mutant forms. E46K and A53T share almost identical kinetics

(measured by Thioflavin T (ThT) fluorescence).

It has been shown that amyloid-β and prion protein both cause disease. Aβ has been linked with Alzheimer's Disease since the 1980s, and oxidative stress is believed to be the method by which cells are killed (Varadarajan *et al.*, 2000). It has been known for many years (reviewed in 1994 by D. Selkoe) that different forms of Alzheimer's Disease could be caused by genetic alterations in several aspects of the relevant cellular biochemistry: the trafficking of amyloid precursor protein (APP), the processing enzymes that interact with APP, heterogeneity (or otherwise) of Aβ peptides, proteolytic systems that could degrade Aβ, kinetics of fibrillogenesis, and the other proteins that can interact with Aβ aggregates. All of these associated proteins can lead to Alzheimer's Disease if mutated in some way (Selkoe, 1994).

PrP is believed to exert its toxic effect through aggregation at the cellular membrane. If enough of the protein accumulates, biochemical pathways are interrupted or altered (*e.g.* proteosomal or other degradation pathways), thereby triggering apoptosis (Simoneau *et al.*, 2007). Wild type PrP, known as PrP^C, does not cause disease. Its function is not yet understood, but may be neuroprotective to oxidative stress or apoptotic signals (Solomon *et al.*, 2010). This would then imply that when the protein is damaged by mutation, leading to its aggregation and failure of function, cells subjected to previously non-effective apoptotic signals would die.

The studies discussed above make clear the importance of the interaction of amyloid proteins in general with membranes. In the next section, this general amyloid-lipid interaction is probed more specifically, to determine the relevance of work on α-synuclein and lipids.

1.2 Protein-Membrane interaction and toxicity

A comparison was also made between how well the different α-synuclein mutants bound two different types of liposome. Lipids used were brain PC and brain PS (phosphocholine and phosphoserine), *i.e.* with a mixture of head groups and charges. The liposome proportions were PC:PS:cholesterol 52.5:17.5:30 mol% and 35:35:30 mol%, with the former being more similar to synaptic vesicle construction. The liposomes were fluorescence labelled with 3,3′-dioctadecyloxocarbocyanine perchlorate (DiO). The E46K mutant had 88 % stronger binding to the first liposome type than wild type (WT) α-synuclein. It also bound the second liposome type 56 % more strongly. Other disease-associated forms of α-synuclein have different effects: A53T mutation does not significantly alter liposome binding, whereas A30P reduces the ability of the protein to bind liposome. This supports the hypotheses set out by Auluck, Caraveo and Lindquist into the modes of toxicity of mutant α-synuclein. These authors suggested that E46K and A53T α-synuclein caused disease by not releasing reserve pool vesicles to the synapse, whereas A30P would cause disease by releasing too much too quickly (effectively the same as having no α-synuclein present) (Auluck *et al.*, 2010; Choi *et al.*, 2004).

Mice expressing the A53T mutant show marked degeneration of motor neurones, and other data suggest that normal α-synuclein function might be in neuronal or synaptic maintenance. The protein has been shown to associate with the synaptic region of neurones, with up to 50 % being bound either to the cell membrane, or to vesicles. Mutated forms of the protein have less ability to bind membranes: A30P has no capacity to form these interactions, possibly due to a kinked structure, and A53T loses some of its ability to bind planar lipid membrane, though it may still bind vesicles (Lotharius & Brundin, 2002).

Measurements of how effective oligomeric α-synuclein could be at membrane disruption

have been made by Stöckl, Claessens and Subramaniam (Stöckl *et al.*, 2012a). The authors discuss the two leading models for how this would occur: either oligomers forming pores through the membrane allowing molecules to pass, or by simply disrupting the membrane structure enough to cause problems for the integrity of the cell. By using a kinetic measurement approach, the authors hoped to gain an insight into which of these is more likely to be the case. The kinetics of permeabilisation would appear different for the different effects of destabilising the membrane or punching a hole through it.

Vesicles containing C6-NBD-PC (a fluorescent lipid) were exposed to a solution of 10 mM dithionite – a species that bleaches C6-NBD-PC. This was performed at a range of concentrations of α-synuclein. By measuring the change in fluorescence, it was possible to deduce how much dithionite was passing through the vesicle membrane, and therefore how permeable the vesicle was. In all cases, the fluorescence dropped quickly after the addition of dithionite, but only to around 50 % of maximum in the 0 α-synuclein control experiment. It was shown that fluorescence decreased further for every higher α-synuclein concentration; with 1 μM α-synuclein the amount of C6-NBD-PC remaining unbleached decreased to below 20 %, thereby showing that α-synuclein increased membrane permeability according to its concentration (Stöckl *et al.*, 2012a).

Membranes containing the lipids POPG and POPC (1-palmitoyl-2-oleoyl-sn-glycero-3-phospho-(1′-rac-glycerol), and 1-palmitoyl-2-oleoyl -sn-glycero-3-phosphocholine) at various ratios were prepared. POPG is negatively charged, and is therefore the lipid to which α-synuclein will bind. Again, the vesicles contained C6-NBD-PC, and were exposed to dithionite. A difference in fluorescence for different amounts of POPG would show that lipid composition influences the ability of α-synuclein to permeabilise the membrane. It was shown that over 90 % of the vesicle membrane had to be composed of POPG for α-synuclein to affect the rate at which permeabilisation occurred. Therefore, the protein is only able to disrupt membranes substantially if the lipids in the membrane are mainly negatively charged. Due to the calculated rate constants by which dithionite influx occurs,

and the rate at which other phenomena such as flip-flop occur, where flip-flop is defined as lipid molecules swapping to the other leaflet of the membrane, the authors conclude that permeabilisation is by membrane destabilisation, rather than pore formation (Stöckl *et al.*, 2012a; D M Michaelson, 1983).

Auluck, Caraveo and Lindquist presented a review of the theories behind the toxicity of α-synuclein. They discuss the strong association, shown in many model systems, between α-synuclein and membranes *in vivo* and *in vitro*. It was shown in yeast models that both the wild type and A53T forms of the protein localise to the cell membrane. At higher levels of expression, both forms of the protein accumulated in so-called foci in the cytoplasm, shown by EM to be vesicles decorated with the protein (Auluck *et al.*, 2010; Outeiro & Lindquist, 2003; Gitler *et al.*, 2009). This reinforces the view discussed by Lotharius and Brundin that α-synuclein has a role in vesicle maintenance and recycling (Lotharius & Brundin, 2002), so that defects in the protein result in defects in this system. In yeast, high levels of α-synuclein have been shown to affect the endoplasmic reticulum (ER)–Golgi vesicle transport system: vesicles are formed at the ER correctly, but on reaching the Golgi they do not fuse in the expected manner (Gitler *et al.*, 2008).

It has also been shown that dopaminergic neurones in *Caenorhabditis elegans* made to express α-synuclein will be lost within 72 hours. Genes for endocytosis and protein degradation are up-regulated in these animals, and if endocytotic genes are down-regulated instead α-synuclein has increased toxicity (Lasko *et al.*, 2003). Overexpression of human α-synuclein in *Drosophila* has resulted in the observation of cytoplasmic inclusions, reminiscent of Lewy Bodies and Neurites, and further experiments have shown that lipid metabolism is damaged in these insects (Feany & Bender, 2000; Scherzer *et al.*, 2003).

Auluck *et al.* describe their model for how α-synuclein exerts its toxicity. They propose that under normal conditions, α-synuclein exists as an unfolded cytoplasmic protein. When the protein comes into contact with lipid membrane, the structure changes to

give rise to α-helical domains at the lipid surface. Mutant α-synuclein, on the other hand, exhibits different behaviour. On lipid membrane, or in the cytoplasm, it is able to dimerise, forming β-sheet structures. These dimers may further oligomerise, forming toxic species as they do so, spreading throughout the cell damaging membrane around many organelles (Auluck *et al.*, 2010). These processes are depicted in Figure 1.3.

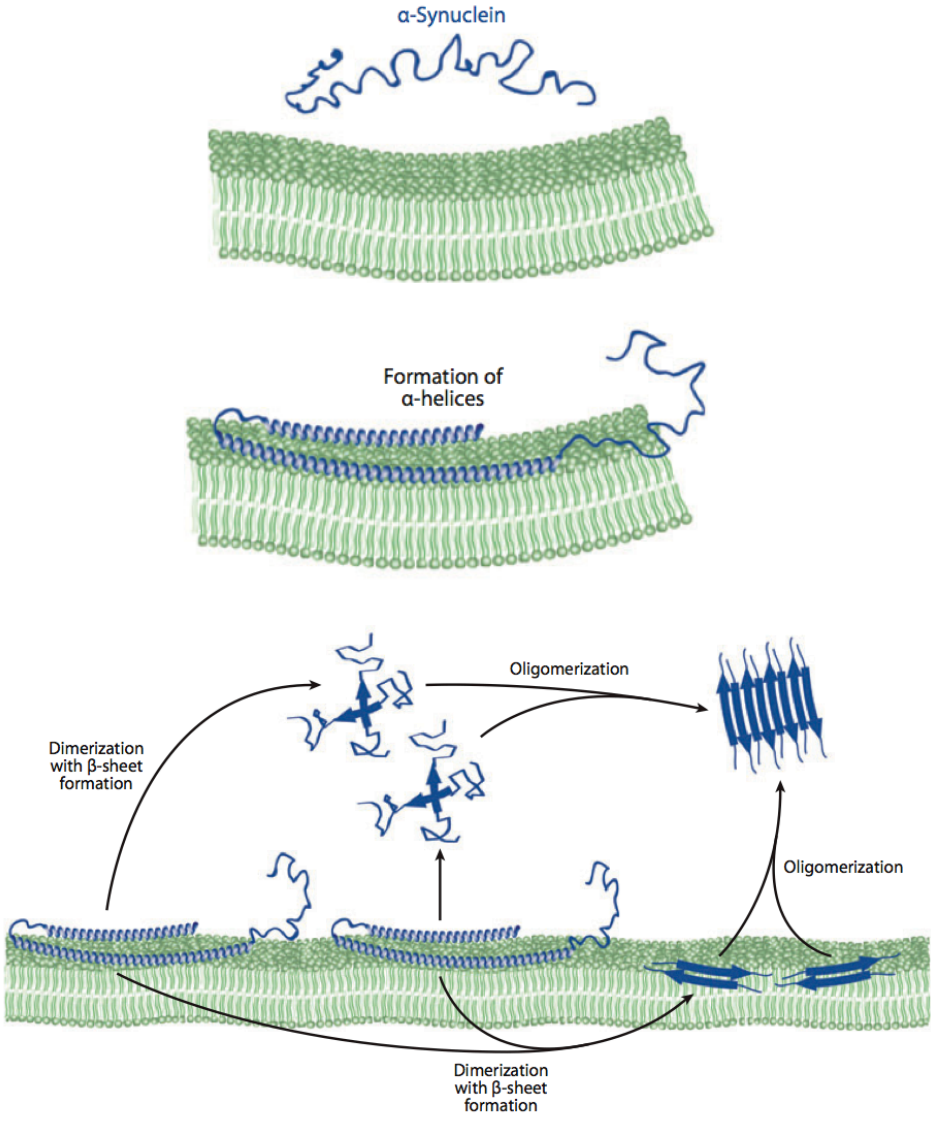

Figure 1.3: *(Top)* Normal cytoplasmic alpha-synuclein, *(middle)* alpha-synuclein associating with membrane, *(bottom)* mutant alpha-synuclein associating with membrane in an incorrect manner, then oligomerising. Reproduced from Auluck *et al.*, 2010 (Auluck *et al.*, 2010)

Intriguingly, the five sites of PD-causing mutation mentioned so far (A30, E46, H50, A53, G51) are within a very compact region, Four are spatially close, with three on the same side of one of the α-helices formed on lipid binding. This is illustrated in Figure 1.4 (Pettersen *et al.*, 2004; Ulmer *et al.*, 2005). This may suggest that the nature of helix formed on lipid binding is influential in whether disease occurs, but this is yet to be proven.

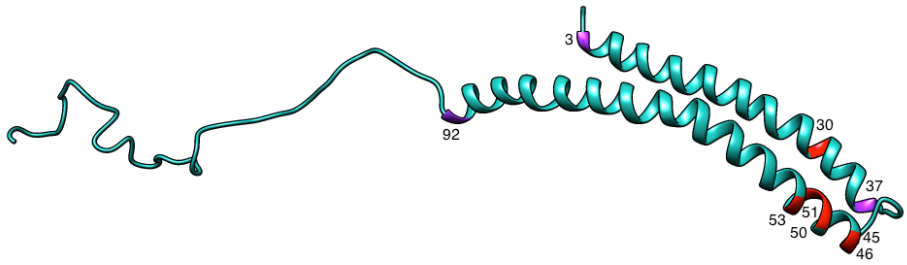

Figure 1.4: Micelle-bound α-synuclein, with polypeptide chain in blue, and residues 30, 46, 50, 51, and 53 in red. Note the proximity of E46, H50, G51, and A53, as well as the similarity in orientation around the α-helix. Initial and final residues of helices are coloured purple, and labelled with their sequence number. Image prepared using Chimera, coordinate file downloaded from the protein database, PDB ID: 1XQ8.

Auluck *et al.* discuss the different α-synuclein mutants and their likely effect on synapse behaviour. During spells of repeated stimulation, additional vesicles must be recruited from a so-called reserve pool (Lotharius & Brundin, 2002). The wild type protein maintains the reserve pool of synaptic vesicles by forming interactions between small numbers of the structures. Mutants A53T and E46K alter the vesicles on binding, since they have a different binding affinity to WT α-synuclein, and lead to far too many vesicles being kept in the reserve pool, reducing synaptic transmission. A30P mutant α-synuclein reflects the consequence of lacking α-synuclein altogether, with the protein unable to bind to the vesicles efficiently. This leads to depletion of the reserve pool as vesicles are released too frequently (Auluck *et al.*, 2010).

It is the conclusion of the Auluck *et al.* review that toxicity comes as a result of dimerisation of mutant protein at the synapse. Dimers form soluble oligomers which may then disperse into the rest of the cell, damaging the organelles they come into contact with, particularly

the endoplasmic reticulum and mitochondria, possibly by oxidative stress mechanisms. The key pathogenic effect would be at the synapse, where vesicles would inappropriately release their contents, and neurones would be stimulated incorrectly. When dopaminergic neurones are affected, motor defects would result. These conclusions echo the earlier conclusions of Lotharius and Brundin (Lotharius & Brundin, 2002; Auluck *et al.*, 2010).

Two recent reviews have collected the information on how α-synuclein structure relates to membrane interaction. Dikiy and Eliezer focussed on the structural information gathered for the protein in its bound states. It is known that under various conditions, α-synuclein may fold into an extended-helix structure, or into a broken-helix (Bussell & Eliezer, 2004; Bussell *et al.*, 2005; Georgieva *et al.*, 2008). The authors postulate that the broken-helix conformation is only adopted when the vesicle upon which the protein is bound, approaches the synaptic membrane (Dikiy & Eliezer, 2012). Their summary of the current models is presented in Figure 1.5.

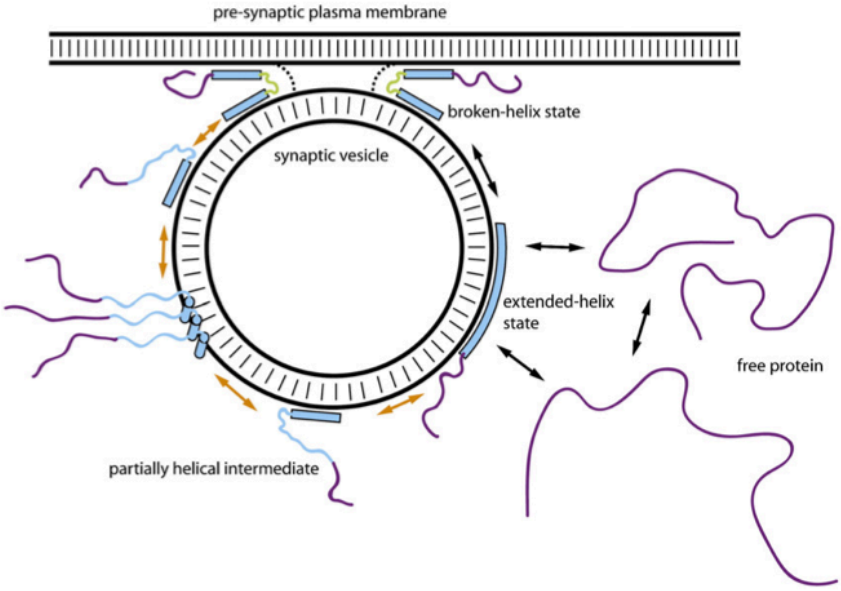

Figure 1.5: Summary of various membrane interaction models, reproduced from Dikiy and Eliezer, 2012 (Dikiy & Eliezer, 2012). Note the changes from randomly structured free protein, to extended-helix, to broken-helix.

The findings of Dikiy and Eliezer are repeated, and elaborated upon by Pfefferkorn, Jiang, and Lee (2012). In their review, the authors discuss the wide range of techniques used to probe α-synuclein behaviour at membranes. A focus of the review is that the dimensions of the lipid structure, to which the protein is binding, may have substantial impact on the structure of α-synuclein. NMR structures for micelle-bound α-synuclein show clearly the broken-helix, but, when larger vesicles are used, the extended-helix is observed. There is also an effect on how easily α-synuclein binds lipids: the protein appears to bind more readily to smaller vesicles, perhaps due to packing defects. Finally, the authors examined evidence describing the interaction of disease-related mutants with lipid structures. A53T does not appear to alter lipid binding, A30P appears to reduce lipid-binding, and E46K appears to enhance lipid-binding (Pfefferkorn *et al.*, 2012).

It is important to address the question of how α-synuclein binds membrane, because this may lead to either an understanding of the method of toxicity, or to potential treatment targets for PD, and many laboratories have contributed to the literature addressing this question (Zhu *et al.*, 2003; Lee *et al.*, 2004; Lashuel *et al.*, 2007; Ferreon *et al.*, 2009; Burke *et al.*, 2013; Khalaf *et al.*, 2014). Using circular dichroism (*CD*) and other techniques, Martinez *et al.* investigated the interaction of α-synuclein and gangliosides to determine which of these lipids would bond with the protein, and what the effects were of such an interaction (Martinez *et al.*, 2007). It was shown that α-synuclein has specificity for GM1 (Monosialotetrahexosylganglioside) over other forms of lipid. Measured by circular dichroism, the α-helical proportion of the protein was shown to change when exposed to different lipid mixtures. The protein on its own, or with DPPC (1,2-dipalmitoyl-sn-glycero-3-phosphocholine) and cerebrosides, or with ceramides, gave *CD* spectra as for an unfolded protein. When exposed to total brain gangliosides, the *CD* spectra displayed some signs of α-helix structure, but not significantly. When exposed to vesicles containing only GM1, the *CD* spectra showed the characteristics of that for α-helically folded protein, showing significant interaction with this lipid, and much greater interaction than that for

with other lipids.

Specificity for GM1 has been observed in Aβ (Yanagisawa *et al.*, 1995; Matsuzaki *et al.*, 2010), and the influence of GM1 and lipid rafts on prion aggregation and toxicity has also been seen (Fantini *et al.*, 2002; Sanghera *et al.*, 2011). GM1, therefore, is likely to be involved at a key step in all amyloid diseases: the step in which the protein binds membrane. It is also likely to be essential to the normal function of the protein, with some structural change needed to make this interaction pathogenic.

Martinez *et al.* were able to show that GM1 influenced the formation of α-synuclein oligomers. Atomic Force Microscopy was used to analyse α-synuclein structures following incubation in different conditions. The authors examined samples incubated with and without vesicles containing GM1. In the sample exposed to GM1, oligomers of α-synuclein were observed that were not seen in samples incubated without vesicles. Bands corresponding to oligomers were also seen by native polyacrylamide gel electrophoresis (PAGE) at two different sizes. No oligomers were observed in samples exposed to different lipids, or even total brain gangliosides (Martinez *et al.*, 2007).

Interestingly, it was shown that fibrils were likely to form when Martinez *et al.* exposed the protein to total brain lipid, but not when it was exposed only to GM1. Exposure of α-synuclein to vesicles of total brain lipid extract – containing approximately 10 % phosphotidylserine (PS) – lead to accelerated fibril formation. This accelerated fibrillation is counteracted by a higher GM1 content in the vesicles to which α-synuclein is exposed. Vesicles containing 20 % GM1 removed the acceleration effect completely, and by 50 % GM1 fibrillation was eliminated. This was confirmed by ThT fluorescence and TEM (Martinez *et al.*, 2007).

CD showed no significant formation of secondary structure in the 20 % GM1 vesicle samples, but in the 50 % GM1 samples α-helical structure was shown. These results confirmed previous findings that α-helical α-synuclein inhibits or eliminates its fibrillation

(Zhu *et al.*, 2003). After incubation, β-structure was seen by circular dichroism, suggesting that these non-fibrillar oligomers possess significant β-sheet regions. Martinez *et al.* conclude that, since they have shown interaction between the two species, α-synuclein would localise to regions of the membrane enriched with GM1 – so-called rafts or caveolae – which are present at synapses. In these regions there is sometimes as much as 50 % GM1, due to ganglioside self-association, thereby presenting a large area of lipid that may interact with α-synuclein. Here, with wild type α-synuclein, fibrillation would have an extremely low chance of occurring. This interaction, they deduce, must be essential to the function of the protein, and therefore requires detailed further study (Martinez *et al.*, 2007).

Given that it has been shown that α-synuclein interacts with the gangliosides GM1 and GM3 (Martinez *et al.*, 2007; Di Pasquale *et al.*, 2010), Fantini and Yahi decided to use a theoretical approach to investigate how this is accomplished, and the consequences of this interaction (Fantini & Yahi, 2010, 2011). The authors compared the primary structures of the glycosphingolipid–binding motif (GBM) of α-synuclein to that of *Helicobacter pylori* adhesin, HIV-1 gp120 v3 loop, GM1–binding peptide, human Prion Protein (PrP), and human amyloid-β. This analysis revealed that the domains share a common sequence, written as: (K/H/R)-X_{1-4}-(Y/F)-X_{4-5}-(K/H/R). At least one of X_{1-4} must be G and X_{4-5} are usually G or T. They make further interesting points with regard to the central aromatic residue: Y39 for α-synuclein and Y10 for Aβ. This amino acid is found in the same location both in the fragment analysed for alignment comparison, and in the whole protein. It is flanked by basic residues in both α-synuclein and Aβ. Through molecular dynamics simulations, several mutants of α-synuclein were examined for interaction with GM3. It was found that Y39A had much lower affinity for GM3, showing that this interaction depends heavily on the amino acid at position 39. Y39F, a mutant replacing the tyrosine with phenylalanine (another aromatic residue), was able to interact almost as strongly as the wild type protein. Therefore, the aromatic group at this point is presumed

to be essential to lipid binding of α-synuclein. The Fantini and Yahi model for binding of α-synuclein to gangliosides is shown in Figure 1.6.

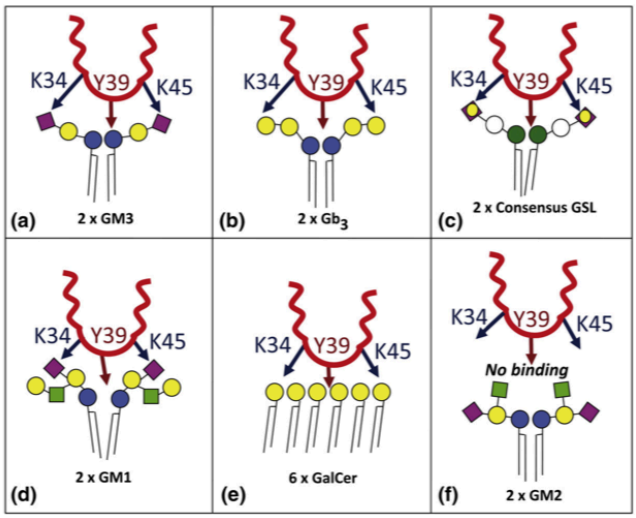

Figure 1.6: Figure reproduced from Fantini and Yahi, 2011, showing the interactions of α-synuclein with gangliosides, around residue Y39. Of particular relevance is panel (d), in which Y39 is coordinated by interactions of K34 and K45 with the sugar moieties of GM1.

It has been discussed in this Section that both lipid choice and protein have impact on the interaction between protein and membrane. In the next Section more detail on membrane composition is presented, and the vesicles used in work presented later in this thesis are introduced.

1.3 Model membranes for lipid-binding studies

Efforts by some researchers to employ lipid vesicles in their studies have been discussed above. For the studies presented in this thesis, it was necessary to choose a set of suitable and interesting lipids that may have roles in the interaction between α-synuclein and membranes. A single lipid species alone does not provide an accurate representation of neuronal membrane. Cotman *et al.* and Breckenridge *et al.* examined neuronal membranes in 1969 and 1972, respectively (Cotman *et al.*, 1969; Breckenridge *et al.*, 1972).

In the former study, it was found that phospholipids PC and phosphoethanolamine (PE) constituted ∼60 % of total membrane lipid, with cholesterol and ceramides making up ∼ 20 %. PI (phosphoinositol) and PS also make up around 10 %, as do glycolipids in total brain lipid. However, glycolipids were found to be a smaller component at synapses, making up only 1 % of lipid there.

Breckenridge *et al.* realised that the Cotman study had not investigated the proportion of lipid that was ganglioside; a matter of concern because in fact gangliosides are a major component of neuronal membrane. This study found that ganglioside is approximately 13 %, with phospholipids PC, PE, PS, and PI making up ∼ 71 % altogether. Cholesterol, they found, is only 15 % of total lipid. Discrepancies can be accounted for by the missing ganglioside fraction from the Cotman study.

Potentially key lipid head groups for the present work are, therefore, PC, PA (phosphate), PG (phosphoglycerol), PE, PS, PI, cholesterol, and GM1. These represent measurable components of real neuronal membranes, *i.e.* the lipids that α-synuclein would typically encounter. Zhu, Li and Fink carried out early work to determine how strongly α-synuclein interacts with different lipids (Zhu *et al.*, 2003). They found that binding affinity is greatest for PA, with PG, PS, and PE being slightly lower. These lipids have charged head groups, thereby suggesting a means of interaction with α-synuclein. Another key decision in selecting lipids for this study was the length of the acyl chains in the molecules. Since pure lipids were to be used, it was impossible to replicate the complexity of true neuronal membranes. Yu *et al.* determined the composition of a brain lipid extract by NMR, and found that lipids with longer acyl chains accounted for larger proportions of the total mixture than those with smaller chains (Yu *et al.*, 2006).

It was decided that for the primary α-synuclein–lipid binding studies the optimal balance of natural occurrence and ability to work with the lipid was to use lipids with acyl chains of lengths 18 and 16 carbon atoms. The chains were also minimally unsaturated, with only one double bond per molecule, introducing some fluidity without compromising the structural integrity. These are known as PO lipids, where PO is defined as 1-palmitoyl-2-oleoyl-sn-glycero-3-R, and R is defined as the lipid head group. The structure of these lipids is shown in Figure 1.7.

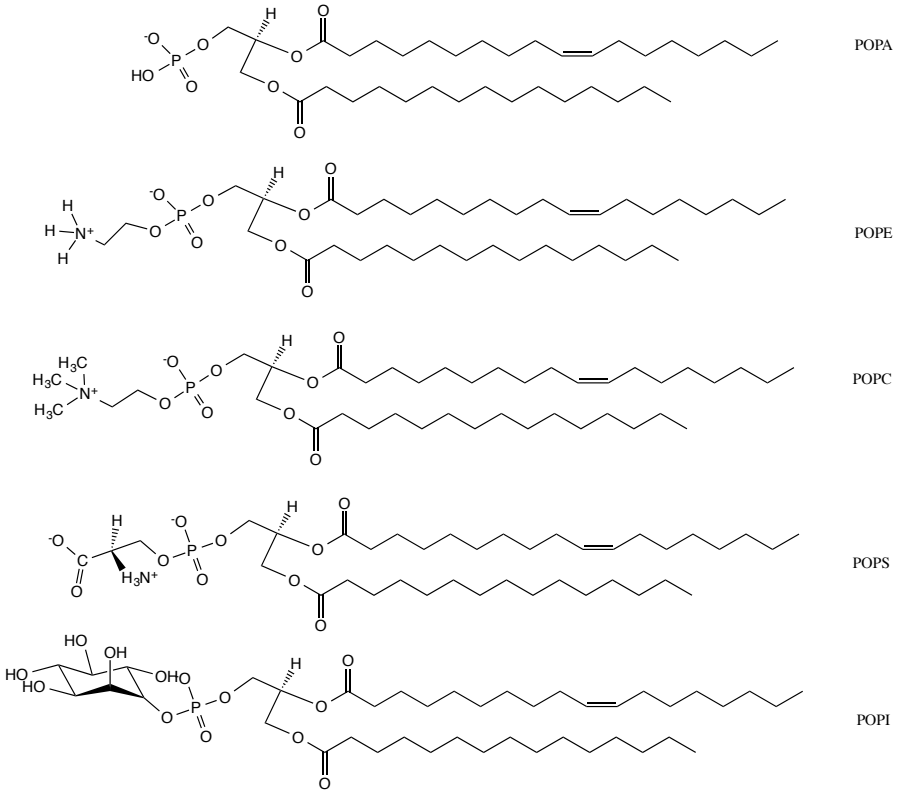

Figure 1.7: Commonly used phospholipids, some referred to in this thesis, and in references. From top: POPA, POPE, POPC, POPS, POPI.

Also used in the present work is cholesterol. This molecule has a key role in stabilising cellular membranes, and can be responsible for fluidity and rigidity properties of lipid structures. It is necessary to use cholesterol here to more accurately simulate real cell membranes, and reflect conditions α-synuclein would encounter in cells. Cholesterol is shown in Figure 1.8 (Ohvo-Rekilä *et al.*, 2002).

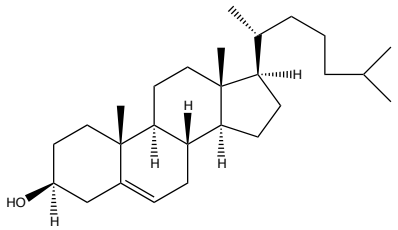

Figure 1.8: Cholesterol

The sphingolipid sphingomyelin (SM1) was incorporated into vesicles for some of the studies in this work. Its structure is shown in Figure 1.9. SM1 has been implicated in signalling pathways, and apoptotic pathways, and it has many putative roles in binding events. Since it it prevalent in neurones, SM1 was judged to be a good candidate for amyloid binding (Zhang *et al.*, 1997).

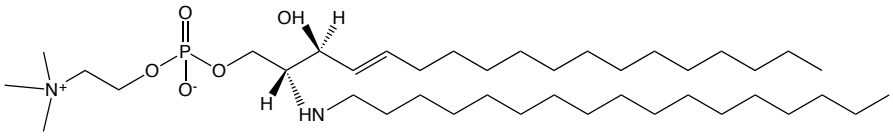

Figure 1.9: Sphingomyelin

Finally, the ganglioside GM1 was incorporated into our model membranes. GM1 is an important lipid for many binding processes, including binding the cholera toxin, and is found in large quantities in neuronal membranes. GM1 is found *in vivo* partitioned into lipid rafts, which have been reconstituted *in vitro* (Dietrich *et al.*, 2001a,b; Mocchetti, 2005). It seems likely that these would be areas of major affinity for α-synuclein. GM1 is shown in Figure 1.10. It is the plentiful charged groups and side chains that make the

molecule able to bind the protein.

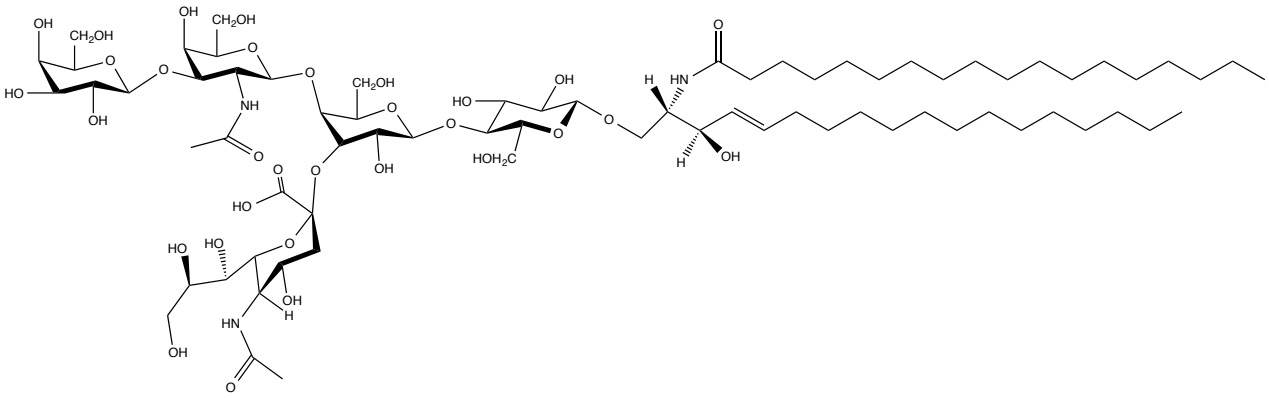

Figure 1.10: GM1

The lipids discussed above, particularly SM1 and cholesterol, have often been implicated in the formation of lipid raft domains, where narrower lipid molecules are able to pack together more closely and present an concentrated region of head groups to the bulk solution. Figure 1.11 shows how this kind of domain may exist as part of the lipid bilayer. These domains have often been suggested as binding targets for amyloid proteins, though other researchers dispute their existence (Dietrich *et al.*, 2001b; Fantini *et al.*, 2002; Pinheiro, 2006; Lingwood & Simons, 2010). Whether they are permanent, transient, or merely hypothetical, these domains incorporate lipids that may influence the binding of α-synuclein to membranes, and therefore are rightly considered here.

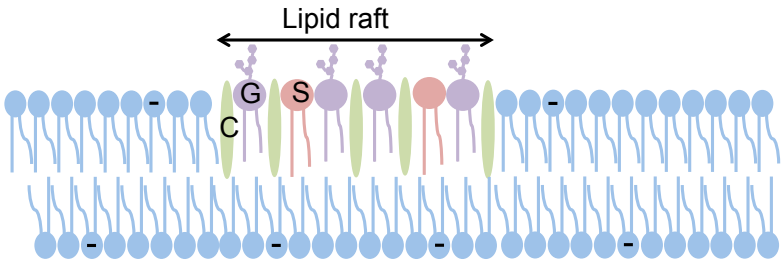

Figure 1.11: Schematic of lipid raft domain contained within a bilayer. Blue lipids are POPC or POPS. Symbol "-" indicates the negatively charged POPS. Green ovals labelled "C" indicate cholesterol, orange lipids labelled "S" indicate sphingolipid, purple lipids labelled "G" indicate gangliosides.

Two lipid mixtures were used in the work presented in this thesis: soybean PC, and brain total lipid extract (BTLE). Soybean PC is an extract from soybeans of all lipids containing the PC head group. A variety of acyl chain lengths and unsaturation levels is present in this mixture, but the predominant species is shown in Figure 1.12. BTLE is not characterised by the suppliers, but a breakdown of the head groups present is given in Table 1.1. Soybean PC was chosen as an extract that is easy to handle at room temperature, suitably soluble, and representative of some natural lipid membranes. BTLE was chosen as α-synuclein is found mainly in the brain, and these lipids would be representative of those it would encounter.

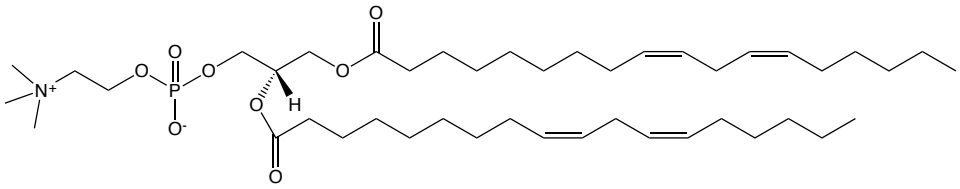

Figure 1.12: The predominant species found in soybean PC extract.

Table 1.1: Proportions of lipid head groups found in brain total lipid extract.

Head Group	wt/wt %
PC	9.6
PE	16.7
PI	1.6
PS	10.6
PA	2.8
Unknown	58.7
Total	100.0

1.4 Annular, amyloid oligomers

Oligomers of amyloid proteins have been introduced briefly in Section 1.1, but clarification is needed to refine this concept and focus on those chemical species relevant to this work. Kim *et al.* produced work characterising oligomers they derived from broken-down fibrils

of α-synuclein (Kim *et al.*, 2009). It has long been suspected that the fibrillar aggregates found in brains of PD sufferers, as in other amyloid conditions, are not the most neurotoxic species (Hardy & Selkoe, 2002). It is believed that soluble oligomers, formed either as an intermediate to fibrils or formed on a separate pathway, are much more toxic to cells. The similarities in the oligomers led to the view that the amyloid proteins may share a method of toxicity (Kayed *et al.*, 2008). As such, this paper investigated properties of soluble oligomers that may form pores in neurones, thereby leading to cell death. The oligomers used in this study were not representative of those that are to be used in the present work, however, there may be useful insights to gain from the Kim *et al.* approach, certainly with regard to techniques employed in the characterisation.

Techniques used to probe the structure of the oligomers included Atomic Force Microscopy (AFM), Transmission Electron Microscopy (TEM), Polyacrylamide Gel Electrophoresis (PAGE), Dynamic Light Scattering (DLS), Circular Dichroism (*CD*), Nuclear Magnetic Resonance (NMR), and small angle X-ray scattering (Kim *et al.*, 2009; Sweers *et al.*, 2012; Lorenzen *et al.*, 2014). Some of these techniques were combined by Kim *et al.* to assess the size of the oligomers, whether they would form pores in membrane, and whether they maintained fibrillar characteristics in oligomeric species. The oligomers were prepared by breaking up fibrils, and were shown by Thioflavin T (ThT) fluorescence to easily re-form fibrils, so these were defined as "on-pathway" oligomers: an intermediate step before full fibrils are formed. Other oligomers can be synthesised that would never lead to fibril formation. These would be known as off-pathway oligomers (Kim *et al.*, 2009).

Antibody A11 has been shown to bind to neurotoxic oligomers in a sequence-independent manner; *i.e.* they bind to the protein in this configuration regardless of which protein is involved (Kayed *et al.*, 2008). This is down to a very similar structure; as one group puts it, the proteins form "morphologically indistinguishable annular protofibrils" (Lashuel *et al.*, 2002b). Kim *et al.* succeeded in showing that the antibody bound the oligomer they had synthesised, but not monomer or fibril, confirming that this species was of the toxic

oligomer type they were seeking.

It was found by Yoshiike *et al.* that fully-assembled α-haemolysin (αHL, a bacterial toxin) heptamers were detectable by A11, suggesting strongly that they share a conformation epitope with amyloid oligomers. This is intriguing, pointing to mechanisms of amyloid toxicity, among other things. The group simultaneously detected Aβ during this experiment, confirming that the A11 used was detecting the correct species. The human pore-forming protein (PFP) perforin (released by cytotoxic T-lymphocytes and natural killer cells) was also shown to be detectable by A11, again showing that its mode of action might be very similar to the mode of toxicity of amyloid proteins (Yoshiike *et al.*, 2007).

The aggregation of αHL and perforin were compared to that of Aβ by the ThT fluorescence assay discussed earlier. It was expected that the change in fluorescence would be similar for all three, but the two non-amyloid proteins did not show the characteristic amyloid aggregation ThT curve, perhaps due to limitations of the assay. However, by electron microscopy, it could be confirmed that oligomers resembling amyloid rings were present in samples of αHL, and even structures resembling amyloid fibrils were seen in perforin samples. This gives further clues to the similarities between amyloid proteins and PFPs (Yoshiike *et al.*, 2007).

Several groups have been able to show that α-synuclein oligomers were able to form well-defined pores in lipid membrane (as other amyloid proteins have been shown to do) (Lashuel *et al.*, 2002b; Danzer *et al.*, 2007; Kim *et al.*, 2009). This is a suspected method of toxicity, since pores would change the environment of the cell leading to incorrect concentrations of metabolites and other ions. Interestingly, despite Kim *et al.* breaking down fibrils to form their oligomers, it was shown by solid-state NMR that the small oligomers are not fibrillar. This was confirmed by TEM and AFM, in which no fibrils were seen, and is reflected in experiments on Aβ (Kim *et al.*, 2009).

1.5 Oligomer preparation

It is important to reinforce that oligomers used in the Kim *et al.* study were made in an entirely different way to the oligomers that will be used in this project. These oligomers may in fact be more correctly classed as protofibrils, since it is likely that the change from oligomer to fibril requires a major structural change. An oligomer of the type we require would not go on to form a fibril, but would be off-pathway. Our oligomers are formed *in vitro* from a solution of monomer, and are stable enough not to form fibrils, even over time, when frozen. Therefore, we conclude that the species is not on the same pathway. Indeed, several oligomer preparations have been reported, resulting in different secondary and tertiary structures (Lashuel *et al.*, 2002b,a; Danzer *et al.*, 2007; Kayed *et al.*, 2008; Kim *et al.*, 2009).

Various preparations of α-synuclein oligomers have been reported. Apetri *et al.* describe a method involving incubation at 37 °C, until aggregates had formed, detected by AFM. This method would lead to many species being formed, but the authors mainly discuss spheroidal oligomers. These were separated from the mixture by filtration centrifugation (Apetri *et al.*, 2006).

Danzer *et al.* describe another oligomer preparation. The lyophilised protein is resuspended in sodium phosphate buffer, with ethanol at low concentration. Depending on their required product, the group may add $FeCl_3$, or may leave this out. They use three modifications to the protocol, involving agitation and incubation for different lengths of time. They do obtain annular oligomers from these protocols (Danzer *et al.*, 2007).

The method used by the Lansbury group to prepare α-synuclein oligomers, has been adapted for use in the present work (Lashuel *et al.*, 2002b,a). Briefly, according to the original procedure, freeze-dried protein aliquots were resuspended in phosphate-buffered saline (PBS) to a concentration of 300 – 700 μM. After an hour incubation on ice, the

solution was refrigerated for up to four weeks. Regular samples were taken and subjected to immunoblot using A11 antibody. This allows the progress of oligomerisation to be monitored over time. When the A11 blot is successful (indicating successful oligomerisation), the sample is separated by size-exclusion chromatography, using a gel filtration column.

1.6 Recent development

Bartels, Choi, and Selkoe recently challenged common knowledge of α-synuclein – the belief that the native state of the protein is an unfolded monomer until it binds lipid. The authors examined evidence that may show that the true native state of α-synuclein is a helically-folded tetramer (Bartels *et al.*, 2011). This is at odds with evidence gathered up to this point, however, the authors argue that this is due to the use in previous research of recombinant (as opposed to human) α-synuclein. The experiments performed to back up this claim were thorough. Several cell lines were chosen that all express α-synuclein endogenously: M17D (neuroblastoma cell line), HEK293 (embryonic kidney cells), HeLa (human cancer cell line) and COS-7 (simian kidney cell line). In addition, mouse cortex and fresh human red blood cells were used, since they too express α-synuclein.

Through various forms of gel electrophoresis (SDS-PAGE both with and without *in vitro* cross-linkers, CN-PAGE and BN-PAGE) a non-denatured species with molecular weight $\sim$45–50 kDa was identified. Coomassie blue stain may have effects on protein migration through gels, however, and under CN-PAGE the main species in all cell types had molecular weight $\sim$55–60 kDa. Since we know that the molecular weight of an α-synuclein monomer is approximately 14.8 kDA, the detected mass corresponds very well to a tetramer. Other analyses, including ultracentrifugation, confirmed that the average mass of α-synuclein species in the cells was just over 55 kDa. By circular dichroism, the structure of these tetramers was found to be strongly α-helical. The authors compared this to recombinant α-synuclein and confirmed that it exists as an unfolded monomer. When exposed to

PC/PS lipid, both species were α-helically folded (Bartels *et al.*, 2011).

Wang *et al.* also reported data seeming to show a tetramer, this time in recombinant α-synuclein (Wang *et al.*, 2011). This group expressed α-synuclein as a Glutathione S-Transferase (GST)–fused protein, and required the GST tag to be removed for experiment. They avoided denaturing conditions throughout their study. When purified on a size-exclusion column, the construct used here eluted as a single sharp peak, with an apparent molecular weight of around 56 kDa. Using chemical cross-linking, the group were also able to show that four species are visible by SDS-PAGE, indicating the existence of tetramer. Their analysis also found that the wild type construct here had α-helical structure by *CD* spectroscopy. This was no longer the case after denaturation by heating. The Wang *et al.* tetramer is shown in Figure 1.13.

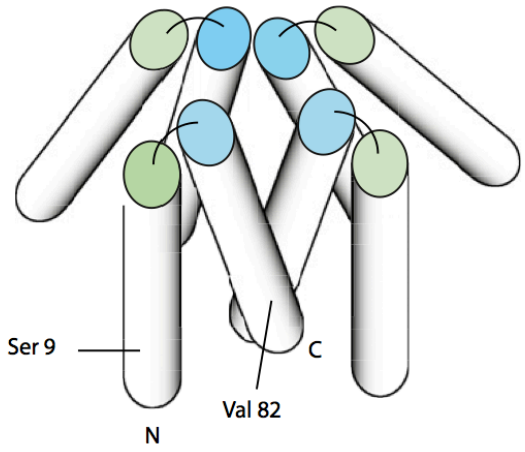

Figure 1.13: The α-synuclein tetramer hypothesised by Wang *et al.*, reproduced from Wang *et al.*, 2011.

In 2012, however, the Bartels *et al.* and Wang *et al.* papers were subjected to strong criticism by a large collaborative publication including the group (Fauvet *et al.*, 2012). This study involved multiple groups, and multiple, independent, experiments, that all failed to find the helical tetramer. Results from Fauvet *et al.* show that, as expected, recombinant α-synuclein exists as a disordered monomer. With native, or heat-denaturing

conditions, only disordered monomer was observed by a variety of methods. It was suggested that the helical structure may have been observed by the other groups after α-synuclein had interacted with membrane and retained its altered structure. Fauvet *et al.* examined this hypothesis by mixing the protein with lipid and observing its α-helical structure by *CD*, then removing the lipid. After lipid removal the protein reverted to disordered structure.

Secondly, α-synuclein purified from mouse and rat brains was shown to have similar properties to recombinant α-synuclein. The unfolded recombinant monomer standard ran to an apparent molecular weight of around 66 kDa on CN-PAGE. This was also seen in several mouse and rat samples, indicating similar electrophoretic properties (size and charge, for example). On SDS-PAGE all samples ran to the same molecular weight, though this time around the expected monomer weight. It was also found that human α-synuclein (recovered from brain tissue *post mortem*), and α-synuclein derived from cell lines (including HeLa and COS-7 amongst many others), migrated the same distance on CN- and SDS-PAGE as unfolded monomer. Various expressions of the protein were shown to elute from gel-filtration columns at the same elution time as native α-synuclein, and heating did not alter this property, suggesting further that the proteins behave similarly (Fauvet *et al.*, 2012).

Whether the tetramer *is* the native form of α-synuclein, or whether it is a step on the pathway to fibrils or oligomers, is not yet known. Data presented by Bartels *et al.* and Wang *et al.* revealing the existence of the tetramer are compelling, but so are the data presented by Fauvet *et al.* disputing the tetramer. While the studies presented in this thesis did not actively seek tetrameric structure, all researchers in the α-synuclein field have become aware of this potential species, and its putative roles in pathways to toxic species. One point that is very clear, though, is that structural studies are essential for work on understanding α-synuclein, and structural work requires robust, validated techniques in order to be accepted by the field.

1.7 Melittin

A second protein was used in the studies presented here to provide comparisons and context for α-synuclein data. Melittin is known as the major component of bee venom, and up-regulates phospholipase A2. It has cell membrane lysis abilities in some circumstances (Terwilliger & Eisenberg, 1982a,b; Pettersen *et al.*, 2004). This protein has been studied by various laboratories, including the Rodger laboratory, its structure measured by *CD*, and its linear dichroism *(LD)* spectra have been reported (Sui *et al.*, 1994; Damianoglou *et al.*, 2010; Svensson *et al.*, 2011). Like α-synuclein, the secondary structure of melittin changes when it interacts with membranes. The structure of the melittin dimer (adopted in lipidic environments) is shown in Figure 1.14. The change in structure exhibited by melittin, and its previously-studied *LD* make it ideal as a tool with which to verify and calibrate the *CD* and *LD* methods applied in this work.

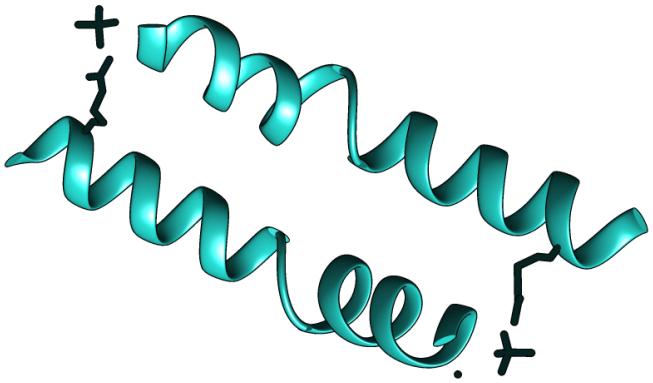

Figure 1.14: Structure of melittin in lipid environments. Image prepared using Chimera, and coordinate file downloaded from the protein database, PDB ID: 2MLT.

1.8 Techniques used in these studies

It has been emphasised above that key to understanding the toxicity of amyloid proteins, is understanding the interactions they make with membranes. This has implications for whether they form pores in organelles or vesicles, whether they transport vesicles at or near the synapse, or whether their role is elsewhere. Spectroscopic techniques have been used in studies discussed above, and these were judged to be the most appropriate in this work. Since vesicles would be used, studies were undertaken into the behaviour of such lipid structures, especially in flow. Circular dichroism was used as the most appropriate way to track changes in the secondary structure of the proteins. Tryptophan fluorescence was chosen as this technique is very sensitive, and allows a single region of the protein to be monitored during interaction with the membrane. Finally, linear dichroism was used as it provides data that complements the other spectroscopic techniques and is, as yet, underused by the field.

1.8.1 Vesicle behaviour studies

This project includes work carried out in order to understand some of the processes that occur when Couette flow is applied to lipid vesicles, and therefore improve spectroscopic work using protein-lipid systems. By monitoring the leakiness of vesicles, it was possible to determine how damaging the effects of Couette flow are on these structures. Calcein leakage was chosen as an easily-measured indicator of vesicles permeability, as demonstrated in literature for many years (Calissano *et al.*, 1972; Papahadjopoulos *et al.*, 1973; Gliozzi *et al.*, 2002; Jesorka & Orwar, 2008). Calcein fluorescence is different when packed into a vesicle at high concentration, and when in dilute solution, so by monitoring fluorescence emission during an experiment it is possible to draw conclusions about the stresses a vesicle is under.

McLachlan *et al.* developed methods for determining the alignment of vesicles in Couette flow. Here, this method was combined with some straightforward mathematical modelling, determining the geometry adopted by vesicles in shear flow. This gave an experimentally verifiable indicator of the degree to which a vesicles must change shape in order to adapt to the strong shear flow used in linear dichroism measurements.

The effect of flow on vesicles has also been studied previously, but mostly by theoretical means, and with little application to relevant studies (de Haas *et al.*, 1997; Noguchi & Gompper, 2005; Mader *et al.*, 2006; Kaoui *et al.*, 2009; Deschamps *et al.*, 2009; Bagchi & Kalluri, 2009). While this work is doubtless essential to the field at large, questions about whether certain lipids should fare better in a linear dichroism experiment, for example, have hardly been touched on. It was possible in this work to combine much more basic modelling with experimental results, and determine some fundamental points about using vesicles in these kinds of experiments.

1.8.2 Intrinsic tryptophan fluorescence

Fluorescence occurs due to the excitation of a fluorophore through absorbance of light at a specific wavelength. Absorbance describes the process of photons causing electrons in the fluorophore to move to a different, higher, electronic state of higher energy. This energy must be lost by the fluorophore as it returns to its ground state, and is lost in the form of emitted photons at a different wavelength than those used to excite the fluorophore. This process may be described by Figure 1.15.

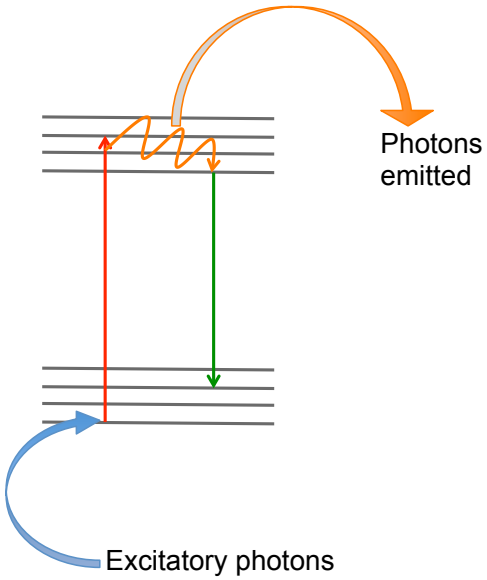

Figure 1.15: The principle of the process of fluorescence, demonstrating that absorbed photons cause a change in energy level of fluorophore electrons, and as the fluorophore returns to ground state other photons are emitted.

In the experiments described here, the fluorophore used is the amino acid tryptophan. Tryptophan is known to emit fluorescence when excited by light at around 295 nm (Ladokhin *et al.*, 2000; Dusa *et al.*, 2006; Pfefferkorn & Lee, 2010; Pfefferkorn *et al.*, 2012). The wavelength of the emitted light varies according to the environment of the tryptophan, so monitoring this wavelength allows conclusions to be drawn about whether the tryptophan has undergone some kind of environmental change. One such change is the burying of the

residue in a lipid membrane away from aqueous solution, therefore allowing deductions to be made about the interaction of the protein containing the tryptophan with a lipid vesicle.

1.8.3 Circular dichroism and linear dichroism

Circular dichroism *(CD)* is long established as the technique of choice for determination of protein secondary structure, not least in the field of amyloid proteins, as mentioned in Section 1.2 (Sui *et al.*, 1994; Kelly & Price, 1997; Davidson *et al.*, 1998; Johnson, 1999; Eliezer *et al.*, 2001; Munishkina *et al.*, 2003; Martinez *et al.*, 2007). Light is circularly polarised in opposite directions, and the absorbance of this light in one direction, subtracted from the absorbance of light in the opposite direction. A signal is observed, therefore, when these absorbances are different – the case occurring for chiral molecules, and molecules with chiral domains such as peptides and α-helices. It is possible to use this technique to monitor the development of structure such as α-helix under different conditions and draw conclusions about how these conditions influence the molecular secondary structure. Protein secondary structures have characteristic *CD* spectra, demonstrated in Figure 1.16, reproduced from an early computational *CD* study (Greenfield & Fasman, 1969).

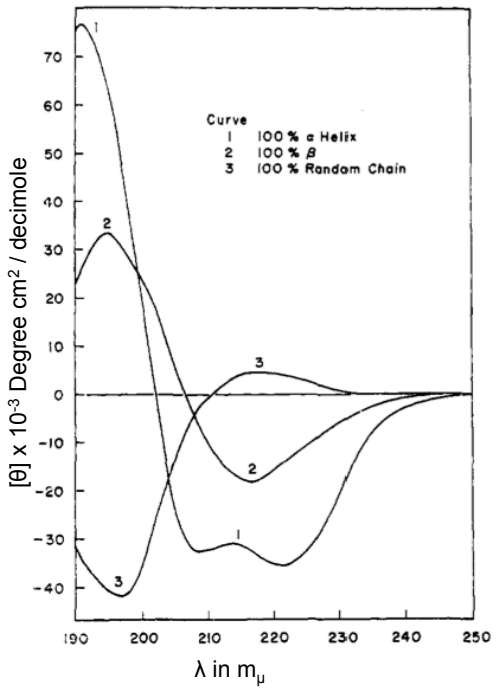

Figure 1.16: Computed, characteristic, *CD* spectra for the major protein secondary structure types, reproduced from Greenfield and Fasman, 1969.

The characteristic bands observed in Figure 1.16 are usually seen in some kind of combination, *e.g.* if a protein is partly disordered but partly α-helical, the α-helix band around 190 nm will usually be much reduced or not present. Therefore, by monitoring the development of particular bands, we may make inferences about the state of the overall structure.

Linear dichroism *(LD)* is a lesser-used optical technique, related to *CD*, that measures differential absorbance of light by oriented molecules. When aligned, molecules containing chromophores are more readily able to absorb light in some directions than others. *LD* measures the difference in absorbance of light polarised parallel to the direction of alignment, and perpendicular to it. In this way, we gain insight into whether a system of molecules do align, or whether, for example, a chromophore interacting with a vesicle surface is inserted into the membrane or across it (Nordén *et al.*, 1992; Ardhammar *et al.*, 1998; Rajendra *et al.*, 2004, 2006).

Figure 1.17 shows the expected position of *LD* bands for α-helices and β-sheet protein structures interacting with vesicle membrane.

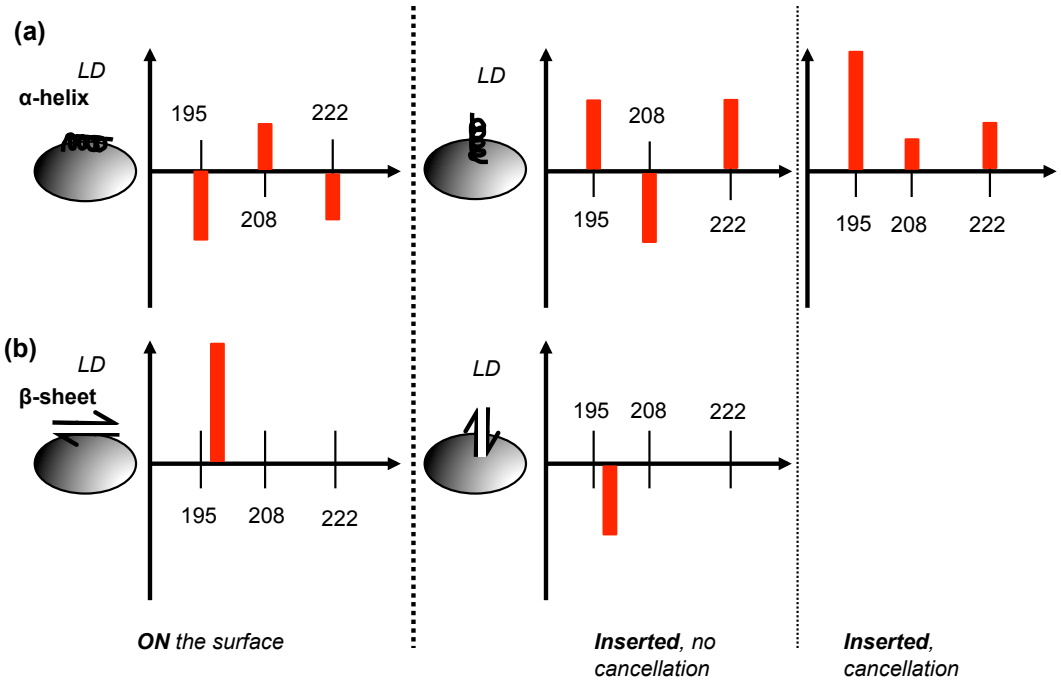

Figure 1.17: Characteristic band positions for (a) α-helices, and (b) β-sheets interacting with vesicle membrane. *(Left)* structures on the vesicle surface, *(right)* structures inserted across vesicle membrane. For α-helix, the bands may cancel when the protein inserts into the membrane, hence two sets of *LD* bands are shown. Figure based on figure from Nordén, Rodger and Dafforn, 2010.

The bands observed in *CD* and *LD* spectroscopy are due to the presence of the peptide

bonds between each amino acid in the protein. These bonds contain bonding, non-bonding, and delocalised electrons, the transitions of which occur at 210-230 nm ($n \longrightarrow \pi^*$), and around 190 nm ($\pi \longrightarrow \pi^*$) (Nordén *et al.*, 2010).

Various groups have set out to use *LD* to gain insight into protein-lipid interactions, following on from attempts to use oriented *CD* to determine protein orientation (de Jongh *et al.*, 1994). The *CD* technique has not been widely adopted, but *LD* has shown more promise since it is more straightforward and more logical. An *LD* signal should be obtained if several protein molecules align together on the surface of a vesicle, for example, or if peptides cross the membrane, and insert parallel to lipid molecules. The first key step, in an experiment of this nature, is to set up a system that encourages alignment. In this case, Couette flow is used. Figure 1.18 demonstrates how this is achieved. The sample chamber is a space between a hollow quartz capillary and a quartz rod. The capillary is set to rotate, thereby generating flow in the sample buffer. Since the buffer is under flow, long molecules in solution are encouraged to align in the direction of the flow.

Plane-polarised light is transmitted trough the sample in two orientations (parallel to the direction of alignment, and perpendicular), and absorbance at each wavelength measured. *LD* signal is calculated as:

$$LD = A_{\parallel} - A_{\perp}.$$

Deductions are made about the molecules in solution based on properties of the resulting spectrum, such as whether bands are positive or negative, at what wavelengths bands occur, *etc.* (Nordén *et al.*, 2010).

LD is extended by probing what happens to alignment when some extra condition is applied to the molecules under study. In the case of membrane-interacting proteins, we ask whether the protein lies across the surface of a vesicle, or if it might insert across a membrane (Damianoglou *et al.*, 2010). A vesicle under Couette flow is believed to flatten, from its stable sphere conformation, into an ellipsoid, and an α-helical protein

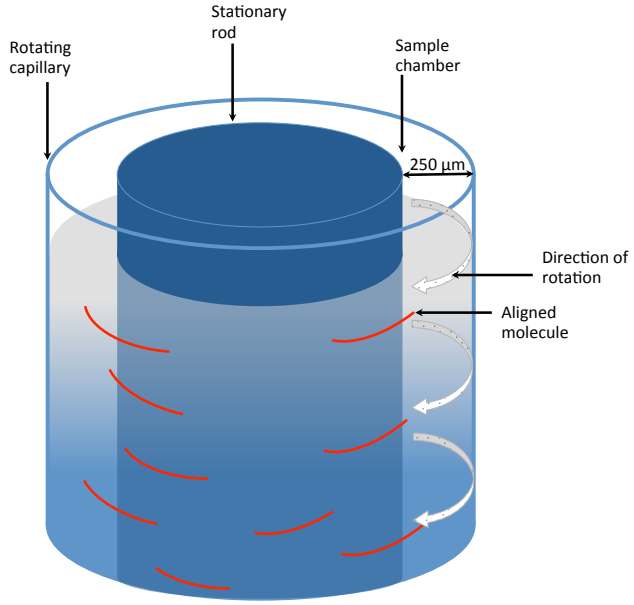

Figure 1.18: Schematic of *LD* cell generating alignment by Couette flow. Torque produced by the rotating capillary induces long molecules to orient in the direction of flow. The capillary has inner diameter 2.9 mm, the rod has diameter 2.4 mm. Both rod and capillary are optical-quality quartz, so light may be shone through the cell at any angle.

on the surface ought to act as a stabilising rib, giving the ellipsoid an axis of alignment. Therefore, a strong alignment signal should be seen for this sort of protein-membrane interaction. The expected bands on such an *LD* spectrum would be positive at 195 nm, negative at 208 nm, and positive at 222 nm. Conversely, if peptides insert across the bilayer, parallel to membrane normal, the *LD* bands would have opposite signs (Nordén *et al.*, 2010).

There are technical issues with *LD*, however, that have hindered progress in the past. *LD* of membrane protein depends on a reliable membrane system, and does not give reproducible results if the membrane vesicles are unstable. Another issue is the as-yet poorly understood nature of vesicle deformation under flow – just how the shape of the vesicle changes, and how this affects its volume or surface area, is not known. This project

uses a combination of experimental and theoretical approaches, in order to establish how volume and orientation of vesicles may change in different conditions of flow. Probe molecules may be added to lipid preparations in order to indirectly measure the *LD* of the vesicles themselves. Probes may interact with the lipids in two ways, shown in Figure 1.19.

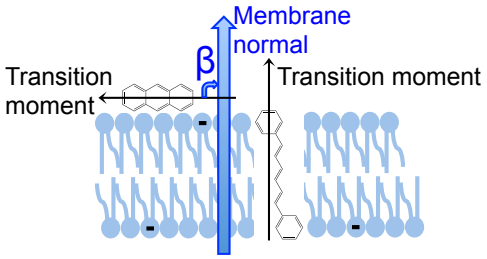

Figure 1.19: Schematic of small molecule-membrane interactions, and their relationship to the membrane normal. On the left is anthracene. In this case, its transition moment being perpendicular to membrane normal, and therefore its angle β being 90°. On the right is diphenylhexatriene, with its major transition being parallel to membrane normal, and angle β being 0.

Vesicles in flow are compressed in the direction of the flow, *i.e.* they develop long sides and short sides (Mader *et al.*, 2006). If a probe, such as the diphenylhexatriene shown in Figure 1.19, is uniformly incorporated into the lipid mixture there would be no *LD* signal until an orientation force was applied by Couette flow, as positive and negative signals in the bulk suspension would cancel each other out. In flow, there would be more probe molecules along the long sides of the vesicles, therefore resulting in *LD* signal.

1.9 Work presented in this thesis

There were several objectives to this work. These overlap, and provide insights for researchers at the interface of amyloid protein biochemistry and spectroscopy. In order to understand amyloid toxicity it is necessary to fully understand the way the proteins interact with lipid membranes, and therefore one must understand the lipids themselves.

The studies presented in this thesis include theoretical and experimental investigations into vesicles behaviour, *CD*, *LD*, and fluorescence investigation into α-synuclein–lipid interaction, and work done to improve *LD* itself. The work was broken-down into the following themes:

- **Develop the practical knowledge of vesicle behaviour in flow**

  The theoretical literature on lipid vesicles in flow is extensive, but does not translate into effective practical work, especially in a Couette flow system. This work aims to take current knowledge and laboratory experience and extend it. Some theoretical work is described in order to understand the expected dimensions a vesicle would achieve during flow, and how this would affect its volume. Experimental work was also carried out to measure how resilient vesicles of different types are in Couette flow – only those that can withstand Couette flow for extended periods are suitable for linear dichroism.

- **Use tryptophan fluorescence to study α-synuclein–lipid interaction**

  The ability of α-synuclein to bind lipid vesicles has been investigated previously, but certain lipids (POPC, POPS, GM1, SM1, cholesterol) have not been studied in depth. It is important, if the true role of α-synuclein in health or disease is to be understood, that any plausible interaction is studied in some detail. By using an inserted tryptophan as a reporter of protein environment, the data presented in this thesis aim to explain the interaction of the protein with POPC and POPS in much more detail than previously known. GM1, SM1 and cholesterol are also investigated for any effect on the binding.

- **Use circular dichroism to study melittin and α-synuclein–lipid interaction**

  By using the same preparations of protein and lipid as for fluorescence studies, much more information on these interactions is gained through making circular dichroism

measurements of the samples. The work presented here shows how the rate structural change undergone on lipid binding is similar to the rates of change in fluorescence, indicating that the two processes occur in parallel.

Melittin was used in these studies as a model protein, well-known to biophysics. In the experiments presented here, *CD* of melittin was pushed to technically challenging levels, measuring *CD* spectra in the *LD* cell. By demonstrating that this experimental set-up was able to deliver good quality *CD*, this work has opened new experimental options for other protein-lipid systems. This approach was then applied to α-synuclein, both its monomeric and oligomeric forms. This *CD* data is an essential partner to the *LD* data also gathered.

- **Develop robust methodology for protein–lipid interaction linear dichroism studies**

  At times, researchers have achieved good *LD* data for proteins and lipids, and at other times the data has been poor. Much of the lower quality data may be attributed to poor sample preparation or unsuitable lipid selection. The final aim of this work was to report on the successes achieved here in generating meaningful *LD* spectra, and how sample preparation and lipid selection influenced the spectra. By first using melittin, the well-studied model peptide, the data reported here validate the methodology used as appropriate and sound. This method was then applied to α-synuclein, giving a simple spectroscopic measurement of oligomeric amyloid protein interacting with lipid membranes for the first time.

Chapter 2

Experimental

2.1 Introduction

The reasons and motivations for researching α-synuclein are discussed in Chapter 1, enabling the design of experiments presented in this chapter. The techniques selected were predominantly spectroscopic, and often represent extensions of techniques used in the literature. Circular dichroism is a crucial tool in structural biology, giving secondary structure information. By monitoring changes in secondary structure, researchers have been able to shed light on many protein-based systems, including amyloid folding and misfolding (Sui *et al.*, 1994; Kelly & Price, 1997; Davidson *et al.*, 1998; Johnson, 1999; Eliezer *et al.*, 2001; Munishkina *et al.*, 2003). In this study, it was necessary to monitor the change in the secondary structure of α-synuclein as it interacts with lipids, making *CD* an ideal technique.

Intrinsic tryptophan fluorescence has been used in many previous studies, since this amino acid has a strong fluorescence emission that changes in response to its environment. This is also an established technique in protein folding studies, both for amyloid research and other categories of protein biophysics (Ladokhin *et al.*, 2000; Dusa *et al.*, 2006; Pfefferkorn & Lee, 2010; Pfefferkorn *et al.*, 2012). Wild type (WT) α-synuclein has no tryptophan residues, so the insertion of a single Trp is discussed in this chapter.

Linear dichroism, as yet, has a smaller field of associated research, but its use here has been

essential in extending the tools available for studying protein-lipid interactions. These methods are developments from those previously utilised in the Nordén, Rodger, and Dafforn laboratories (Rodger & Nordén, 1997; Rodger *et al.*, 2002; Nordén *et al.*, 1992, 2010).

In this study, E46K α-synuclein is compared to α-synuclein without the E46K mutation on a structural level, and through interactions with lipids. The protein was required in large quantities (on the order of tens of milligrams), and this was achieved by expressing the protein in *Escherichia coli*. The methods presented here draw on laboratory experience and knowledge, as well as that of other groups, to produce an efficient expression process for two constructs of α-synuclein, Y39W, and E46K:Y39W (Lashuel *et al.*, 2002b,a). Work by Timothy Kaufmann and Rachel Smith in the Pinheiro laboratory has led to an improvement in production of α-synuclein oligomers, the method for production of which is detailed below, and this process has been employed for the material for our *LD* studies.

2.2 Materials and methods

2.2.1 Materials

Consumables procured

The following were obtained from Abcam (Cambridge, UK): Full length wild type human α-synuclein for control experiment.

From Agilent (Santa Clara, CA, USA): Stratagene site-directed mutagenesis QuikChange II kit.

From Avanti Polar Lipids (Alabaster, AL, USA): POPC, DPPC, DMPC, POPS, BTLE, SM1, soybean PC.

From Bio-Rad (Hercules, CA, USA): Bradford assay reagent, SDS-PAGE kit, SDS-PAGE low molecular weight protein markers.

From Integrated DNA Technologies (IDT) (Coralville, IA, USA): DNA primers, IDTE buffer.

From Invitrogen (Carlsbad, CA, USA): SYBR Safe DNA gel stain

From Melford (Ipswich, UK): Tris, IPTG.

From Merck (Kenilworth, NJ, USA): $MgCl_2$, yeast extract, pepton.

From National Diagnostics (Atlanta, GA, USA): 30 % acrylamide mixture.

From QIAGEN (Limburg, Netherlands): QIAprep miniprep kit, QIAquick Gel Extraction kit.

From Severn Biotech (Kidderminster, UK): Coomassie Blue G-250.

From Sigma-Aldrich (Poole, Dorset, UK): RbCl, $CaCl_2$, $MgSO_4$, $MnCl_2$, bromophenol blue, phosphoric acid, 3-(N-morpholino)propanesulfonic acid (MOPS), GM1, sepharose 4B N,N,N′,N′-tetramethylethane-1,2-diamine (TEMED), Ethylenediaminetetraacetic acid (EDTA), Phenylmethylsulfonyl fluoride (PMSF), calcein, diphenylhexatriene (DPH), N-[Tris(hydroxymethyl)methyl]-2-aminoethanesulfonic acid (TES).

From Thermo Fisher Scientific (Waltham, MA, USA): NaH_2PO_4, Na_2HPO_4, NaCl, $(NH_4)_2S_2O_8$, $(NH_4)_2SO_4$, CH_3CO_2K, KH_2PO_4, K_2HPO_4, glycine, glycerol, 2-mercaptoethanol, sodium dodecyl sulphate (SDS), snake skin pleated dialysis tubing (3,500 MWCO), DNA standard 1 kb ladder, 6 × DNA loading dye solution.

Buffers and solutions prepared in the laboratory

For cell culture

Lysogeny broth (LB): 10 g peptone, 5 g yeast extract, and 10 g NaCl, made up to 1 L with distilled water, and autoclaved to sterilise.

Terrific broth (TB): 12 g peptone, 24 g yeast extract, 4 mL glycerol, made up to 900 L with distilled water, and autoclaved to sterilise. 100 mL of TB salts solution contained: 0.17 M KH_2PO_4, and 0.72 M K_2HPO_4, autoclaved. The two components were mixed on day of use.

For competent cell production

TFB1: 30 mM CH_3CO_2K, 10 mM $CaCl_2$, 50 mM $MnCl_2$, 100 mM RbCl, 15 % (v/v) glycerol, pH 5.8.

TFB2: 10 mM MOPS, 75 mM $CaCl_2$, 10 mM RbCl, 15 % (v/v) glycerol, pH 6.5.

For SDS-PAGE

Resolving gel: 375 mM Tris pH 8.8, 15 % acrylamide, 0.1 % SDS, 0.1 % $(NH_4)_2S_2O_8$, 0.0004 % TEMED.

Stacking gel: 100 mM Tris pH 6.8, 5 % acrylamide, 0.1 % SDS, 0.1 % $(NH_4)_2S_2O_8$, 0.0004 % TEMED.

Sample buffer: 62.5 mM Tris-HCl pH 6.8, 10 % (v/v) glycerol, 2 % SDS, 5 % 2-mercaptoethanol, 0.05 % bromophenol blue.

Running buffer: 25 mM Tris base, 192 mM glycine, 0.1 % SDS, pH 8.3.

Colloidal Coomassie blue stain: 10 % $(NH_4)_2SO_4$, 0.1 % Coomassie G250, 20 % ethanol, 3 % phosphoric acid.

For purification and fast protein liquid chromatography (FPLC)

Lysis buffer: 10 mM Tris-HCl, 1 mM EDTA, 1 mM PMSF, pH 8.0.

Buffer A: 10 mM Tris-HCl, pH7.4. Filtered and degassed on day of use.

Buffer B: 10 mM Tris-HCl, 2 M NaCl, pH 7.4. Filtered and degassed on day of use.

Phosphate-buffered saline (PBS): 137 mM NaCl, 2.7 mM KCl, 10 mM Na_2HPO_4, 1.8 mM KH_2PO_4.

Sodium phosphate buffer: 10 mM mixture of Na_2HPO_4 and NaH_2PO_4, mixed at proportion resulting in pH of 7.4.

2.2.2 Expression of α-synuclein

Preparation of competent cells

E. coli strain BL21* Rosetta cells from Dr Kelly Walker (University of Warwick) were were streaked onto an LB agar plate, and incubated overnight at 37 °C. These cells have resistance to chloramphenicol, so any *E. coli* growth in chloramphenicol-containing media should occur only from this strain, allowing selection from wild type bacteria. Single, typical, *E. coli* colonies were selected with which to inoculate 2.5 mL of LB medium[1]. These cultures were incubated overnight at 37 °C with shaking at 160 rpm. The entire overnight culture was added to 250 mL LB containing 20 mM $MgSO_4$, and grown at 37 °C with shaking at 160 rpm until the optical density at 600 nm (OD_{600}) was between 0.4 and 0.6. The cells were harvested by centrifugation at 4,500 *g* for 5 minutes at 4 °C, and the pellet resuspended in 100 mL ice cold TFB1. The centrifuge step was repeated, with resuspension in 10 mL ice-cold TFB2. After 30 minutes incubation on ice, the cells were transferred to 200 μL aliquots, and flash frozen with dry ice, for storage at – 80 °C.

[1]Typical *E. coli* colonies were defined as 1-3 mm white-yellow circular colonies on LB agar plates, after overnight incubation.

Expression plasmid

The PGS-21a plasmid encoding α-synuclein with Y39W insert was obtained from Prof. Fiona Benson (Lancaster University). The gene is controlled by a T7 promotor, and expression was initiated by the addition of IPTG. In order to be used for mutagenesis, the plasmid was amplified by expression in *E. coli*. This plasmid confers resistance to the antibiotic ampicillin, enabling the use of this antibiotic as a selective tool: any *E. coli* growth in media containing ampicillin would be from bacteria containing this plasmid.

The plasmid was defrosted on ice for 2 minutes and 1 μL was mixed with 100 μL of competent *E. coli* strain DH5-α from Pinheiro laboratory stocks, prepared similarly to the method for BL21* above. After incubating on ice for 30 minutes, the cells were exposed to heat shock at 42 °C for 45 seconds, followed by incubation on ice for 2 minutes. After adding 900 μL of LB, to give a total volume of 1 mL, the cells were incubated for 1 hour at 37 °C. The cells were then centrifuged at 5,000 g for 2 minutes. The supernatant was discarded and the cells resuspended in 100 μL of LB, then plated onto LB agar with ampicillin at 100 μg/mL, to be incubated overnight at 37 °C. One colony was transferred to 5 mL of LB with ampicillin at 100 μg/mL and incubated overnight at 37 °C with shaking.

The plasmid template was purified from the DH5-α strain *E. coli* using a QIAprep Miniprep Kit (QIAGEN, Netherlands). PCR mutagenesis was carried out by Anthony Wambua in the Pinheiro laboratory as detailed below, resulting in the production of E46K:Y39W to complement the Y39W construct.

Site-directed mutagenesis

Primers for PCR mutagenesis were designed manually using sequence data supplied by the manufacturer for the PGS-21a plasmid. Forward and reverse primers were designed

with seven codons flanking the inserted mutation on either side. Primers were supplied by Integrated DNA technologies (IDT, USA) and had the following sequences:

1: 5′–TGG GTC GGC TCT AAA ACG AAA[2] AAA GGC GTG GTG CAT GGC GTG GCG–3′

2: 5′–CGC CAC GCC ATG CAC CAC GCC TTT TTT CGT TTT AGA GCC CAC CCA–3′

The concentration of the primers obtained was 100 μM in 285 μL IDTE buffer pH8. 10 pM/μL solutions of each primer were prepared, and mixed according to Table 2.1.

Table 2.1: Quantities of reagents used in PCR mutagenesis.

Reagent	Volume (μL)
Sterile water	39.0
10x buffer	5.0
dNTPs	1.5
Primer 1	1.5
Primer 2	1.5
Template	0.5
PfuUltra DNA polymerase	1.0

The PCR cycle was performed according to the Stratagene site-directed mutagenesis QuikChange II kit (Agilent, USA). PCR was performed overnight, with the following steps: Parental DNA was denatured at 95 °C for 30 seconds, followed by 18 cycles of 95 °C for 30 seconds and 55 °C for 1 minute, in order to denature parental DNA and anneal the primers. This stage was followed by 68 °C for 1 minute/kb plasmid length, plus 5 minutes, to allow complete extension of primers.

PCR products were purified from other DNA by extraction from agarose gel. 2 g of high-melting point agarose was added to 250 mL TAE (40 mM Tris acetate, 1 mM EDTA) giving a 0.8 % (w/v) agarose solution. This was heated by microwave oven until all the agarose had dissolved, then allowed to cool until safe to handle. 25 μL of 10,000× SYBR Safe DNA

[2]This AAA codon in the forward primer encodes lysine. It is different by a single nucleotide to the wild type GAA codon for glutamic acid.

gel stain was added (Invitrogen, USA), and the gel was poured into the relevant mould to set. Once set, the gel was submerged in the gel tank in 1× TAE. DNA was loaded with 6× DNA loading dye solution in a 5:1 ratio. 5 μL of DNA standard 1 Kb ladder was loaded into a lane for size comparison. Electrophoresis was performed at 100 V for 40 minutes, and the gel was visualised using ultraviolet light on a GeneSnap gel illuminator system (Syngene, India). The correct PCR product was excised with a razor blade, then purified by QIAquick Gel Extraction kit (Agilent, USA).

Expression and purification of α-synuclein

A 200 μL aliquot of competent *E. coli* BL21* Rosetta cells were thawed on ice. 1 μL of the relevant plasmid solution (Y39W or E46K:Y39W) was added, and the mixture incubated for 30 minutes on ice. The mixture was exposed to heat shock of 42 °C for 60 seconds, then incubated for 2 minutes on ice. This mixture was added to 3 mL of LB medium and incubated for 45 minutes at 37 °C with shaking at 160 rpm, then spread onto an LB plate with ampicillin at 100 μg/mL and chloramphenicol at 20 μg/mL. The plates were incubated at 37 °C overnight.

Single, typical, *E. coli* colonies were picked from the plates, and used to inoculate 10 mL of LB with ampicillin at 100 μg/mL and chloramphenicol at 20 μg/mL. These starter cultures were incubated overnight at 37 °C with shaking at 160 rpm. The following day, individual starter cultures were added to 1 L TB in 2 L flasks. These were incubated at 37 °C with shaking at 160 rpm until the OD_{600} was between 0.4 and 0.6. At this point, 1 mL 1 M IPTG was added to the flask to induce expression of α-synuclein. Incubation was continued for 4 hours, and the cells harvested by centrifugation at 10,000 *g*, the supernatant discarded and the pellet frozen.

The pellet was resuspended in 15 mL lysis buffer. Cell lysis was performed by freeze-thawing, followed by sonication. After another centrifugation step, the supernatant was

collected. The supernatant was made up to 60 mL with Tris buffer at pH 8.0, and placed, in a flask, in a water bath at approximately 100 °C for around 10 minutes. Depending on cell density, a more-or-less visible film of proteins precipitated out around the flask. Ammonium sulfate was added to 50 % saturation, causing more proteins, α-synuclein included, to precipitate. After centrifugation, and re-suspension of the pellet in in Tris buffer at pH 7.4, a solution was obtained containing all the α-synuclein, with some impurities.

The protein was purified by FPLC, first using a Source 30Q anion exchange column (GE Healthcare, UK), then determining by sodium dodecyl sulfate-polyacrylamide gel electrophoresis (SDS-PAGE) in which fractions the α-synuclein had eluted. Anion exchange used buffers A and B described in Section 2.2.1. Buffer A was the buffer used to load protein onto the column, and buffer B as the elution buffer, was incorporated on a gradient up to 35 % over 150 mL. Anion exchange fractions that contained α-synuclein were pooled, freeze-dried, and dialysed into 0.01 M sodium phosphate buffer, pH 7.4, using Snake skin pleated dialysis tubing. The sample was then put through a second round of chromatography, this time by Sephacryl S-300 high-resolution size-exclusion column (GE Healthcare, UK), SDS-PAGE performed, α-synuclein-containing fractions pooled, and dialysed again into 10 mM sodium phosphate buffer at pH 7.4.

Characterisation of purified α-synuclein

At various stages of expression and purification, expression of α-synuclein was analysed by SDS-PAGE. The protein was over-expressed, thanks to the T7 promotor and addition of 1 mM IPTG, and has a known molecular weight of around 14,440 kDa. The position and relative size of the over-expressed protein band on the gel allowed a crude first test of whether expression had been successful or not.

SDS-PAGE was performed by diluting 20 μL of protein sample with 20 μL sample buffer,

before heating the samples to 90 °C for 5 minutes. The samples were loaded onto a 15 % polyacrylamide gel, made using the solutions outlined in Section 2.2.1. The gels were stained by colloidal Coomassie blue staining solution overnight to visualise the proteins.

Since this stage of the protocol was completed before carrying out other checks, *E. coli* were judged to have expressed α-synuclein when the characteristic over-expression band was observed on SDS-PAGE gel of total cell extract. SDS-PAGE was carried out using the solutions described in Section 2.2.1, and using SDS-PAGE gel casting equipment from Bio-Rad (Hercules, CA, USA). Electrophoresis was performed at 170 V for around 1 hour, or until the sample buffer approached the base of the gel. 20 μL of sample was loaded into each well, 10 μL of protein markers were loaded into one lane on each gel used.

Figure 2.1 shows images taken of SDS-PAGE gels onto which total cell extracts were loaded. These cells had been transformed with α-synuclein containing one or two mutations: one with Y39W (tyrosine to tryptophan), and one with Y39W and E46K (glutamic acid to lysine), referred to as E46K:Y39W. The purpose of these gels was to demonstrate that over-expression had taken place, demonstrated by swelling around 17 kDa (the characteristic SDS-PAGE position for α-synuclein) and overspill and smearing.

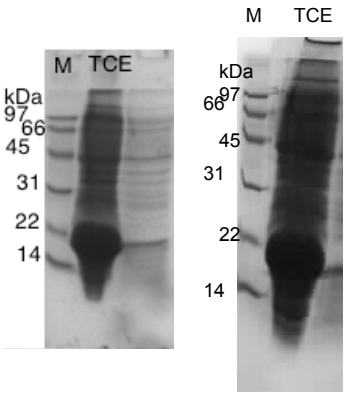

Figure 2.1: Polyacrylamide gels for a typical expression of *(left)* E46K:Y39W α-synuclein, and *(right)* Y39W α-synuclein. Lanes shown are protein molecular weight markers, and cell extracts.

Following each FPLC stage, various fractions were selected to be tested for α-synuclein presence. These usually corresponded to peaks on the chromatogram. Examples of chromatograms from which fractions were selected for SDS-PAGE are shown in Figure 2.2. These are typical for both Y39W and E46K:Y39W expression, with no discernible difference observed by this method.

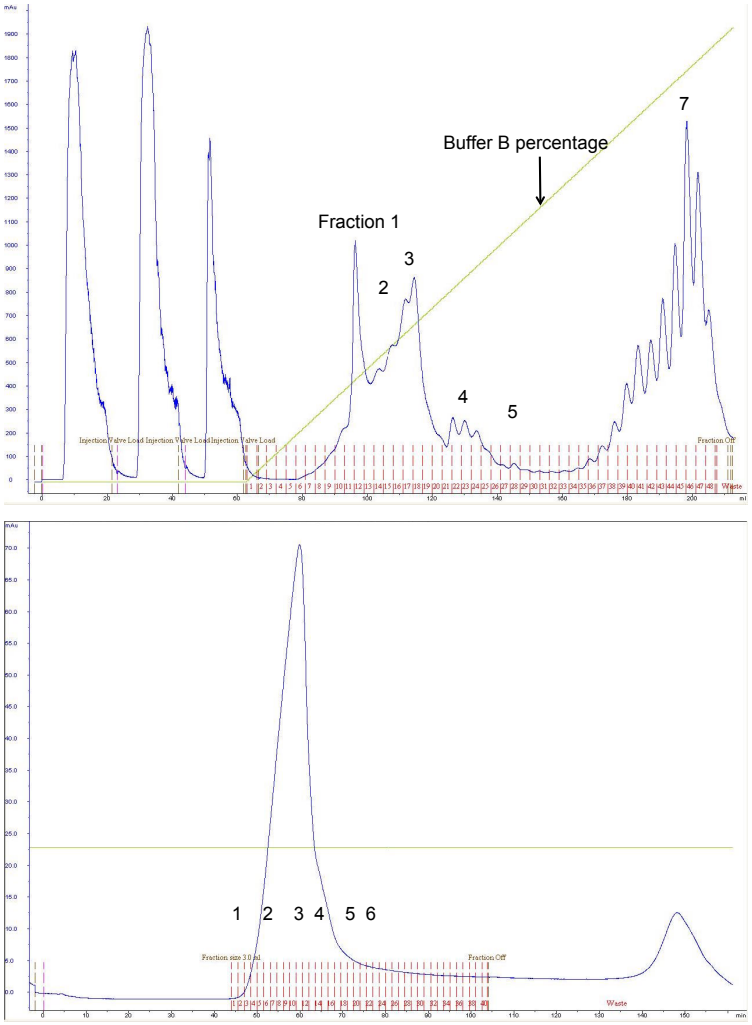

Figure 2.2: FPLC chromatograms for α-synuclein expression. *(top)* Anion exchange, with A_{280} in blue, % buffer B (2 M NaCl) in green, fractions in red; *(bottom)* gel filtration, with A_{280} in blue, fractions in red. Numbers noted on plots indicate fractions used in SDS-PAGE.

The quality and purity of α-synuclein was monitored by SDS-PAGE at various stages, demonstrating that purity was at acceptable levels only after gel filtration FPLC. E46K:Y39W fractions taken from samples labelled 1-7 and 1-6 in Figure 2.2, were used for SDS-PAGE, with the corresponding gels shown in Figure 2.3.

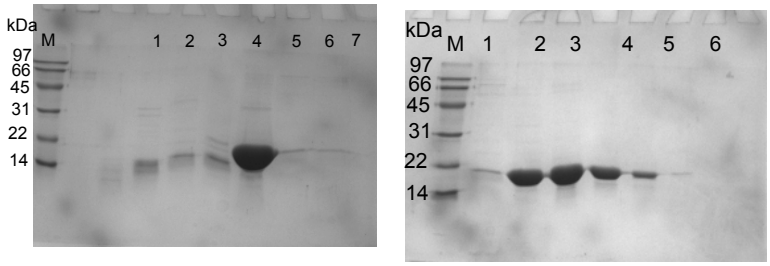

Figure 2.3: SDS-PAGE for fractions gathered after FPLC, for a typical expression of E46K:Y39W α-synuclein: *(left)* anion exchange FPLC, *(right)* size exclusion FPLC. Lanes shown are protein molecular weight markers, and FPLC fractions. Numbered lanes correspond to numbered labels on chromatograms.

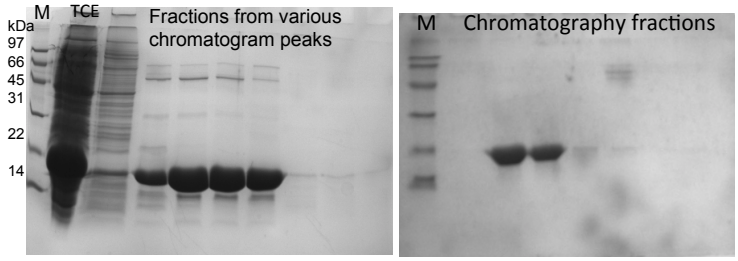

Figure 2.4: SDS-PAGE for fractions gathered after FPLC, for a typical expression of E46K:Y39W α-synuclein: *(left)* anion exchange FPLC, *(right)* size exclusion FPLC. Lanes shown are protein molecular weight markers, diluted cell extract, collected waste, and fractions from chromatography. The corresponding chromatograms are not shown in this thesis, as they are indistinguishable from those for E46K:Y39W.

Three methods were used to confirm that the expression product was in fact α-synuclein, and not some *E. coli* protein: fluorimetry, *CD*, and ESI-MS.

Fluorescence spectra were recorded on either a Photon Technology International Master Series spectrofluorimeter (PTI, New Jersey, USA), or a Jasco FP-6500 spectrofluorimeter (Jasco, UK). Quartz cells of 4 mm path length were used, and an excitation wavelength of 295 nm (2 nm bandwidth). Emission spectra were recorded from 300 to 450 nm (2 nm bandwidth), and 4 scans were averaged per spectrum. The corresponding appropriate backgrounds were subtracted from the final spectra, *i.e.* for demonstrating α-synuclein production, 10 mM sodium phosphate buffer, pH 7.4 was used.

Fluorimetry is a very sensitive technique in the right circumstances. Both α-synuclein constructs used here have an inserted tryptophan residue (Y39W), which gives a characteristic fluorescence. When tryptophan is in aqueous solution, and excited with light at 295 nm, the fluorescence it gives off will have a maximum wavelength (λ_{max}) of around 350 nm. Figure 2.5 shows the emission spectra for both expressed proteins, excited at 295 nm. The spectra show strong fluorescence, with peaks around 350 nm. Recombinant α-synuclein exists as a disordered monomer, exposing the inserted tryptophan residue to its solvent. This, therefore, also suggests that the proteins expressed were Y39W α-synuclein, and the Trp residues were exposed to the solution, as expected for unfolded protein. The presence of the fluorescence peak for Trp shows that Trp is present and therefore if the protein is α-synuclein it is the correct construct, however it does not prove presence of α-synuclein.

Circular dichroism spectroscopy *(CD)* was carried out using a Jasco J-815 Spectropolarimeter (Jasco, UK) using a 1 mm quartz cuvette (Optiglass Ltd., Hainault). Measurements were typically carried out between 190 and 260 nm at room temperature. The scanning speed was 100 nm/min, bandwidth 2 nm, response time 1 second, and a resolution 1 nm. Typically, 8 accumulations were averaged per spectrum, and appropriate backgrounds

subtracted from the final spectra. Figure 2.5 shows the *CD* spectra generated for both recombinant α-synuclein constructs: Y39W, and the E46K:Y39W double mutant. Both spectra conform to the characteristic spectrum for a random coil protein, with the strong negative band around 200 nm. This is evidence that the proteins produced are both constructs of monomeric α-synuclein, without structure in aqueous solution, as expected.

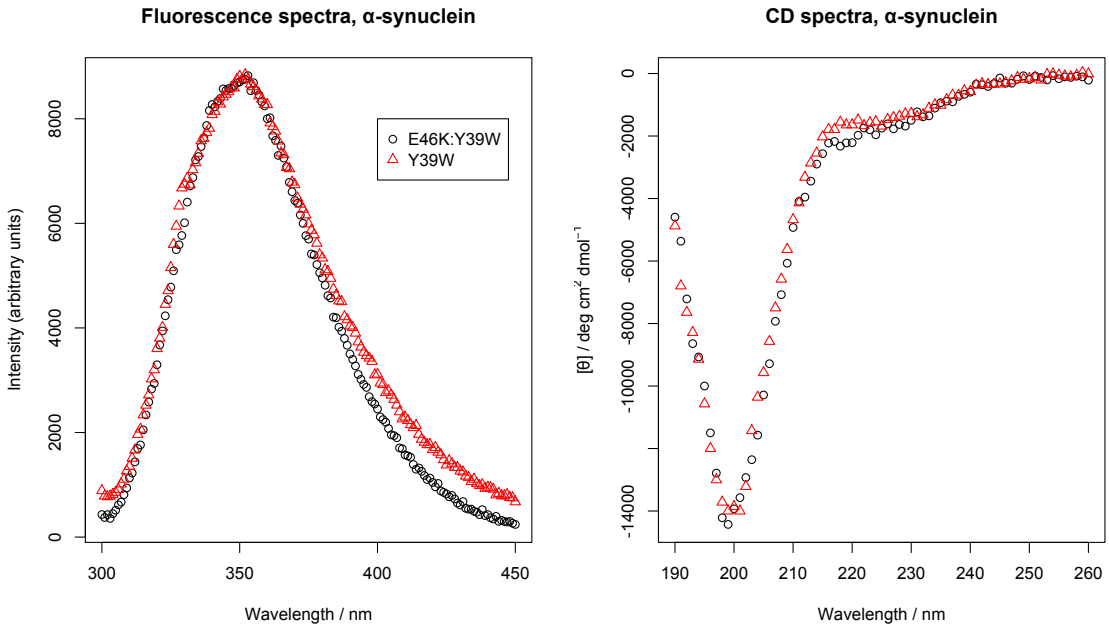

Figure 2.5: *(left)* Fluorescence emission spectra for α-synuclein constructs excited at 295 nm. Black circles are data points for the E46:Y39W construct, red triangles are data points for the Y39W mutant. *(right) CD* spectra for the same samples. Presence of Trp fluorescence indicates that the Y39W mutation has been successful.

The molecular weight of purified α-synuclein was confirmed by electrospray ionisation mass spectrometry (ESI-MS). Samples were sprayed in 10 % methanol in positive ion mode. Analysis was carried out by the Warwick/Waters BioMedical Mass Spectrometry Facility at the School of Life Sciences, University of Warwick. ESI-MS allows the most certain quality check of the expression product, compared to the pseudo-quantitative results from SDS-PAGE, for example. Examples of mass spectra from a typical α-synuclein expression are shown in Figure 2.6, demonstrating that the purification process left one major protein

at the expected molecular weights of 14458.6 and 14459.1 Da.

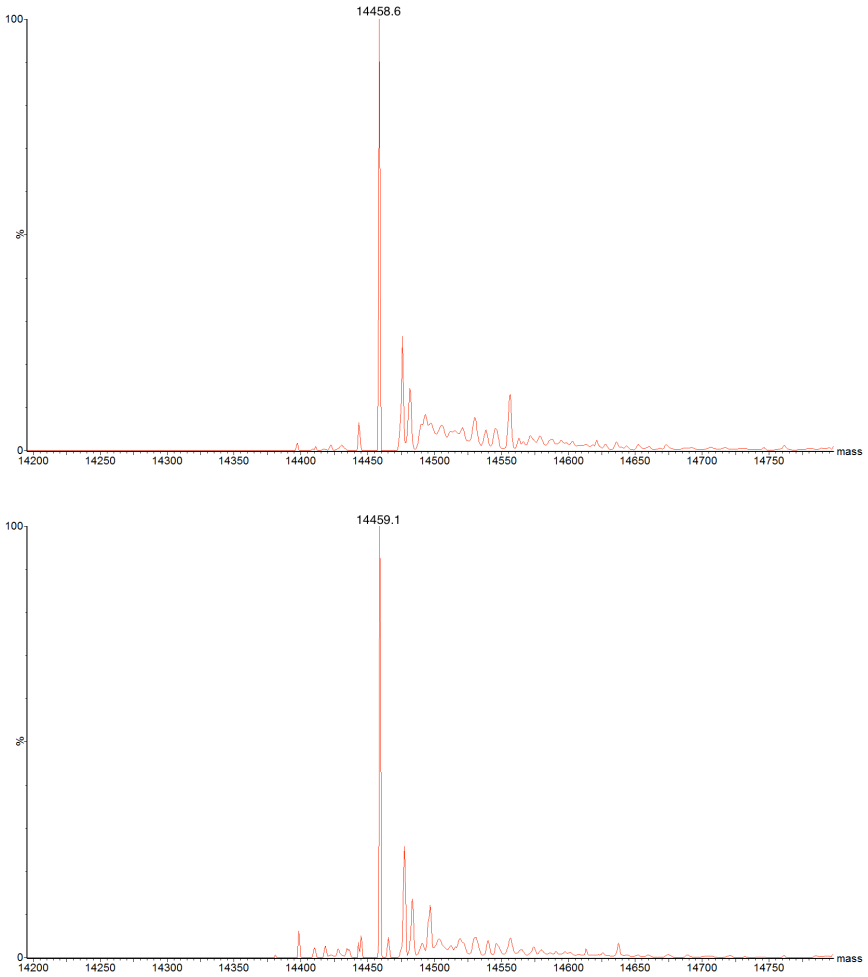

Figure 2.6: Deconvoluted mass spectra gathered for one expression each of Y39W α-synuclein *(top)*, and E46K:Y39W α-synuclein *(bottom)*. Regions are focused around primary product, at approximately 14,400 Da.

The expression of α-synuclein was accepted as true from the cumulative evidence of DNA sequencing (carried out by Anthony Wambua), picking colonies of *E. coli* selected by antibiotic resistance, over-expression bands observed on gels, protein folding and fluorescence as expected, and mass spectra as expected. The Pinheiro laboratory had produced α-synuclein in preliminary work before this project, and confirmed the production of the protein by Western blotting. This blotting was reproduced during the undergraduate research project undertaken by Rachel Smith in the Pinheiro laboratory. Under my supervision and instruction, Figure 2.7 was produced. The same expression and purification methods described above were used to produce the protein.

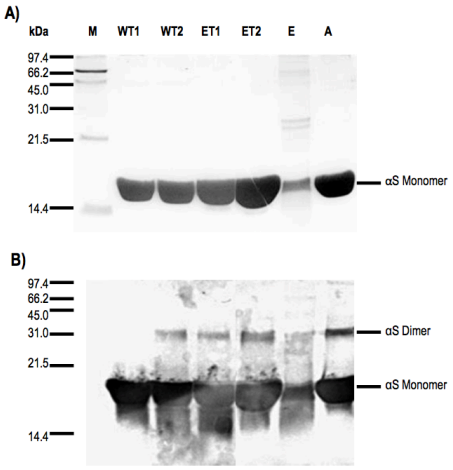

Figure 2.7: *(Top)* SDS-PAGE and *(bottom)* Western blot of α-synuclein constructs following purification by anion exchange and size exclusion chromatography. Lanes labelled M are protein markers, WT are Y39W, ET are E46K:Y39W, E are E46K, and A are A53T. Reproduced with permission of the author (Smith, 2013).

2.2.3 Monomeric protein-lipid binding experiments

Lipids provided as solids were dissolved in chloroform, or methanol if solubility in chloroform was low. Lipids were mixed to the required molar ratios, then dried thoroughly under N_2 or by rotary evaporation. The resulting films of lipid were desiccated overnight. They were resuspended in sodium phosphate buffer at 10 mM, pH 7.4. The resuspension volume was

such that the final concentration of lipid was 20 mM. This suspension was sonicated until clear – typically 30 minutes. This provided enough energy over a long enough time period to cause vesicles to convert from multi-lamellar to unilamellar structure.

CD measurements were made on protein-lipid samples, using the parameters noted above. The subtracted background spectrum for each measurement contained the same amount of lipid, but diluted with buffer, rather than protein solution. We were then able to plot *CD* as a function of concentration of lipid, in the wavelength range of relevance for identifying secondary structure: 190-260 nm.

Fluorescence measurements were made on protein-lipid samples, using the parameters discussed above. The subtracted background spectrum for each measurement were obtained using the same amount of lipid, but diluted with buffer, rather than protein solution. We then plotted the shift in maximum emitted fluorescence ($\lambda_{\max}$) as a function of lipid concentration. A value of $\lambda_{\max}$ around 350 nm indicated that the protein was unfolded. A value around 340 nm indicated that the tryptophan residue was in a hydrophobic environment.

LD spectra were gathered using a Jasco J-815 spectropolarimeter (Jasco, Dunmow, UK) adapted for *LD* by fitting with a Couette flow *LD* cell (Dioptica Scientific Ltd., Rugby, UK). Flow was typically at a speed of 3000 rpm, with bandwidth of 2 nm. 8 accumulations were made for each measurement, with non-spinning spectra taken as baselines.

2.2.4 Linear dichroism method development

The conditions described in this section represent starting points for the developments in linear dichroism methods. These are typical experimental conditions, but are not optimised for any specific system, particularly lipid and protein systems. In Chapter 6, several conditions are described, leading to recommendations for more optimal methods.

Lipids supplied as solids were dissolved in chloroform or methanol, and then mixed as needed. Lipids supplied as solutions in chloroform were mixed at appropriate molar ratios, without further solvent addition. Diphenylhexatriene (DPH) was added to lipids for *LD* at 1 % w/w as an *LD* probe. The dissolved mixtures were dried in a rotary evaporator resulting in a film of lipid around the inside of a round-bottomed flask. This took at least 2 hours. They were resuspended in appropriate buffers, before being frozen at –20 °C.

LD was carried out in Jasco spectropolarimeters: J-1500, J-815, J-720 (Jasco, Dunmow, UK). These were adapted for *LD* by fitting with Couette flow cells (Dioptica Scientific Ltd, Rugby, UK) (Marrington *et al.*, 2004). A schematic of a Couette flow cell for *LD* is shown in Figure 1.18. The width of the sample chamber (between stationary rod and rotating capillary) was 250 μm. Spectra were initially measured between 190 and 260 nm, later between 180 and 500 nm. Rotation speed was 3000 rpm. Typically, spectra were the average of 8 accumulations. The lipid resuspension buffer in this case was 10 mM sodium phosphate, pH 7.4.

2.2.5 Vesicle leakage studies

Vesicle leakage experiments were carried out in a Bio-Logic MOS-450 spectrometer (Bio-Logic, Claix, France) fitted with a Couette flow cell as for *LD*. Fluorescence of calcein over time, with or without Couette flow at 3000 rpm, was recorded. The lipid resuspension buffer in this case was 0.1 mM EDTA, 10 mM TES, 50 mM calcein.

The dimensions of a compressed vesicle under Couette flow were approximated by a capsule shape – a cylinder with hemispherical ends – and the method of McLachlan *et al.* applied in MATLAB to calculate orientation of the vesicle (MATLAB, 2013; McLachlan *et al.*, 2013).

2.2.6 Preparation of oligomeric α-synuclein

While interactions of monomeric amyloid proteins with membranes are interesting and may answer questions about their role in diseases, it is oligomeric forms of these proteins that are presently believed to be the most cytotoxic. In the present work, oligomeric α-synuclein was studied by *CD* and *LD*, while interacting with lipid membranes.

To prepare oligomeric α-synuclein, freeze-dried protein was resuspended in PBS containing 0.01 % w/w sodium azide, to a final concentration of approximately 12 mg/mL. This preparation was incubated at 37 °C at 900 rpm for 3 hours using a Thermomixer (Eppendorf, Germany). The solution was subjected to ultracentrifugation at 100,000 *g* for 10 minutes, and the supernatant purified by FPLC. Using a Superdex 200 FPLC column, two distinct peaks are observed: one for oligomer, and a later, larger peak for monomeric protein. A chromatogram of this stage is shown in Figure 2.8. This protein may be collected and allowed to oligomerise again. The fractions collected for the oligomer peak were concentrated using Amicon centrifugal filters (Sigma-Aldrich, UK), 3 kDa MWCO. The same filters were used to exchange the buffer from PBS to 10 mM sodium phosphate (pH 7.4) for spectroscopy.

This protocol has been adapted and optimised in the Pinheiro laboratory by Timothy Kaufmann and Rachel Smith, from various sources (Danzer *et al.*, 2007; van Rooijen *et al.*, 2008; van Rooijen & van Leijenhorst-Groener, 2009; Fauvet *et al.*, 2012; Stöckl *et al.*, 2012a). The chromatogram shown in Figure 2.8 is highly reproducible, and the presence of α-synuclein oligomer was confirmed by immunoblot using the A11 confirmation detection antibody (Lesné *et al.*, 2006; Smith, 2013). Figure 2.10 was prepared by Rachel Smith under my supervision, demonstrating the presence of A11-reactive oligomers prepared by the methods described above. Different α-synuclein constructs were used, and A53T, E46K:Y39W, and Y39W oligomers all show A11-reactivity. Oligomers prepared using metal ions were not detectable here, just as α-synuclein monomer or bovine serum albumin

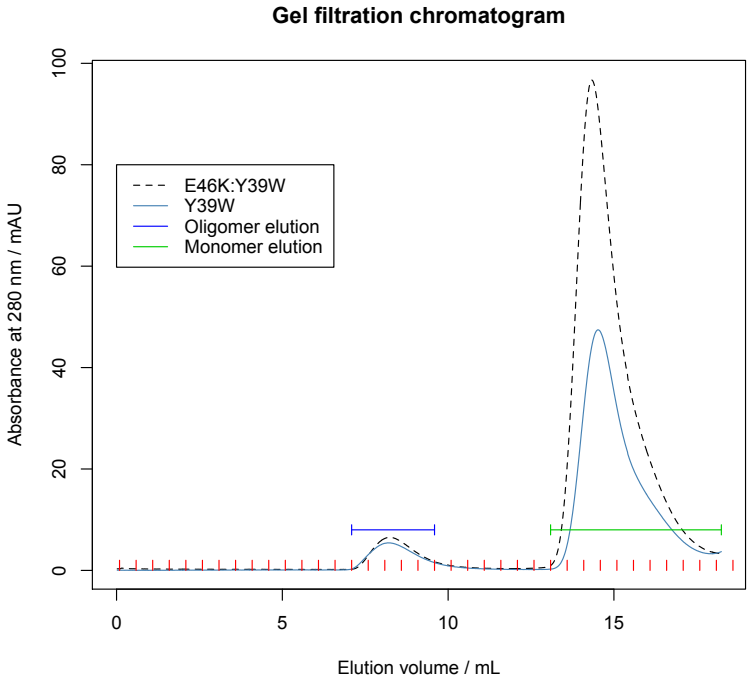

Figure 2.8: Gel filtration size-exclusion chromatogram of α-synuclein post after oligomerisation was carried out. The large peaks are residual monomeric protein that may be collected for later use. The small peaks are oligomeric protein desired here.

were not detected.

In Chapter 1, the annular nature of amyloid oligomers was discussed, as this morphology may be key to the ability of the oligomer to cause cell death. It was confirmed by Rachel Smith and Timothy Kaufmann that the oligomers produced by this method are annular (ring-shaped), and therefore of the same type as discussed in the literature. A scanning electron micrograph taken of one such preparation is shown in Figure 2.9. The outer diameter of the ring in this case was around 8 nm, and the inner was around 1 nm, though the outer was found to be as big as 14 nm and the inner as big as 3 nm (Smith, 2013).

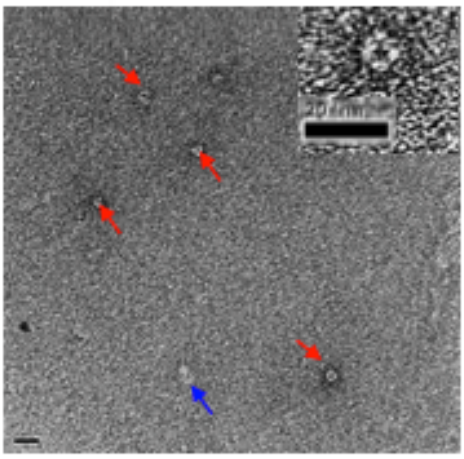

Figure 2.9: Electron micrograph showing oligomeric E46K:Y39W. Inset shows single oligomer, with inner diameter 1 nm, and outer diameter around 8 nm. Reproduced with permission of the author (Smith, 2013).

Dot blotting was carried out by drying droplets of protein solutions on nitrocellulose membrane ($5 \times 3\,\mu$L), then incubating in blocking solution. This stage was followed by incubating with the A11 antibody, then an anti-A11 secondary antibody. The membrane was stained so the image could be captured.

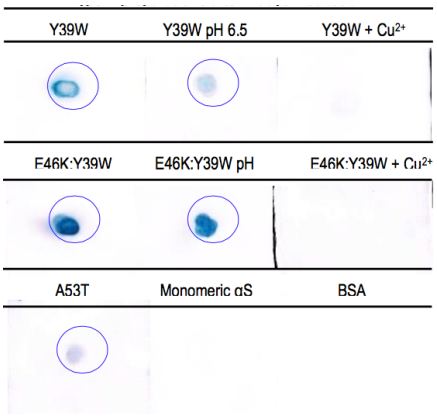

Figure 2.10: Dot blot of α-synuclein size exclusion chromatography fractions gathered after oligomer preparation. Blue colour indicates presence of A11-reactive species; the samples showing positive for presence of oligomer were Y39W, Y39W incubated at reduced pH, E46K:Y39W, E46K:Y39W at reduced pH, and A53T. In this case, metal ion presence during incubation, monomeric α-synuclein, and BSA (control protein) all showed negative for oligomer presence. Reproduced with permission of the author (Smith, 2013).

Chapter 3

The behaviour of lipid vesicles in Couette flow

3.1 Introduction

Lipid vesicles have been used extensively in this work, as they are a convenient model for the cell membrane. Much is still unknown, however, about the behaviour of vesicles in different conditions, particularly in a shear flow system such as that of a Couette flow linear dichroism experiment. Many studies concentrate on the behaviour of lipid molecules, but often neglect the effect of flow on the vesicle as a whole, whereas other studies look at vesicles in flow but do not connect their modelling to experimental work (Mader *et al.*, 2006; Bagchi & Kalluri, 2009; Biben *et al.*, 2011). In order to study the alignment of lipid-interacting proteins using *LD*, the lipid systems used must be understood and characterised. It must be known whether vesicles withstand Couette flow as the orientation technique, and whether they align successfully. It must also be known whether different lipids behave in the same way under flow, or whether lipid choice plays a role in the success of these experiments. Theoretical work is reported in this chapter, describing the relationship between vesicle shape, deformation of this shape, and orientation in flow. Experimental work is also reported, showing how various types of lipid vesicle respond to Couette flow, and how they leak their contents.

A small molecule compound was used in the experiments described in this chapter: calcein. Calcein, shown in Figure 3.1, is a very highly fluorescent, but also strongly self-quenching, compound that was employed in measuring vesicle leakage, as in other studies of lipid vesicle leakage when influenced by amyloid proteins (Sanghera & Pinheiro, 2002).

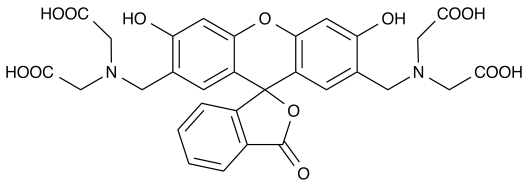

Figure 3.1: The structure of calcein, demonstrating several light-absorbing ring structures.

The data from this chapter contribute to the wider understanding that choices such as lipid selection, made during experimental design, must be validated for their appropriateness for downstream techniques.

3.2 Methods

3.2.1 Measuring calcein fluorescence

Calcein was sequentially diluted from 50 mM by factors of two, and the fluorescence measured at each concentration using a Jasco FP-6500 fluorimeter. Four measurements were averaged for each spectrum, and the process was repeated in triplicate. The spectra were plotted together, and the position of maximum fluorescence emission also recorded. As calcein is at 50 mM within the vesicles, fluorescence from within the vesicles may be assumed to be zero; that is to say, any detected fluorescence may be assumed to be from dye that has escaped the vesicles.

3.2.2 Measuring vesicle leakage

Lipids were mixed to the required proportions, and prepared as described in Section 2.2.4, 40 mg at a time. They were then resuspended in 2 mL of buffer containing 0.1 mM EDTA, 10 mM TES, and 50 mM calcein. Once thoroughly resuspended, the lipid was separated into aliquots, and frozen at −20 °C.

Vesicles formed from various mixtures of lipids were tested for their ability to withstand Couette flow for extended periods of time, and for their ability to orient in such a system. It was intended that optimal lipid compositions could be determined, and then recommended for more detailed experiments. The lipids studied are given in Table 3.1. Vesicles used were (molar fraction): 100 % brain total lipid extract (BTLE); 100 % soybean PC; 100 % DMPC, DPPC, or POPC; 75 % DMPC or POPC, 15 % cholesterol, 10 % POPS.

Table 3.1: Lipids used in calcein-leakage and LD studies. The shorthand 16:0, 18:1, for example, denotes a lipid containing one acyl chain 18 carbon atoms long with a single double bond, and one 16 carbon atoms long with no double bonds.

Lipid	Acyl chain length and saturation	Head group nature
DMPC	14:2, 14:2	Zwitterionic
DPPC	16:0, 16:0	Zwitterionic
POPC	16:0, 18:1	Zwitterionic
POPS	16:0, 18:1	Anionic
Cholesterol	—	Neutral
POPC/POPS/cholesterol	16:0, 18:1	Anionic, overall
DMPC/POPS/cholesterol	14:2, 14:2/16:0, 18:1	Anionic, overall
Soybean PC species	18:2, 18:2 (64 %), various	Zwitterionic
BTLE	Various	Various, mixed charges and groups.

Lipids were thawed, then frozen and thawed twice, using dry ice and ethanol to achieve a flash-freeze at around –78 °C. Katherine Lloyd optimised this stage of the protocol within the Rodger group (Lloyd, 2012). Suspensions of lipid were then extruded eleven times using an Avanti mini-extruder, through a membrane with pore size 100 nm. A Nano-series

Zetasizer (Malvern, UK) was used to measure dynamic light scattering (DLS) of the lipid preparation to determine vesicle size. This was typically found to be a narrow distribution around 100 nm. In some cases, vesicles were resuspended and then sonicated for 3 minutes, rather than being extruded, in order to compare the effects of the different treatments on leakage.

Columns of sepharose 4B were made using Pasteur pipettes by cutting excess length from the tip and blocking with a small amount of cotton wool, before adding around 4 cm of resin and allowing to settle. This was washed with sample buffer containing 0.1 mM EDTA, 10 mM TES, and 100 mM NaCl. 50 μL of calcein-loaded, post-extrusion lipids were purified through the column at a time by carefully depositing the vesicles onto the resin bed and adding a drop of buffer. Finally, one column volume of buffer was added and the vesicle-containing fraction collected manually. This was the second coloured band, after the free dye had run though the resin. The resulting volume of size-separated vesicle suspension was approximately 100 μL.

A Bio-Logic MOS-450 spectrometer (Bio-Logic, Claix, France), was used to measure leakage of the vesicle suspensions. Calcein fluoresces above 500 nm when excited by light at 460 nm, so an in-line photodetector was fitted with a Hoya Y-50 long-pass wavelength filter (Hoya, Santa Clara, CA, USA) preventing light below 480 nm reaching the detector. A second photodetector, at 90°, had no filter, and therefore detected both fluorescence, and scattered incident light.

The spectrometer was fitted with an *LD* cell (Dioptica Scientific, UK), able to generate Couette flow for samples between 50 and 100 μL. Using this apparatus, we were able to observe the change in fluorescence over time with sample spinning at 3000 rpm, or without spinning, or with intermittent spinning. A typical experiment measured fluorescence and scattering over 30 minutes.

After the final time point, Triton X-100 was added to a final concentration of 0.1 % w/v.

The concentration was such that 1 μL could be added, minimising change in volume. This detergent completely ruptured remaining vesicles, releasing all the calcein present, giving a maximum possible fluorescence signal. This 100 % reference was used to scale measurements over the time course, and show how leakage changed over time. This step provided a correction for the number of vesicles in the suspension (and therefore the concentration of dye in the sample), as this can not be controlled at the size exclusion stage. It was particularly noticeable that for pure DMPC a lower amount of dye (and therefore of vesicles) had been eluted into the sample, so correcting for this effect was crucial.

3.2.3 Changes in geometry

The shape of a flow-distorted spherical vesicle (radius R) was approximated by adding hemispheres to either end of a standard cylinder with radius r, and length h. The hemispheres also have radius r. The domed-cylinder, or capsule, is shown in Figure 3.2.

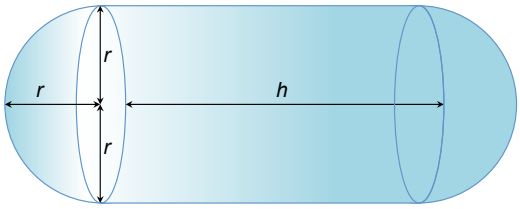

Figure 3.2: Schematic of capsule, or domed-cylinder, with cylinder length h, radius r, and total length $h + 2r$.

This capsule has volume

$$V_c = \frac{4}{3}\pi r^3 + \pi r^2 h, \tag{3.1}$$

and surface area

$$SA_c = 4\pi r^2 + 2\pi r h. \tag{3.2}$$

Surface area (SA) of the compressed vesicle capsule is understood to remain equal to SA of the original sphere (de Haas *et al.*, 1997), so

$$4\pi R^2 = 4\pi r^2 + 2\pi r h, \tag{3.3}$$

which is solved for either h or r:

$$h = \frac{2(R^2 - r^2)}{r}, \tag{3.4}$$

and, by the quadratic formula,

$$r = \frac{-h \pm \sqrt{h^2 - 16R^2}}{4}. \tag{3.5}$$

Two solutions for r were generated for each value of h, but only one was positive, and therefore relevant to this work. By estimating a range of values for the length and radius parameters, we obtained a value for the other, and then calculated how these values altered the volume of the vesicle. This shows us how deformed the vesicle became under flow, and how much of its contents were squeezed out.

3.2.4 Orientation in flow

The *LD* of the angle of an oriented vesicle relative to the direction of orientation is given in Equation 3.6. This equation is essential to quantifying the relationship between vesicle length, radius, and orientation.

$$LD = A_{\text{iso}} \frac{3S}{4}(1 - 3\cos^2\beta), \tag{3.6}$$

Understanding the behaviour of theoretical vesicles in flow required computation of S from Equation 3.6. The method of McLachlan *et al.*, was implemented in MATLAB, in order to compute S, for a range of lengths and radii of the capsule (McLachlan *et al.*, 2013; MATLAB, 2013).

3.3 Results and Discussion

3.3.1 Concentration-dependent fluorescence of calcein

As a self-quenching fluorophore, calcein emits fluorescence well at low concentrations, and emits with very low intensity at high concentrations. Calcein has previously been reported to emit its strongest fluorescence around 520 nm, with this figure being universally accepted (Allen & Cleland, 1980). However, in this work it was noted that the maximum wavelength of emitted fluorescence varies in a concentration-dependent manner, as well as the intensity of emitted light varying as expected. Figure 3.3 shows emission spectra for calcein excited at 460 nm, where the black line represents 50 mM calcein, and dark blue represents 0.19 mM. As concentration decreased, intensity increased as expected. Dilutions were made from 50 mM until intensity began to decrease – 0.19 mM – the point where the dilution effect overtook the effect of elimination of quenching. The Figure also demonstrates a shift effect: as the concentration of calcein was reduced, the emission spectrum undergoes a blue shift, revealing that maximum emission varies at least between the 517 nm and 566 nm observed here.

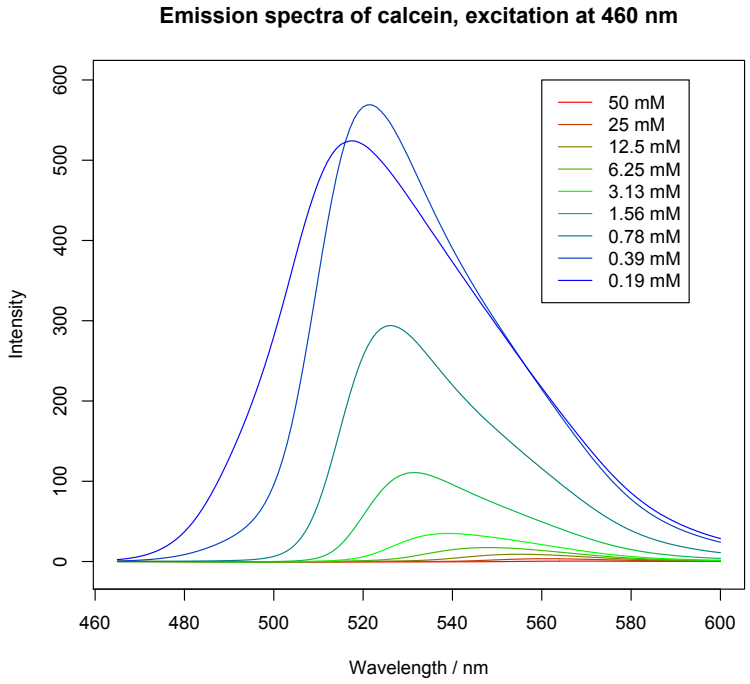

Figure 3.3: Emission spectra for calcein excited at 460 nm. Red spectrum represents emission for the highest concentration, 50 mM, green represents the median concentration, 3.13 mM, and blue represents the lowest concentration tested, 0.19 mM.

Figure 3.4 shows the wavelength of maximum emission ($\lambda_{\max}$) plotted against calcein concentration, and fitted by:

$$\lambda_{\max} = 9.336\ln[\text{calcein}] + 530.11, \tag{3.7}$$

which provided a means to estimate calcein concentration from fluorescence data.

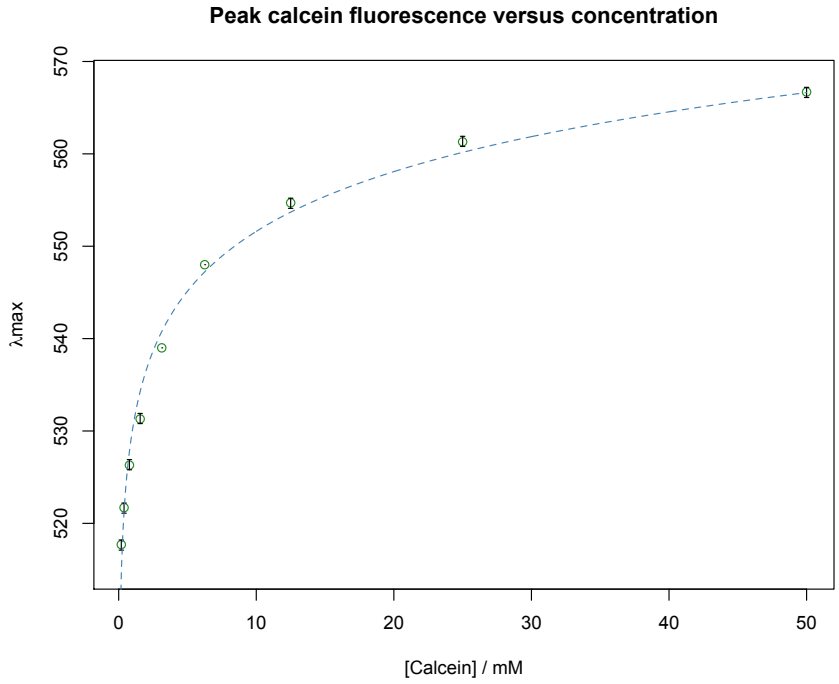

Figure 3.4: Concentration of calcein versus λ_{max} of emitted fluorescence. Green circles are measured values with error bars indicating one standard deviation from the mean after 3 replicates (in some cases 0), dashed line is the curve fitted to the data: $\lambda_{max} = 9.336\ln[\text{calcein}] + 530.11$. The R^2 value for this fit is 0.99021.

A key aspect of the success in gathering these data is the sensitivity of the instrument used, requiring the pre-selection of excitation and emission bandwidths. In this work, fluorescence intensity has been used to measure calcein leakage. However, these data open up potentially better options and opportunities for different experimental design. These data are a proof of principle that using λ_{max} as a dependent variable would be effective, and enable more precise concentration measurements by interpolation.

3.3.2 Calcein leakage measurements to measure vesicle stability

the vesicle preparation method was tested by DLS for reproducibility of vesicle size. DLS data gathered from the lipid samples is shown in Figure 3.5. The Figure demonstrates

that most vesicle types are measured to be around 100 nm diameter after extrusion, though some are bigger before extrusion. In one case a sample was measured after Couette flow (DMPC), and was found to measure around 615 nm, demonstrating the damaging effect of Couette flow on DMPC vesicles.

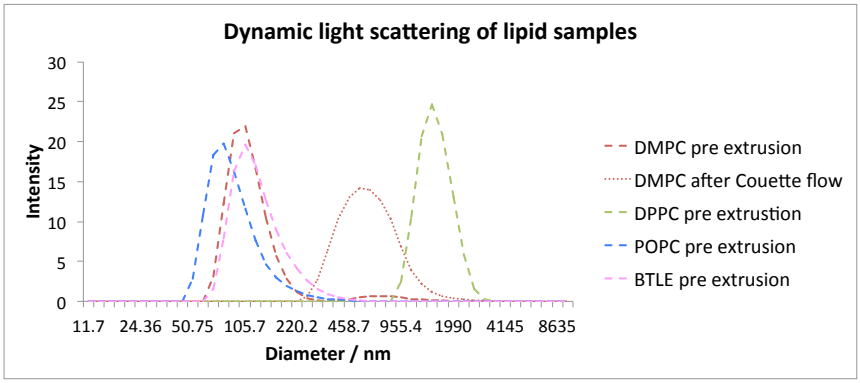

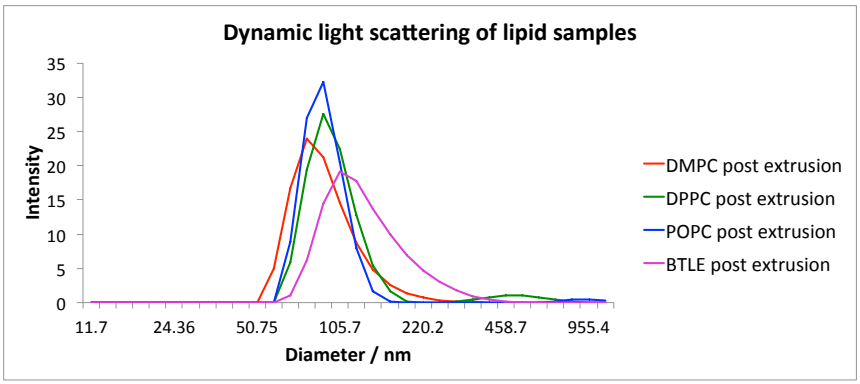

Figure 3.5: DLS gathered for *(top)* vesicles pre-extrusion post-Couette flow, and *(bottom)* vesicles post-extrusion. In DLS, larger particles scatter more light, meaning the higher peaks may represent fewer particles.

Vesicles were prepared containing 50 mM calcein. As demonstrated by the data in Section 3.3.1, calcein at this concentration has negligible fluorescence. After extrusion to 100 nm

diameter, vesicles were purified by size-exclusion chromatography to exclude free dye. In some cases, the extrusion step was swapped for sonication – another lipid preparation method used by some research groups – in order to compare leakage from vesicles prepared by both methods. Vesicles were then loaded into a Couette cell, and fluorescence measured for 30 minutes, with or without rotation at 3000 rpm. Detergent was then added, and the vesicles disrupted. Once all the calcein had been released from the vesicles, a value for 100 % fluorescence was obtained, and used to scale the leakage data. Figure 3.6 shows these collated traces.

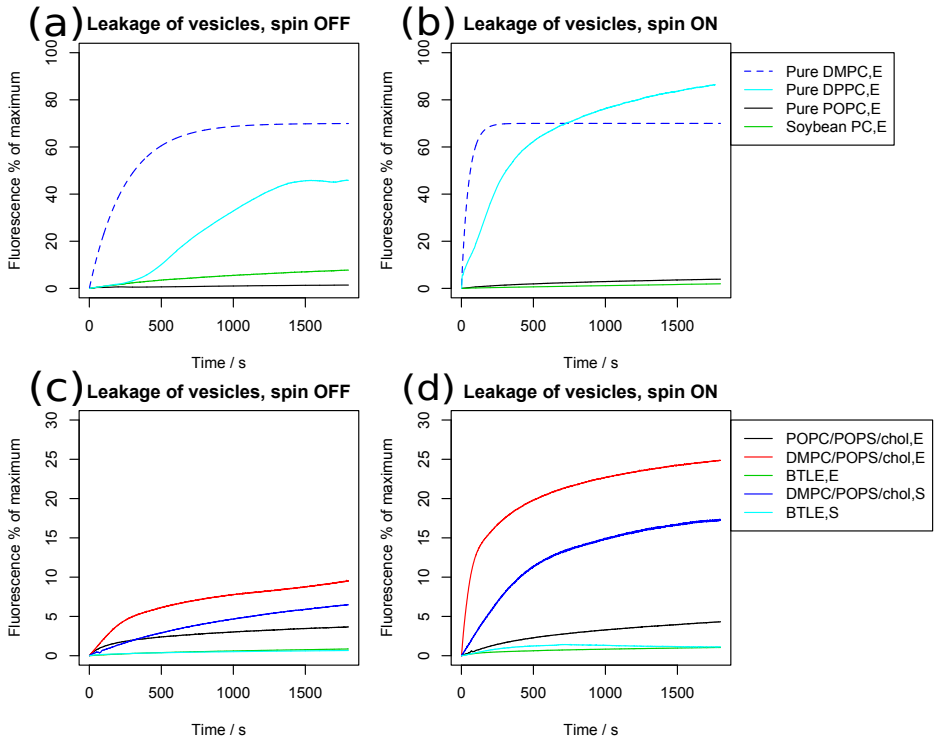

Figure 3.6: Fluorescence of calcein leaked from vesicles: *(a & c)* stationary, and *(b & d)* in Couette flow at 3000 rpm. *(a & b)* show traces for pure DMPC, DPPC, POPC and soybean PC. *(c & d)* show traces for POPC/POPS/ cholesterol, DMPC/POPS/ cholesterol, BTLE. Label "E" indicates extruded lipids, "S" indicates sonicated. Fluorescence was recorded for 1800 seconds, then detergent added to lyse all vesicles, and release 100 % of encapsulated calcein. The resulting fluorescence value was considered 100 %, and all other values described as a percentage of this value, thereby correcting for differences in concentration. Traces for pure DMPC vesicles are shown as dashed lines, indicting values that have been fitted to a curve, since measured values had poor signal:noise.

Signal:noise was so low for pure DMPC data, that these traces were fitted to standard curves, as shown in Figure 3.7.

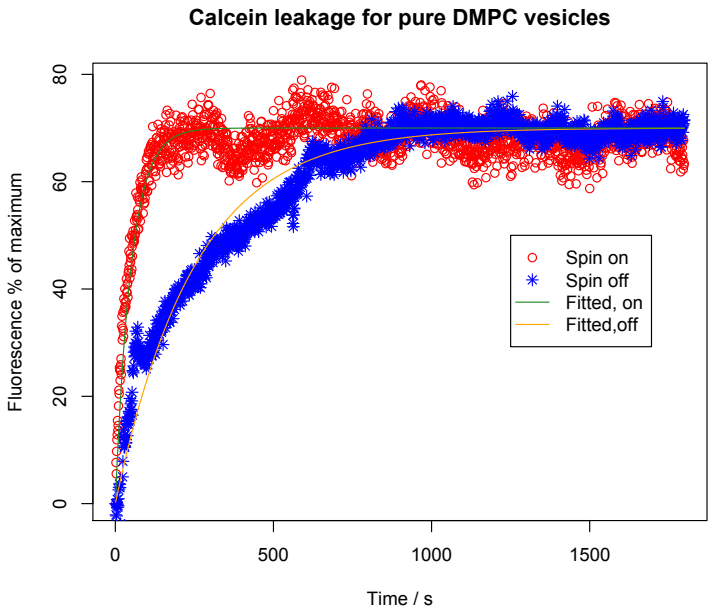

Figure 3.7: Data gathered for calcein leakage from our DMPC vesicles. Blue stars are collected data without Couette flow, red circles for leakage with couette flow. The green line is the curve fluorescence $= 70e^{(-0.02\text{time})}$ fitted to the Couette flow data, the orange line is the curve fluorescence $= 70e^{(-0.004\text{time})}$ fitted to the data without Couette flow.

Taken together, Figures 3.6 and 3.7 demonstrated that certain vesicles cope badly with conditions of Couette flow at 3000 rpm, and some vesicles were extremely leaky even without flow applied. Pure DMPC leaked most of its contents by 500 seconds, whether or not flow was applied. Leakage was exacerbated by Couette flow, however, stabilising at around 100 seconds. DPPC performed similarly to DMPC in flow, though was slightly more resilient over time when flow was not applied. As pure lipids, therefore, these vesicle preparations might be considered too weak to endure an *LD* experiment.

Pure POPC, on the other hand, or the mixed soybean PC, both endured the leakage assay well, with around 5 % leakage after 30 minutes. When produced from other heterogeneous mixtures (POPC or DMPC with POPS, or BTLE), the vesicles also survived better than for pure DMPC or DPPC. The shorter acyl chains of DMPC and DPPC did seem to reduce vesicle stability when present, compared to POPC, but not so dramatically as when the sole vesicle component. Soybean PC and BTLE were both extremely stable over the whole course of the experiment.

Interpretation of these results required further context; it was necessary to understand more deeply the relationship between calcein leakage and vesicle orientation in flow. It may be necessary to study the possibility that the calcein solution is not stable within the vesicle. Should calcein leak without its solvent (aqueous buffer), or should the buffer leak while calcein remains in the vesicles, the internal and external concentrations of calcein would be altered, and our assumptions affected. This could be studied by fluorescence detected linear dichroism, for example, monitoring whether the calcein had partitioned into the lipid membrane.

As noted in Section 3.3.1, if $\lambda_{\max}$ can be measured, following the addition of detergent to cause 100 % dye release, it would be possible to calculate calcein concentration using Equation 3.7. From a typical POPC vesicle sample, a free calcein concentration of 0.403 mM was obtained. Here, this result implies that vesicle contents accounted for

around 1 % of the sample volume (since the vesicles initially contain 50 mM calcein). This result demonstrates that using the λ_{max} method is a useful way to assess the quality of vesicle preparation techniques.

3.3.3 Vesicle Geometry

It was possible to model the effect of flow on the orientation and geometry of vesicles. It was known from previous data that feasible values for the orientation parameter S are around 0.03, *i.e.* a value of S of 0.03 would be suitable orientation for the corresponding LD experiment to generate good signal (Rodger *et al.*, 2002; Nordén *et al.*, 2010). This does not imply that $S = 0.03$ is a prerequisite to generating LD data, but gives the value around which one would expect a particle generating LD signal to have achieved under flow. Previous work in the Rodger group had also generated an analytical method for calculating S for rigid particles, based on a velocity of flow, and on the length and diameter of particles in that flow.

A set of parameter values for the length and radius of a capsule with the same surface area as a sphere with diameter 100 nm was derived. A sample of these values, and the resulting value of S, calculated by the McLachlan *et al.* method, is shown in Table 3.2 (McLachlan *et al.*, 2013). The full data are plotted in Figure 3.8, with $S = 0.03$ indicated on the plots. It may be noted that there is an asymptote to both these plots and we are working in the vicinity of this asymptote. It may be the case that this model does not capture the full experimental range, and could need reformulation in light of later data.

Table 3.2: Calculated values for vesicle volume (V) and the orientation parameter, S, for different values of r and h.

r / nm	h / nm	V / nm^3	S
5.00	990.00	78278.0	0.5882
10.00	480.00	154985.2	0.3391
15.00	303.33	228550.9	0.1757
18.10	240.00	271929.0	0.1122
19.33	220 .00	288512.5	0.0939
20.71	200.00	306717.1	0.0771
26.00	140.31	371596.0	0.0396
26.03	140.00	371971.4	0.0394
27.13	130.00	384382.4	0.0351
28.00	122.57	393846.8	0.0322
28.31	120.00	397167.1	0.0313
30.00	106.67	414690.2	0.0270
37.20	60.00	499628.2	0.0178
38.00	55.58	481979.0	0.0173
40.00	45.00	494277.2	0.0165
40.99	40.00	476529.9	0.0162
45.00	21.11	516006.6	0.0159
45.25	20.00	516733.2	0.0159

When the length and radius of the vesicle is altered, the volume is altered, as any parameter combination has less volume than the original sphere. As shown in Table 3.2, when $S \approx 0.03, V \approx 397000\,\text{nm}^3$, *i.e.* around 75 % the volume of a spherical vesicle with radius 50 nm. Therefore, to achieve $S = 0.03$ a vesicle must lose 25 % of its contents as its shape is altered by Couette flow.

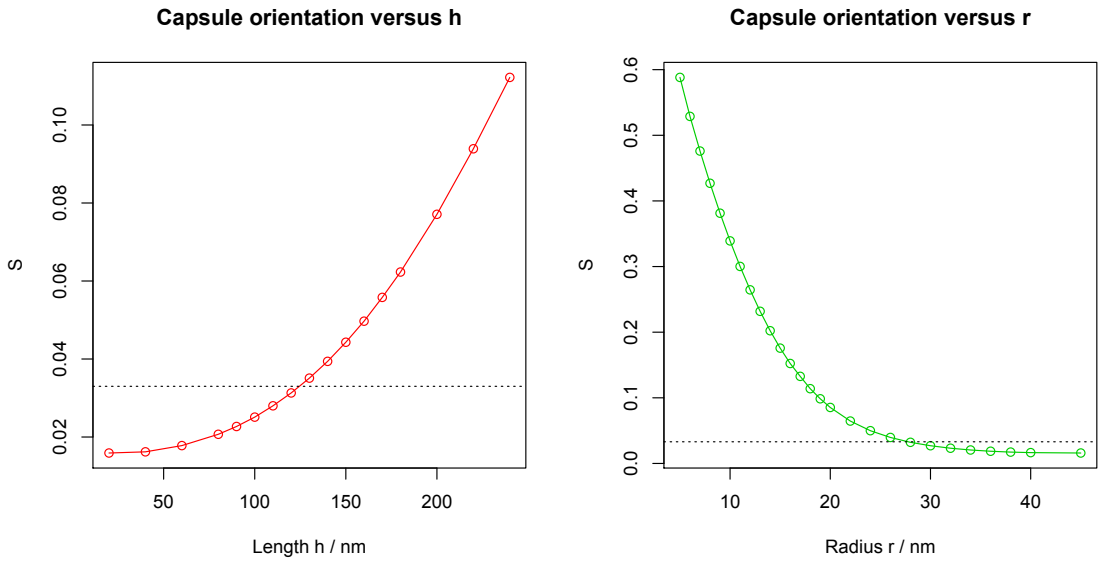

Figure 3.8: Plots demonstrating the effect of changes in h and r on S for compressed vesicles in flow. Surface area was fixed, and volume allowed to change. Dotted line is at $S = 0.03$, an experimental value for vesicle orientation (Nordén *et al.*, 1992; Rodger *et al.*, 2002; Nordén *et al.*, 2010).

3.4 Conclusions

Here, it has been shown that vesicles of different compositions behave very differently in Couette flow. This has serious implications for any *LD* experiment that might seek to use Couette flow and lipids. Couette flow is currently the best choice for orientation of lipids, so the impact of this flow on the lipid must be taken into account. Any investigator attempting *LD* with vesicles must consider these results, and at least compare their lipid selection to those used here. It has been shown that vesicles must undergo significant deformation to orient in Couette flow, but must also be stable enough to maintain their integrity at the same time.

A previously experimentally verified value for the orientation parameter S in a lipid *LD* experiment is 0.03. It was anticipated that if vesicles would give good *LD* signal, their

orientation S would be approximately 0.03. According to the data presented here, a vesicle is required to expel 25 % of its contents in order to conform to this degree of alignment. Some of the lipid systems examined in these experiments leak much more than 25 % of their contents; pure DMPC and DPPC, specifically. These lipids, therefore, are not able to merely align in the flow, but are deformed to a much greater degree, and risk being ruptured completely in a long experiment. The vesicles are extremely porous even without the effect of Couette flow, suggesting that as cell membrane models they are unsuitable anyway.

Some vesicle compositions examined here leak much less than 25 % of their calcein contents: BTLE and soybean PC, for example, lose around 5 % with or without Couette flow. This may imply they are unsuitable for *LD* as they do not deform enough to behave as capsules in flow. They may never orient well enough to give $S = 0.03$, however it would be necessary to establish the quality of any resultant *LD* of using these vesicles. As later work shows, the work in this chapter informs lipid choices for *LD* but is not definitive – successful *LD* may be gathered when using BTLE. More work may be needed to understand the full range of processes occurring.

Finally, two types of vesicle leaked calcein at a rate broadly comparable to the calculated 25 %: POPC/POPS/cholesterol, and DMPC/POPS/cholesterol. These mixtures have some degree of complexity compared to pure lipid preparations, enabling more experiments, and both appear fluid enough to compress under flow, but not likely to rupture completely in these conditions. These data suggest that these lipids are good candidates for *LD*.

Chapter 4

Fluorescence spectroscopy study of α-synuclein lipid binding

4.1 Introduction

Wild type α-synuclein contains four tyrosine residues at positions 4, 39, 94, and 125. Tyrosine is fluorescent, but not strongly so, especially once incorporated into protein. Additionally, the presence of multiple residues per molecule would make conclusions about lipid interaction extremely difficult to draw. This was resolved by introducing a single tryptophan residue in place of one of the tyrosines. Tryptophan is known to emit fluorescence around 352 nm when excited at 295 nm in aqueous solution. When in hydrophobic environments the emission wavelength shifts to lower wavelengths. Y4W and Y94W mutant forms of α-synuclein show this shift strongly, Y39W clearly but less so, and Y125W to a negligible extent (Pfefferkorn & Lee, 2010). The most relevant tryptophan substitution for this work was Y39W, since this puts the tryptophan residue closest to the disease-associated mutations at positions 30, 46, 50, 51, and 53 (Conway *et al.*, 1998; Warner & Schapira, 2003; Zhu *et al.*, 2003; Choi *et al.*, 2004; Zarranz *et al.*, 2004; Appel-Cresswell *et al.*, 2013; Fares *et al.*, 2014).

In this chapter, Y39W α-synuclein was mixed with lipid vesicles of various types, and the fluorescence of the tryptophan residue measured. A second protein construct containing

the E46K disease-associated mutation as well as Y39W was also used in these experiments, allowing for a comparison in lipid interaction at residue 39 for the Parkinson's Disease-linked case, and the non-disease case. The lipids used were selected for biological relevance and prevalence in neurones. They were: POPC, POPS, cholesterol, sphingomyelin (SM1), and the ganglioside GM1.

4.2 Materials and Methods

Table 4.1 shows the range of vesicle compositions used to study the ability of α-synuclein to bind lipid bilayers in the form of vesicles. These mixtures were chosen to observe the binding between α-synuclein and physiologically relevant, negatively charged, POPS, and then to determine the effect of cholesterol, and SM1 on these interactions. Several specific interactions have been proposed between gangliosides and α-synuclein (as well as other amyloid proteins), so GM1 was included in our lipid selection (Martinez *et al.*, 2007; Sanghera *et al.*, 2011). Vesicles were prepared by the sonication method as described in Section 2.2.3.

Table 4.1: Lipid mixtures used in monomer-lipid binding studies.

% POPC	% POPS	%Cholesterol	%Sphingomyelin	%GM1
100	0	0	0	0
90	10	0	0	0
75	25	0	0	0
50	50	0	0	0
75	10	15	0	0
65	10	15	10	0
60	10	15	10	5

Experimental samples were prepared as mixtures of protein and lipid at different molar ratios. In each sample, α-synuclein solution and lipid suspension were mixed in equal volumes, diluting both by a factor of two. After this dilution, protein was at $10\,\mu$M (approximately $0.1\,$mg/mL). Lipid concentrations were such that a range of molar ratios

from 1 mole protein : 1 mole lipid, up to 1 mole protein : 1000 moles lipid were made. The ratios were: 1:1, 1:5, 1:7.5, 1:10, 1:25, 1:50, 1:75, 1:100, 1:250, 1:500, 1:750, and 1:1000 moles. Fluorescence spectra were measured as described in Section 2.2.2, taking care to measure and subtract the appropriate backgrounds for each sample – *i.e.* lipid diluted to the same concentration as in the sample, but protein solution replaced by buffer only. These were measured in the same experimental session, reducing the chance of environmental differences affecting the result.

From each spectrum, the wavelength of maximum intensity of emitted light was obtained, and plotted as a function of lipid concentration. Default fitting algorithms within the data analysis packages Prism® and Sigmaplot® were used to fit one-site ligand-binding curves to the data and extract apparent dissociation constants (Prism, 2015; SigmaPlot, 2013). The method used in this fitting is shown in Appendix B.

4.3 Results and Discussion

4.3.1 Lipid-binding is marked by shift in fluorescence spectra

Tryptophan is hydrophobic and polar, and therefore is often an amino acid involved in interactions with hydrophobic environments, such as a lipid bilayer. Intrinsic tryptophan fluorescence experiments were designed to assess the strength of the interaction between α-synuclein and lipids, by monitoring the characteristic emission wavelength of this residue. The two constructs of α-synuclein were mixed with vesicles prepared from different mixtures of lipids, then fluorescence spectra measured.

POPC was chosen as the predominant, zwitterionic, lipid in our vesicle preparations, with POPS as the anionic component. We studied a range of ratios of these lipids from 100 % POPC to 50 % POPC. Neither of the protein constructs (Y39W and E46K:Y39W) would be expected to bind strongly to POPC, based on previous data (Davidson *et al.*, 1998;

Eliezer *et al.*, 2001; Bussell & Eliezer, 2003; Choi *et al.*, 2004). Indeed, with no POPS present we observe very little interaction. With anionic lipid present, it was expected that pronounced shifts in protein structure would be observed. Figure 4.1 demonstrates the changes observed in fluorescence spectra for Y39W, and Figure 4.2 shows equivalent data gathered for the E46K:Y39W protein.

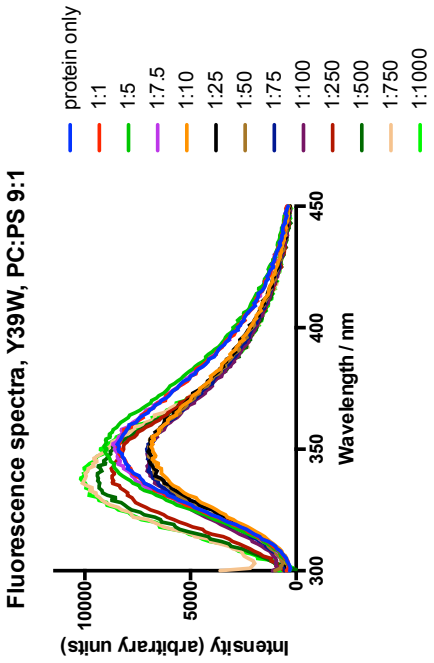

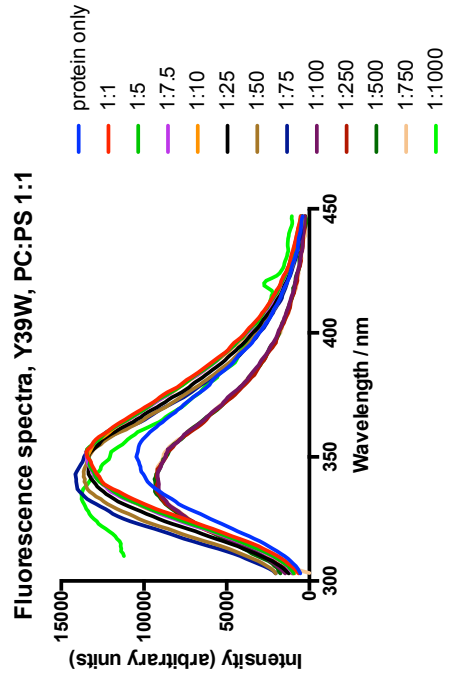

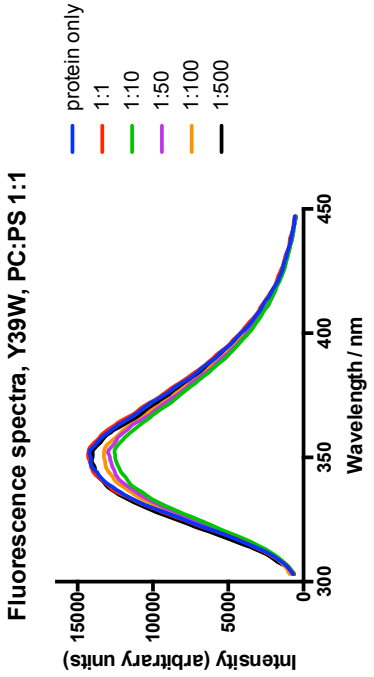

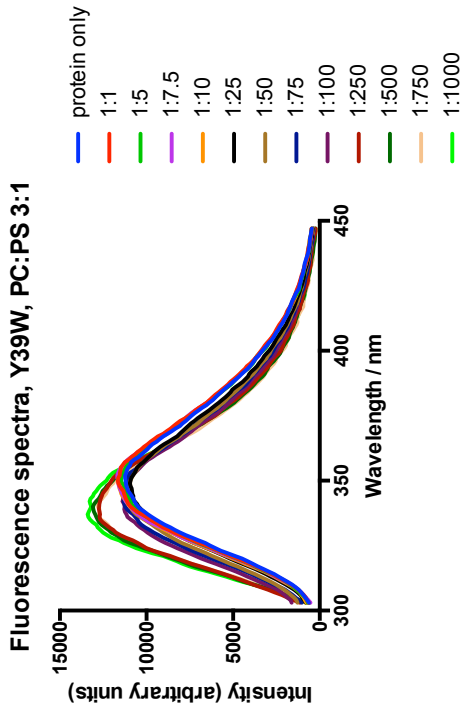

Figure 4.1: Fluorescence emission spectra gathered for Y39W alpha-synuclein mixed with POPC/POPS vesicles. Percentage POPS *(top left, top right, bottom left, bottom right)* is 0, 10, 25, 50. Fluorescence samples excited at 295 nm. Spectra have not been normalised for concentration.

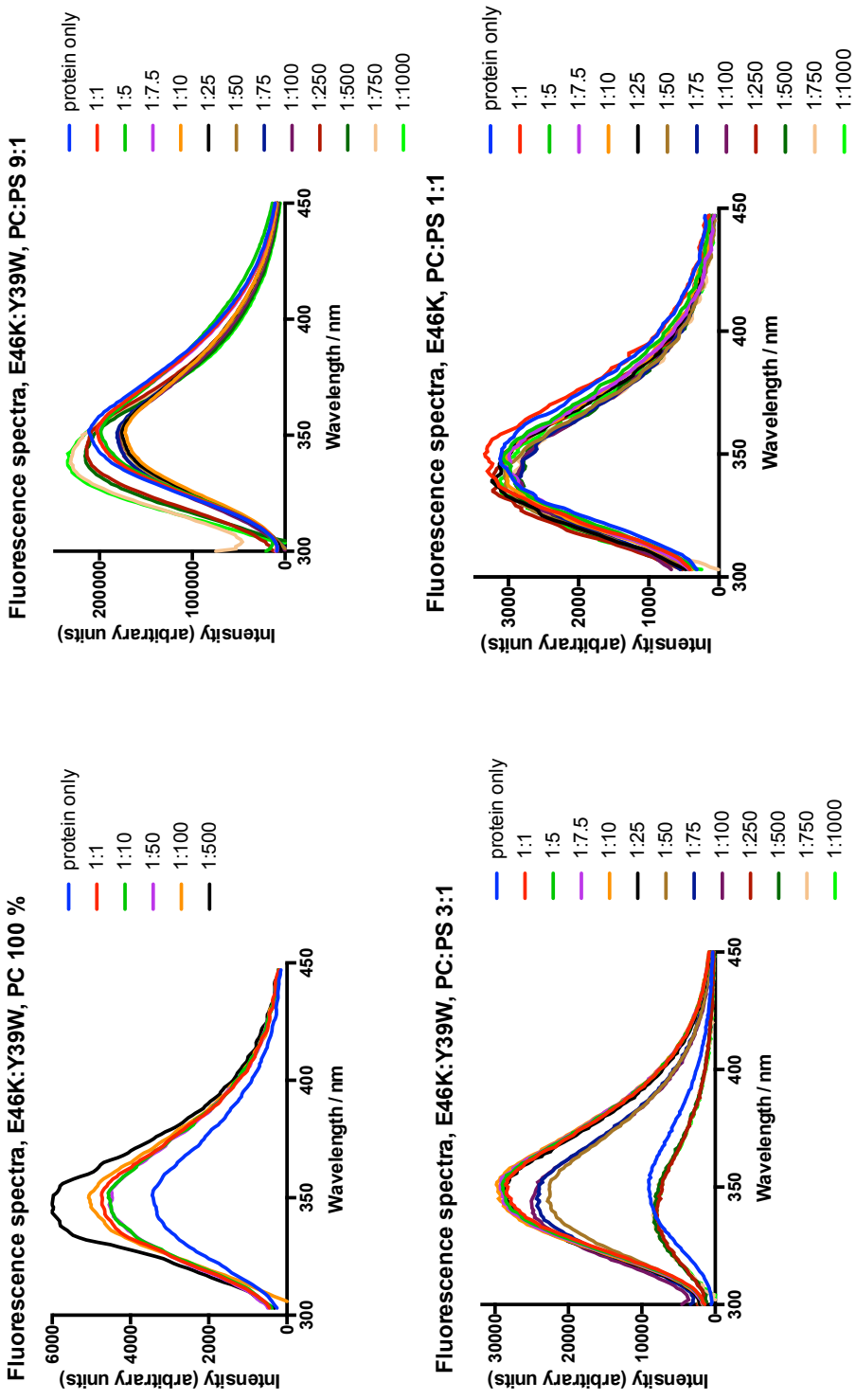

Figure 4.2: Fluorescence emission spectra gathered for E46K:Y39W alpha-synuclein mixed with POPC/POPS vesicles. Percentage POPS *(top left, top right, bottom left, bottom right)* is 0, 10, 25, 50. Fluorescence samples excited at 295 nm. Spectra have not been normalised for concentration.

When no POPS was present, most of the samples showed hardly any deviation from protein in solution (solid black line). We observed shifts in the fluorescence for samples containing 10, 25, and 50 % POPS. These shifts affect the wavelength at which maximum emission is detected ($\lambda_{\max}$): as the tryptophan residue moves from an aqueous to a hydrophobic environment it emits fluoresced light at a lower wavelength. This is known as blue shift. We may deduce that if the blue shift is larger, a greater proportion of Trp residues are inserted into the membrane: a measure of the strength of the binding.

The spectrum appeared to shift for ratios higher than 1:100 moles in the 10 % and 25 % POPS cases. The shift was apparent from around 1:50 moles in the 50 % POPS cases, demonstrating that higher proportions of PS present greater binding opportunity for the protein.

When the blue shift was plotted as a function of lipid concentration, binding curves are produced. These are shown in Figure 4.3. The apparent dissociation constants derived from these plots ($K_{D\text{app}}$) are shown in Table 4.2.

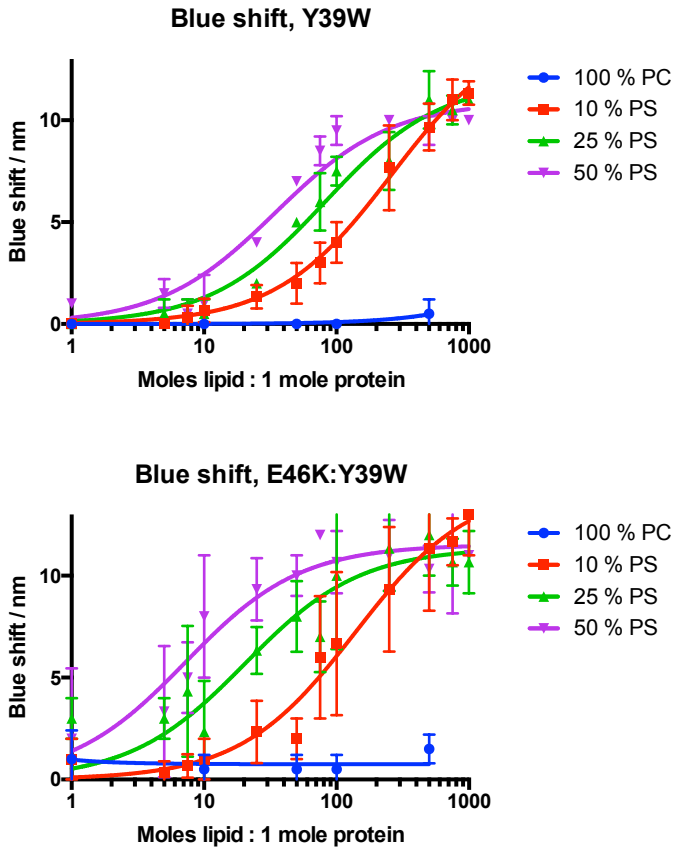

Figure 4.3: Blue shift plotted as a function of lipid concentration for *(top)* Y39W and *(bottom)* E46K:Y39W. Points shown indicate measurements of blue shift for vesicles of 100 % POPC (circles), 10 % POPS (squares), 25 % POPS (filled triangles), and 50 % POPS (downward triangles). Each data point is the average of three measurements, with error bars showing one standard deviation from the mean. Approximate binding curves were fitted using Prism one-site ligand binding algorithms, fitting equation $y = B_{\max}x/(K_d + x)$. Examples of the method used by Prism are shown in Appendix B.

A fluorescence-negative control was carried out using WT α-synuclein. Since no tryptophan residues are present, excitation at 295 nm does not give rise to meaningful fluorescence signals, and only negligible signals are observed. This experiment was carried out using POPC/POPS vesicles, with a molar ratio of 1:1. The data are shown in Figure 4.4.

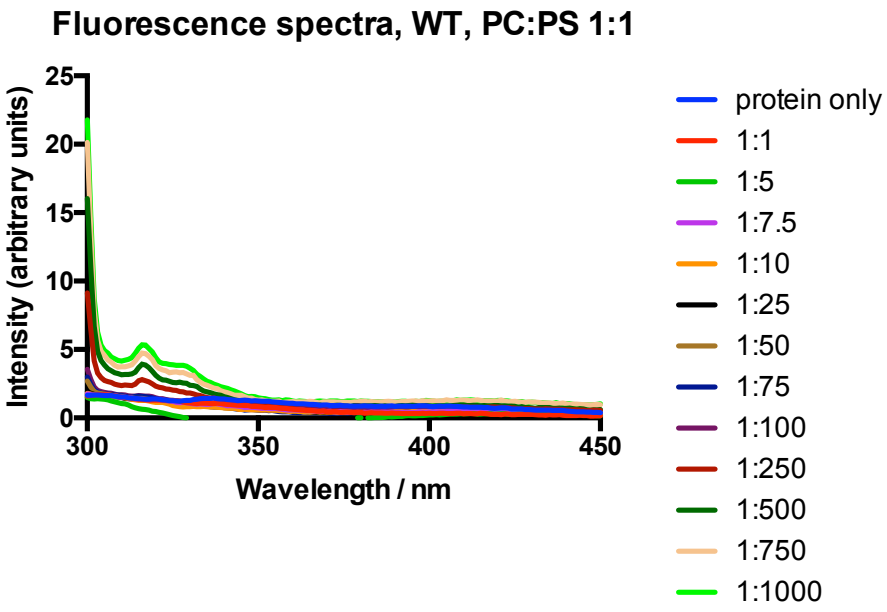

Figure 4.4: Fluorescence spectra for WT α-synuclein mixed with POPC/POPS vesicles. Both lipids were at 50 % mole/mole. Samples excited at 295 nm. Due to the different relative units used by this Jasco fluorimeter, values are smaller by a factor of approximately 500 than they would appear if measured on the PTI fluorimeter used for most of the previous measurements. Spectra have not been normalised for concentration.

Figure 4.4 demonstrates that fluorescence signals observed above (Figure 4.1 and Figure 4.2) were entirely due to the presence of the tryptophan residue, justifying its use. The interaction between α-synuclein and negatively-charged POPS, however, is not believed to be specific, and may not explain the role of the protein in disease. In the literature, for example, binding has been demonstrated using similarly charged PG lipids (Rhoades *et al.*, 2006; Ferreon *et al.*, 2009). It was necessary to attempt to approximate more closely the complexity of native, neuronal membranes, and attempt to discern a specific interaction.

4.3.2 Influence on binding of increased complexity of membranes

Several other lipids play important biological roles in membranes, and some of these were incorporated one at a time in order to deduce which, if any, had the biggest impact on α-synuclein lipid-binding. First, cholesterol: a key lipid for membrane fluidity and stability properties was added. Sphingomyelin (SM1), implicated in signalling pathways, apoptotic pathways, and lipid raft formation (Kolesnick & Golde, 1994), was incorporated. The final lipid to be added to the preparation was the ganglioside GM1, as it has roles in binding events in various systems.

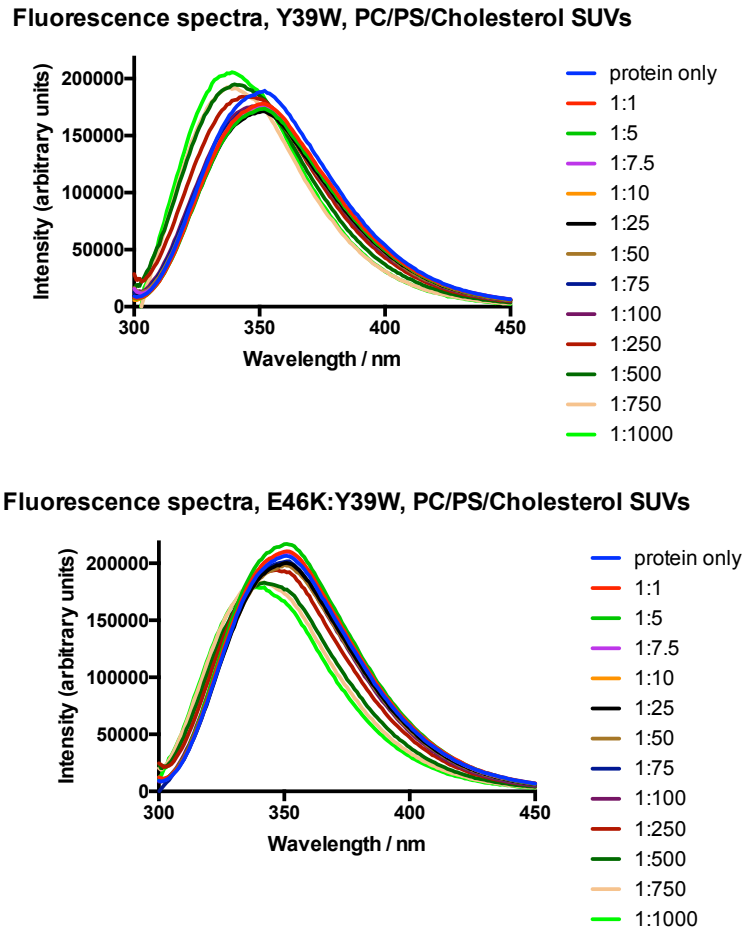

Figure 4.5: Fluorescence spectra gathered for Y39W, and E46K:Y39W alpha-synucleins, mixed with POPC/POPS/cholesterol vesicles. Vesicle composition is 15 % cholesterol, 10 % POPS, 75 % POPC. Spectra have not been normalised for concentration.

Upon addition of 15 % cholesterol, both proteins once more display the same range of shift in λ_{max} from 352 to 340 nm, and both display any shift only once a protein:lipid molar ratio of 1:100 has been passed. This implies that cholesterol does not affect lipid binding. This is in accord with the hypothesis that it is the charged POPS lipid that facilitates the binding process. This result is not surprising, but has not been shown before now.

SM1 was also added to the vesicle preparation. The wide range of reported functions for SM1, especially the role it has in putative lipid rafts, made it a potential binding target for

specific amyloid interactions (Kolesnick & Golde, 1994). These data are shown in Figure 4.6.

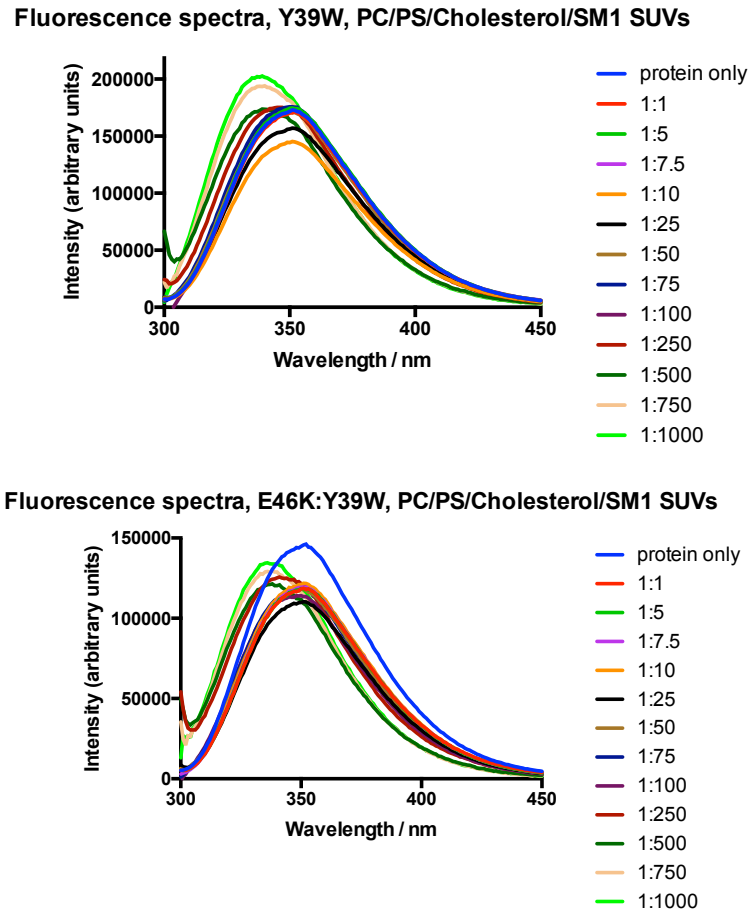

Figure 4.6: Fluorescence spectra gathered for Y39W, and E46K:Y39W alpha-synucleins, mixed with phospholipid vesicles. Vesicle composition is: 10 % SM1, 15 % cholesterol, 10 % POPS, 65 % POPC. Spectra have not been normalised for concentration.

The addition of SM1 also seemed not to affect the position of λ_{max}, or the molar ratio at which blue shift becomes observable, again indicating that any binding in this system is dominated by POPS. No evidence was found in these data that SM1 has enhanced or reduced the binding affinity of the protein for lipids.

Finally, GM1 was incorporated into vesicles, and the experiment repeated. Amyloid-

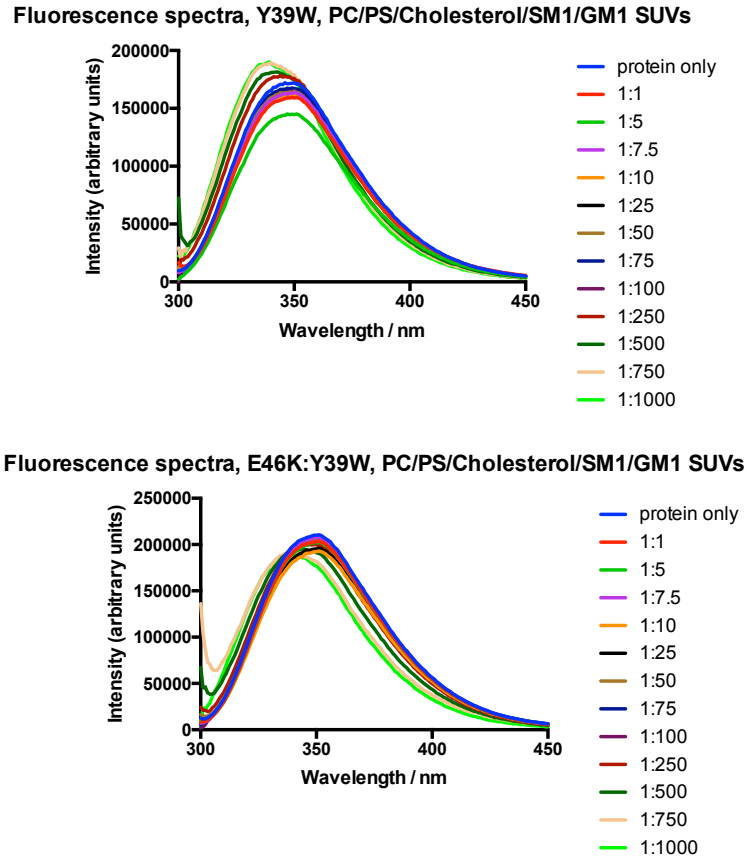

Figure 4.7: Fluorescence spectra gathered for Y39W, and E46K:Y39W alpha-synucleins, mixed with phospholipid vesicles. Vesicle composition is: 5 % GM1, 10 % SM1, 15 % cholesterol, 10 % POPS, 60 % POPC. Spectra have not been normalised for concentration.

ganglioside interactions had been demonstrated previously; an increase in binding ability would have validated these hypotheses further. These spectra are shown in Figure 4.7.

Once again, however, the spectra strongly resemble those for POPC/POPS vesicles, at 10 % PS. The data shown here do not suggest that Y39W or E46K:Y39W α-synuclein interact specifically with GM1, only with POPS. Binding curves for these data, generated as above, are shown in Figure 4.8. When compared to Figure 4.3 it is apparent that the curves are shifted to the right, *i.e.* more lipid is needed to give a binding effect. This became clearer when binding coefficients were compared between Table 4.2 and Table

4.3.

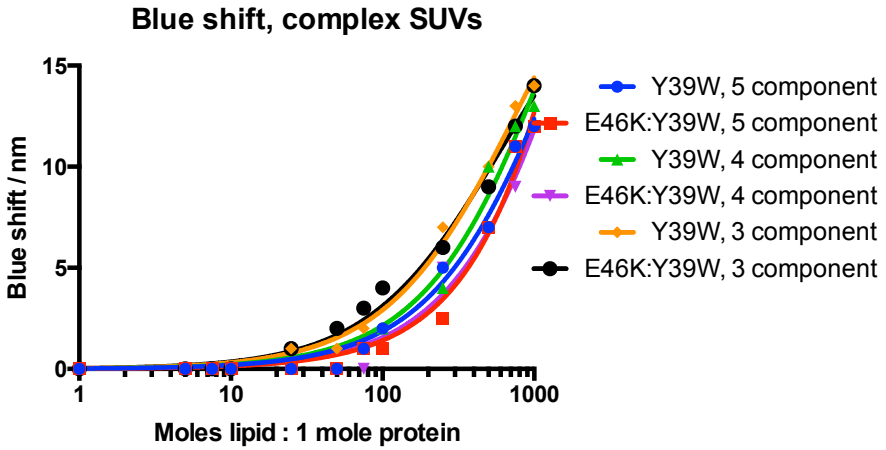

Figure 4.8: Blue shift plotted as a function of lipid concentration for Y39W and E46K:Y39W mixed with lipid vesicles of 3, 4, and 5 component lipids. All vesicles contained 10 % POPS and 15 % cholesterol. 4 component vesicles also contained 10 % SM1, 5 component vesicles also contained 5 % GM1. the remainder was POPC in each case. Diamonds, triangles, and blue circles represent data points for Y39W protein, squares, downward triangles, and black circles represent points for E46K:Y39W. Circles are for 5 component vesicles, triangles for 4 component, and squares for 3 component. Approximate binding curves were fitted using Prism one-site ligand binding algorithms, fitting equation $y = B_{\max}x/(K_d + x)$. Examples of the method used by Prism are shown in Appendix B.

Table 4.2 shows the values for $K_{D\text{app}}$ for α-synuclein binding to small unilamellar vesicles of POPC/POPS in various ratios. These were calculated using a ligand binding algorithm in the SigmaPlot package. These values for $K_{D\text{app}}$ demonstrate the increase in affinity of protein for membrane when more POPS is present. There is an order of magnitude improvement between the 10 % case and the 25 % case. The increase in affinity is smaller between the 25 % and 50 % cases. However, differences between K_D for the two protein constructs are much less pronounced. More data would be required to make conclusions about whether these are truly significant K_D differences, but it appears that both the Y39W and the E46K:Y39W interact with these lipids with similar affinity.

Table 4.2: $K_{D\text{app}}$ calculated within Prism for two α-synuclein constructs, binding to SUVs containing various percentages of POPC and POPS. These figures were calculated using a simple one-site ligand binding algorithm within Prism. Errors given represent the standard error, also calculated within Prism.

	$K_{D\text{app}}$ / μM	
% POPS	Y39W	E46K:Y39W
0	—	—
10	259.9 ± 18.9	398 ± 23.0
25	82.0 ± 12.4	76 ± 5.5
50	34.4 ± 7.6	41 ± 1.4

Table 4.2, showing $K_{D\text{app}}$ for POPC/POPS vesicles, may be compared to Table 4.3, showing $K_{D\text{app}}$ for complex vesicles. The values in Table 4.3, coupled with the curves shown in Figure 4.8 suggest that increasing the complexity of the membranes dramatically reduced the affinity of the protein for the membranes. While some of the values are spurious given that our molar ratios only went up to 1:1000 moles (8538, for example), it is clear that these values are much higher than those in Table 4.2, allowing the conclusion that α-synuclein would bind less readily to complex membranes, and more readily to simple membranes containing large amounts of POPS. This may be due to compartmentalisation of membranes into domains such as lipid rafts - this would, in effect, reduce the number of binding sites, although the sites would be larger.

Table 4.3: $K_{D\text{app}}$ calculated within Prism for two α-synuclein constructs, binding to SUVs containing 10 % POPS and 15 % cholesterol. The latter two contained 10 % SM1, the final data are for SUVs containing 5 % GM1. The remainder of the lipid is made up of POPC. These figures were calculated using a simple one-site ligand binding algorithm. Errors given represent standard error from the mean, also calculated within Prism.

	$K_{D\text{app}}$ / μM	
Component addedd	Y39W	E46K:Y39W
Cholesterol (15 %)	781 ± 146	591 ± 107
Cholesterol and SM1 (10 %)	1518 ± 674	2703 ± 1860
Cholesterol, SM1, GM1 (5 %)	1654 ± 627	8358 ± 12466

This result has implications for experimental design in that if a strong binding effect is required, it may actually be detrimental to use realistic membrane complexity. However, this may at least partly explain why Parkinson's Disease takes so long to develop, as the protein-lipid interaction could be extremely inefficient *in vivo*.

4.3.3 Determination of the ability of GM1 to interact with α-synuclein in the absence of POPS

Since GM1 is known to interact with amyloid proteins (Fantini & Yahi, 2011; Sanghera *et al.*, 2011), a final fluorescence experiment was carried out with only POPC and GM1

present in the vesicle preparation. This was to determine if the proteins used here were able to interact with GM1 at all. The spectra are shown in Figure 4.9, and do not demonstrate any blue shift. It was concluded that constructs of α-synuclein that contain the Y39W mutation are not able interact with GM1. This result contradicts earlier data, specifically that gathered by Fantini and Yahi (Fantini & Yahi, 2011). However, their data do suggest that the tyrosine at position 39 is critical for the interaction with GM1. Although Trp and Tyr are often suggested as functionally interchangeable, due to their similar size and hydrophobicity, it appears that the hydroxyl group on the Tyr residue may be key to this GM1 binding. The Trp mutant used here cannot replicate the effect.

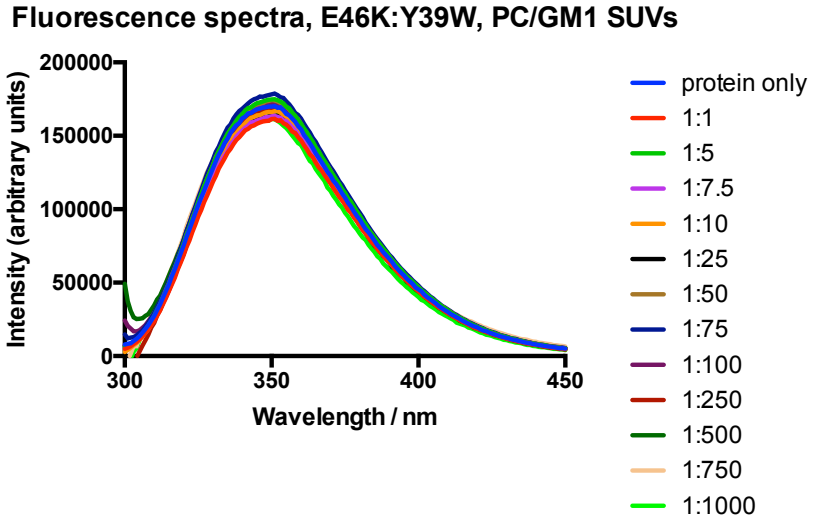

Figure 4.9: Fluorescence spectra gathered for E46K:Y39W alpha-synuclein, mixed with phospholipid vesicles. Vesicle composition is: 5 % GM1, 95 % POPC. Spectra have not been normalised for concentration.

4.4 Conclusions

In this chapter the intrinsic fluorescence of tryptophan has been used to make inferences about how α-synuclein interacts with lipid membranes. The shift in the characteristic

fluorescence spectrum of the residue reveals how readily the indole ring structure inserts into the membrane, away from its aqueous environment. It has been demonstrated that although this process occurs reliably when POPS is present in the lipid mixture, other lipids tested have no influence on this interaction. POPC, cholesterol, SM1, and GM1 have not exhibited any propensity to increase the strength of binding, or at what level of protein:lipid molar ratio it occurs.

Attention has been drawn to the work of other investigators, showing that α-synuclein does have specific interaction with GM1, and evidence has been presented that using Y39W variants of the protein may have eliminated this interaction. Further reference to this conclusion is drawn in other chapters of this work.

In Chapter 5, the samples discussed here were used again for circular dichroism experiments. This enables the context of tryptophan membrane insertion to be understood, and a relationship between that process and other measures of binding to be explained.

Chapter 5

Circular dichroism spectroscopy studies of protein-lipid interaction

5.1 Introduction

To further answer the question of how α-synuclein interacts with lipid membranes, three sets of experiments were carried out. First, using the same samples used in Chapter 4, the *CD* spectrum of α-synuclein was measured for different molar ratios of protein to lipid. Comparisons were made for Y39W and E46K:Y39W α-synuclein, and for lipid systems containing increasingly complex mixtures of lipids. Any differences in binding between the two constructs can be compared, and also compared to the fluorescence data from Chapter 4.

Second, it was desirable to use a model protein so that as much comparable data as possible was obtained. Melittin was selected. This protein has been studied by the Rodger group, and other groups, as its lipid insertion is an interesting case study of a relatively short peptide, with strong, observable, structural changes (Sui *et al.*, 1994; Damianoglou *et al.*, 2010; Svensson *et al.*, 2011). The structure of the melittin dimer (adopted in

lipidic environments) is shown in Figure 1.14 (Terwilliger & Eisenberg, 1982a,b; Pettersen *et al.*, 2004). The experiments presented here give further data on how melittin interacts with lipid membranes, and also provide good context for the lipid binding of α-synuclein. They were carried out in a linear dichroism *LD* cell, also providing validation of this as a development of *CD* instrumentation. Good *CD* data in these sub-optimal conditions represents useful progress for those with very small volumes of sample, for example.

Utilising the *LD* cell for *CD* requires smaller sample volumes than in a conventional *CD* cell, and also minimises the risk of sample loss during cuvette exchange. *CD* and *LD* provide complementary data (secondary structure and orientation), so an experimentalist should seek to gather both spectra during a session. It may be the case that one would wish to measure *CD* before and after the flow of *LD*, so the process again saves time and sample loss during the exchange. The ability to gather two distinct sets of data, reliably, without needing to even open the cover of the instrument would improve efficiency, and uptake of the *LD* cell.

Finally, *CD* measurements were made of α-synuclein monomer and oligomer in the *LD* cell. With all the context from the previous *CD* data, these results can be discussed with confidence, and provide interesting points on how monomeric, and oligomeric, protein appears to adapt to the lipid environment. The oligomeric form of the protein has been characterised in the Pinheiro laboratory by Rachel Smith and Timothy Kaufamnn, and found to be annular and A11 antibody-positive (Smith, 2013). These structures, approximately 10 nm in diameter, would form small pores in the cell membrane on insertion, with their aperture being between 1 and 3 nm wide, so determining whether insertion does or does not occur may go some way to solving the method of toxicity.

A small molecule compound was used in the experiments described in this chapter: 1,6-diphenyl-1,3,5-hexatriene (DPH). As Figure 5.1 shows, DPH is a linear, light-absorbing, fluorescent, hydrophobic, compound, that inserts into lipid films (Prendergast, 1978;

Kaiser & London, 1998; Carafa *et al.*, 1998). It was incorporated at this stage, though its main use would be when the vesicles used here were later used for linear dichroism experiments.

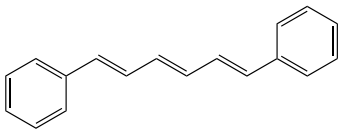

Figure 5.1: Structure of 1,6-Diphenyl-1,3,5-hexatriene, demonstrating hydrophobic acyl chain.

5.2 Methods

Monomeric protein lipid-binding experiments were carried out using the method described in Section 2.2.2. Spectra were measured for protein:lipid ratios of 1:1 moles, up to 1:1000 moles, with α-synuclein at 10 μM. Table 4.1 shows the range of vesicle compositions that were studied in this experiment. Lipids were prepared by the sonication method described in Section 2.2.3, and mixed with protein shortly before use. The same samples were used for fluorescence and *CD* measurements. *CD* signal at 222 and 208 nm was used for calculation of binding curves as for the fluorescence data shown in Chapter 4.

For melittin and the later α-synuclein *CD* experiments, the parameters were changed substantially. Lipids were prepared by the extrusion method described in Section 3.2.2. The resuspension buffer was 10 mM sodium phosphate, pH 7.4. Data were gathered in Jasco J-1500 and J-815 spectropolarimeters, and all data were collected for 80–100 μL of sample in a 0.5 mm path length capillary, stationary in an *LD* cell. Measurement speed was 200 nm/min, integration time was 0.5 seconds, and each spectrum was the average of 8 measurements. Data were gathered from 180 nm to 500 nm in order to gain as much information on the quality of the measurement system as possible, though the protein region between 190 and 260 nm was particularly relevant.

Both melittin and α-synuclein were mixed to a molar ratio of 1:100 (protein:lipid), with

protein at 0.1 mg/mL: approximately 35 μM for melittin and 10 μM for α-synuclein. Monomeric and oligomeric forms of α-synuclein were used, the oligomeric form prepared as described in Section 2.2.6. Lipid vesicles used contained 1 % w/w diphenylhexatriene (DPH), and four different mixtures of lipids: Brain total lipid extract, soybean PC, POPC/POPS/cholesterol (molar ratio 75:10:15), and DMPC/POPS/cholesterol (molar ratio 75:10:15). Lipids were prepared by the extrusion method described in Section 2.2.4, and mixed with protein shortly before use. These samples were also used for linear dichroism measurements.

5.3 Results and Discussion

5.3.1 The secondary structure of α-synuclein on interaction with lipids

Circular dichroism spectra were gathered using the same samples as in fluorescence experiments, with minimal time between measurements. In this case, the change in secondary structure of the protein was the result of interest, demonstrated by the presence or absence of bands at 200, 208, and 222 nm for α-helix, or 200 nm for disordered protein.

Representative spectra for Y39W are shown in Figure 5.2. No folding was demonstrated in the 100 % POPC case until very high lipid:protein ratios: the band at 200 nm was unchanged until 1:500 moles was reached, and even in that case the protein is intermediately folded at best, with only a small shift from the other spectra shown. With higher proportions of POPS, the change from disordered protein to folded protein is strongly evident, with bands at 222 and 208 nm reaching larger magnitudes than the 200 nm random coil band.

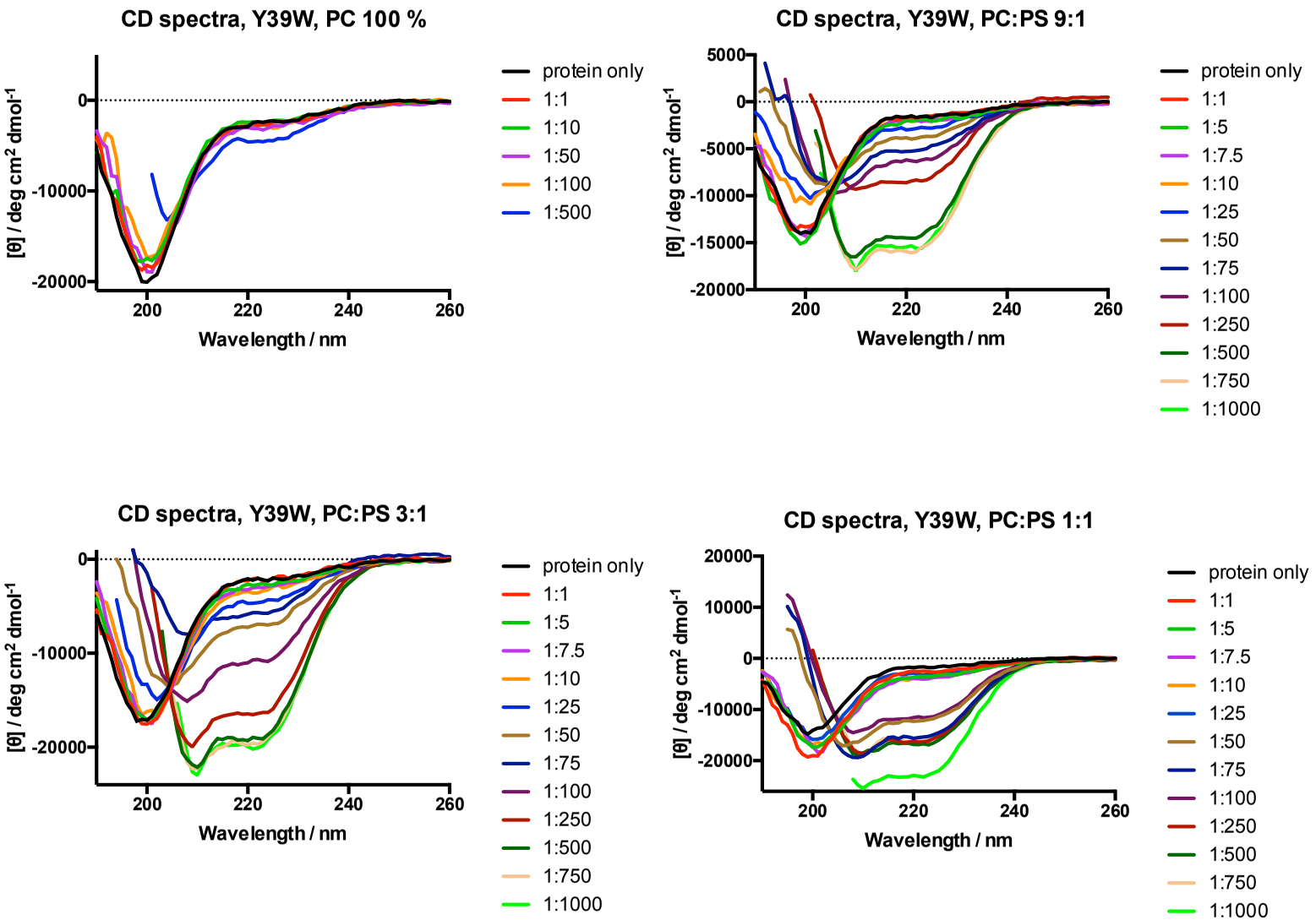

Figure 5.2: *CD* spectra gathered for Y39W α-synuclein mixed with POPC/POPS vesicles. Percentage POPS *(top left, top right, bottom left, bottom right)* is 0, 10, 25, 50. Cuvette path length was 1 mm, and protein concentration was 10 μM.

A control experiment was carried out using wild type (WT) α-synuclein and 50 % POPC/POPS vesicles in order to confirm that the Y39W mutation does not affect interaction of the protein with POPS. These data are shown in Figure 5.3. While these data are noisy, the change from unstructured protein to α-helix evidently occurs at near to the same protein:lipid ratios as in the Y39W case. The fact that the 1:75 moles spectrum in figure 5.3 appears to be random coil may suggest that WT protein (Y39) does not interact quite to readily with the lipid as Y39W.

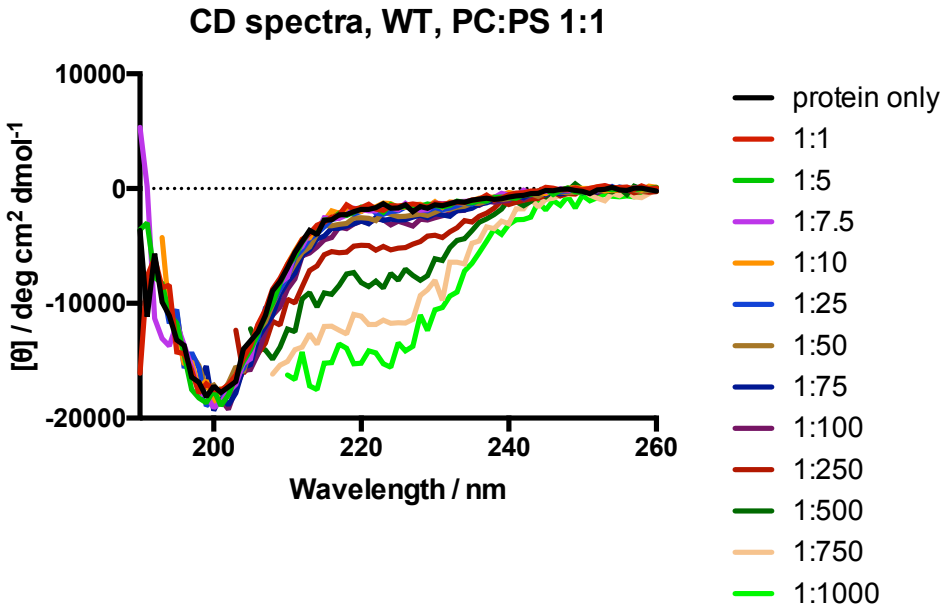

Figure 5.3: *CD* spectra gathered for WT α-synuclein mixed with vesicles containing 50 % POPS, 50 % POPC. Cuvette path length was 1 mm, and protein concentration was 10 μM.

The random coil spectra shown in Figure 5.3 have approximately the same magnitude as for E46K:Y39W α-synuclein, so the trend from random coil to α-helix is judged to be correct. The low signal:noise ratio is presumed to be due to the buffer in which the WT protein was supplied in a buffer containing various components known to generate artefacts on *CD* spectra (NaCl, $MgCl_2$, Tris-HCl). while these were diluted many times from the original stock, it may be the case that they interfered with the spectra.

Representative spectra for E46K:Y39W α-synuclein are shown in in Figure 5.4.

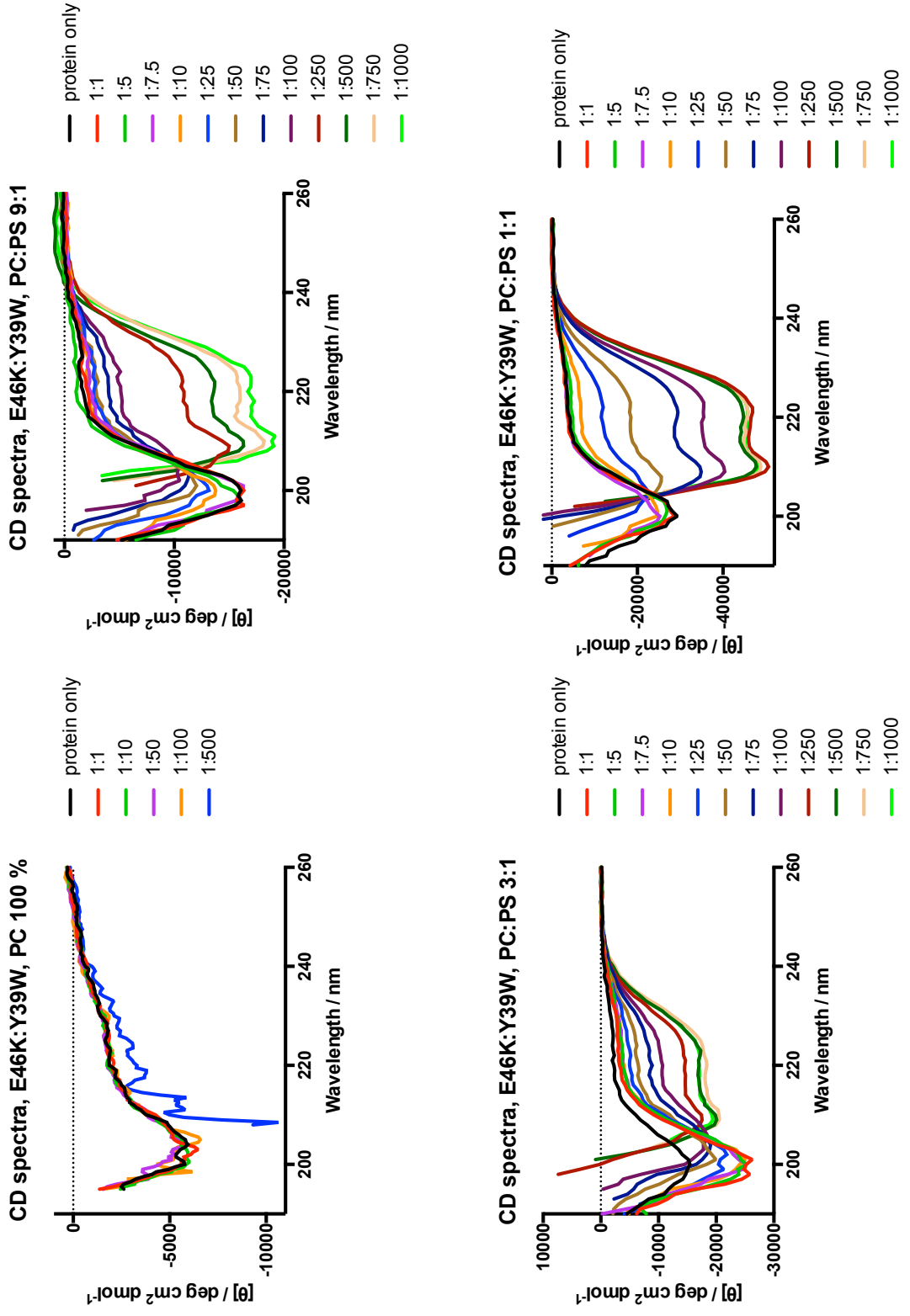

Figure 5.4: *CD* spectra gathered for E46K:Y39W α-synuclein mixed with POPC/POPS vesicles. Percentage POPS *(top left, top right, bottom left, bottom right)* is 0, 10, 25, 50. Cuvette path length was 1 mm, and protein concentration was 10 μM.

Again, little difference was observed when no POPS was present. The band at 200 nm is pronounced, and is the only strong signal visible. In samples where the lipid contains 10, 25, or 50 % POPS, the differences are striking, with the 200 nm band diminishing at ratios above 1:10 moles of protein to moles of lipid. When ratios above 1:500 moles are used, the spectra have no band at 200 nm, and very strong bands at 208 and 222 nm: the protein is clearly α-helical. The band at 200 nm is concealed by scattering due to the nature of lipid vesicles in suspension.

With greater proportions of POPS present, the shift to α-helix may occur at lower ratios of protein to lipid. In the previous chapter, binding curves were generated by plotting lipid:protein ratio against blue shift of the fluorescence spectra. A similar technique is possible in the *CD* case, by plotting the lipid:protein ratio against the change in *CD* signal for the key α-helix band wavelengths at 222 nm and 208 nm. Figure 5.5 shows these fitted curves.

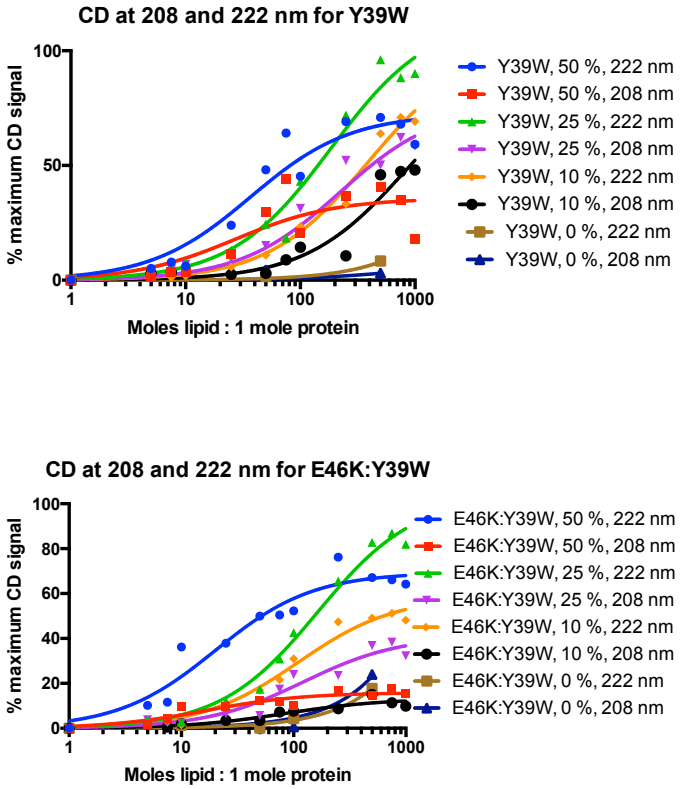

Figure 5.5: Fitted curves for shift in *CD* spectra at 222 nm and 208 nm plotted against lipid:protein ratio for Y39W α-synuclein *(top)* and E46K:Y39W *(bottom)*. Blue, green, yellow, and brown data series represent 222 nm, red, purple, black, and dark blue represent 208 nm. data is scaled by percentage of *CD* signal, where minimum is the signal at 0 lipid, and maximum is that achieved for 50 % POPS. Apparent binding curves were fitted using Prism one-site ligand binding algorithms, fitting equation $y = B_{\max}x/(K_d + x)$.

Figure 5.5 demonstrates that *CD* signal changes in a concentration dependent manner as

the protein interacts with the lipid, *i.e.* the folding of the protein does not take place all at once. From these fits, dissociation constants may be derived, and therefore compared to those gathered from fluorescence data explained in Chapter 4. Table 5.1 shows these calculated values.

Table 5.1: $K_{D\text{app}}$ calculated within Prism for two α-synuclein constructs, binding to SUVs containing 10 % POPS and 15 % cholesterol. The latter two contained 10 % SM1, the final data are for SUVs containing 5 % GM1. The remainder of the lipid is made up of POPC. These figures were calculated using a simple one-site ligand binding algorithm. Errors given represent standard error from the mean, also calculated within Prism.

	$K_{D\text{app}}$ / μM			
	CD_{222}		CD_{208}	
% POPS	Y39W	E46K:Y39W	Y39W	E46K:Y39W
0	—	—	—	—
10	386 ± 75	110 ± 25	819 ± 489	84 ± 35
25	186 ± 41	164 ± 22	222 ± 101	122 ± 35
50	37 ± 10.8	20 ± 5	27 ± 18	17 ± 5

It should be noted that the values presented in Table 5.1 have been taken from one data set only, but despite this limitation, the calculated $K_{D\text{app}}$ are broadly similar to those presented from the fluorescence blue shift data. Values calculated at 208 nm as less accurate than those at 222 nm due to smaller differences between the spectra, and a greater effect of noise at this wavelength. In the 50 % POPS case the values are very close to those calculated in Chapter 4; in the 10 % case the two 222 nm measurements are widely dispersed, but the mean is approximately 248 μM^{-1}, again close to the blue shift data. For 25 % POPS, the *CD* data show a slightly higher dissociation constant, but still comparable to that calculated in Chapter 4. It may be the case that the protein folding event occurs at a lower concentration of POPS than the tryptophan membrane insertion event, and may require higher proportions of POPS to achieve similar affinity. More data would be required to make this case. For the data presented here, the similarities suggest that tryptophan membrane insertion and random coil to α-helix protein folding take place at roughly similar concentrations, and therefore may be considered valid representations of the same binding process.

5.3.2 Addition of different lipids had little effect on *CD*

As in Chapter 4, once the POPC/POPS samples had been studied by *CD*, cholesterol was added to the lipid mixture and the experiment repeated. These data are shown in Figure 5.6. When compared to Figures 5.2 and 5.4, it was clear that cholesterol had not altered the trend – the same number of spectra appear to show random coil signal, and the same show α-helix.

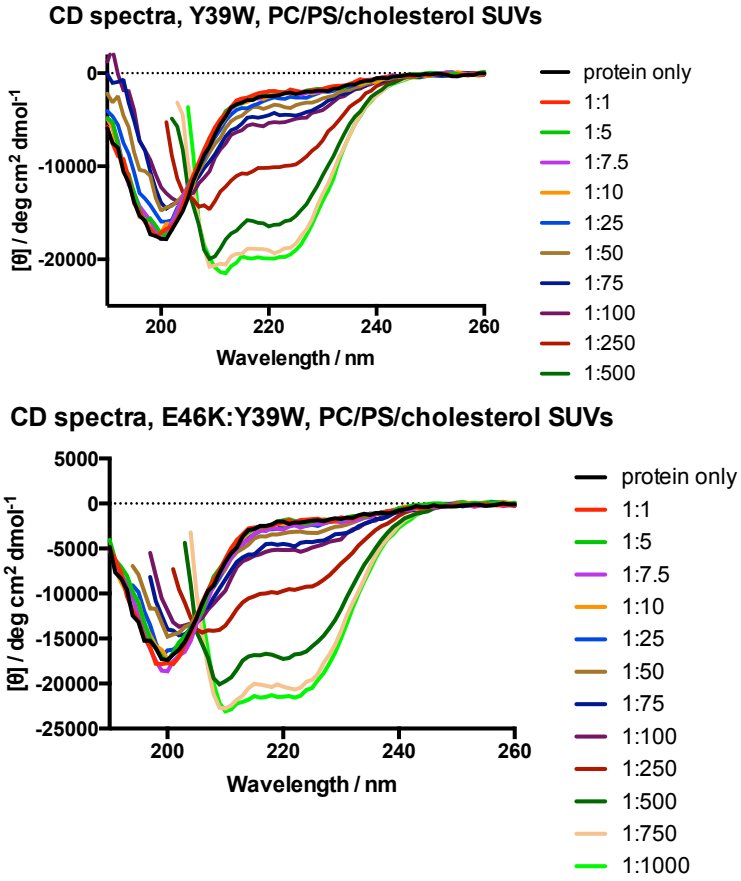

Figure 5.6: *CD* spectra gathered for *(top)* Y39W, and *(bottom)* E46K:Y39W α-synucleins, mixed with POPC/POPS/cholesterol vesicles. Vesicle composition is 15 % cholesterol, 10 % POPS, 75 % POPC. Cuvette path length was 1 mm, and protein concentration was 10 μM.

SM1 was also added to the lipid mixture. These spectra are shown in Figure 5.7, and again there were no differences to the data above. Neither lipid altered the ability of the protein to interact with the membrane.

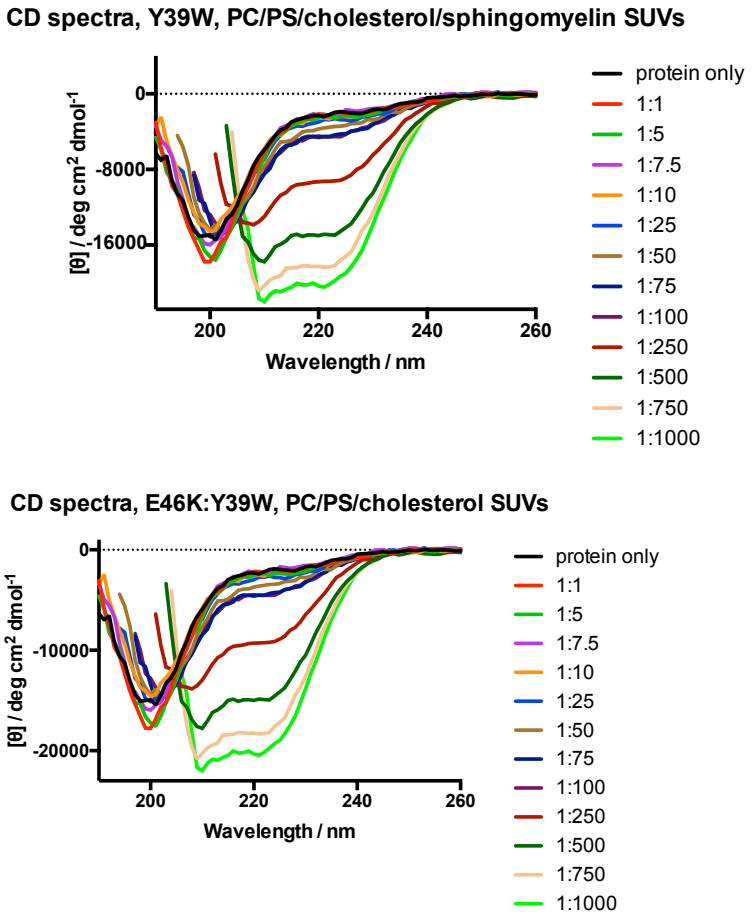

Figure 5.7: *CD* spectra gathered for *top)* Y39W, and *(bottom)* E46K:Y39W α-synucleins, mixed with phospholipid vesicles. Vesicle composition is: 10 % SM1, 15 % cholesterol, 10 % POPS, 65 % POPC. Cuvette path length was 1 mm, and protein concentration was 10 μM.

Finally, GM1 was added to the mixture. This ganglioside is known to interact with amyloid proteins, and this experiment was intended as a means to spot a potentially critical difference in the interaction of WT α-synuclein, and disease-linked E46K α-synuclein. Once again, however, the data did not show any noticeable effect from adding GM1. These spectra are shown in Figure 5.8.

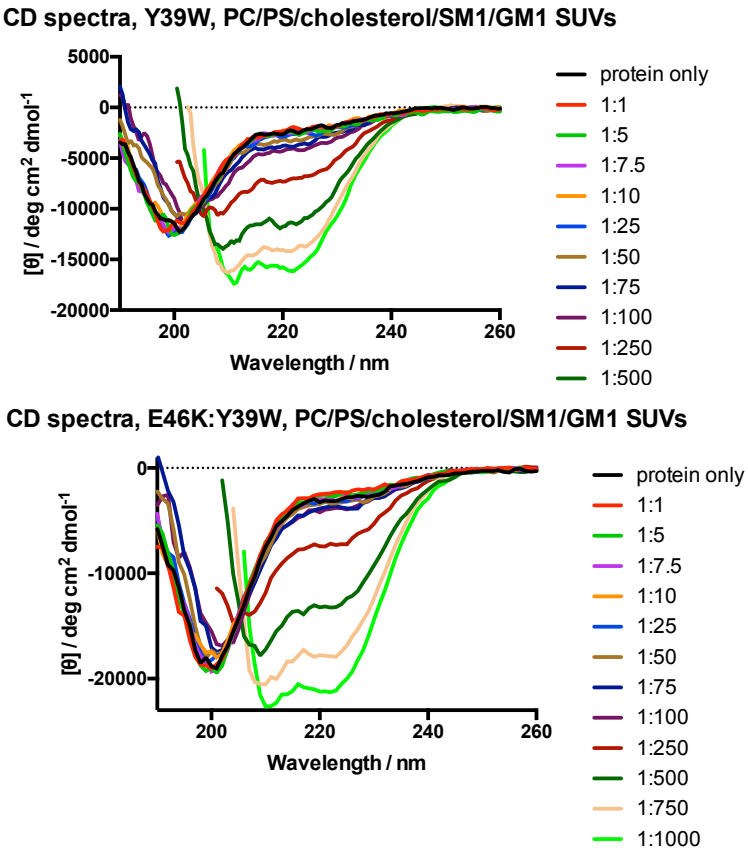

Figure 5.8: *CD* spectra gathered for *(top)* Y39W, and *(bottom)* E46K:Y39W α-synucleins, mixed with phospholipid vesicles. Vesicle composition is: 5 % GM1, 10 % SM1, 15 % cholesterol, 10 % POPS, 60 % POPC. Cuvette path length was 1 mm, and protein concentration was 10 μM.

Figures 5.6, 5.7, and 5.8 taken together confirmed that there is little effect on the binding of Y39W or E46K:Y39W α-synuclein when cholesterol, SM1, or GM1 are added. Therefore, in this system, the protein is able to interact with vesicles containing POPS, but this is the only lipid facilitating the interaction. Interaction with POPS fits well with studies in the literature, describing the tendency of α-synuclein to bind to charged vesicles, though the work presented here goes into greater detail than the one-component vesicles or two-component vesicles considered before (Davidson *et al.*, 1998; Eliezer *et al.*, 2001; Chandra *et al.*, 2003; van Rooijen *et al.*, 2008; Haque *et al.*, 2010; Reynolds *et al.*, 2011; Varkey *et al.*, 2013). This interaction has been shown in greater detail than before, demonstrating a concentration dependence with POPS at many different proportions in the lipid mixture.

However, a discrepancy arose from the observed lack of interaction between the protein and GM1. As discussed in Section 4.3.3, it would be expected that α-synuclein would interact with GM1 specifically (Fantini & Yahi, 2011), but in the spectra presented so far there was no evidence of this interaction. Preliminary data was gathered using E46K:Y39W α-synuclein and vesicles comprising 50 % GM1 and 50 % POPC, prepared and mixed as described above. These spectra are shown in Figure 5.9.

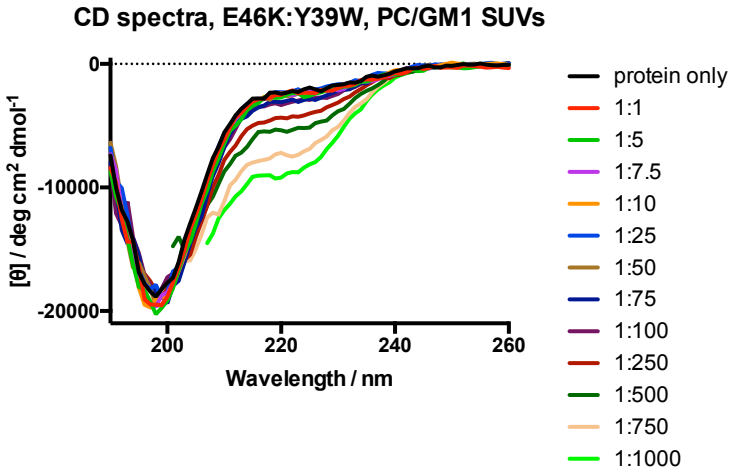

Figure 5.9: *CD* spectra gathered for E46K:Y39W α-synuclein, mixed with phospholipid vesicles. Vesicle composition is: 5 % GM1, 95 % POPC. Cuvette path length was 1 mm, and protein concentration was 10 μM.

Figure 5.9 resembles the POPC-only data shown in Figure 5.2, in that there is almost no structural change. At very high ratios of protein:lipid, around 1:500 moles, the random coil structure is slightly diminished, and α-helix bands have begun to develop, but this effect is not strong, and would require further study to resolve. This result resembles that shown in Figure 4.9, although the *CD* spectra show a *small* structural change, whereas the fluorescence data show nothing. This could indicate that the protein begins to fold in the presence of very high lipid levels regardless of whether the region around residue 39 has interacted with the lipid at all.

5.3.3 Circular dichroism measurements of melittin-lipid systems

Extruded vesicles of several types were mixed with melittin, and the *CD* spectrum measured in the *LD* cell. The *CD* spectrum of melittin without lipid present was also measured. The data are shown in Figure 5.10. These spectra show the unfolded nature of melittin in the absence of lipid, with a band only at 200 nm. When lipid was present at a ratio of 1:100 moles (protein:lipid), α-helix bands developed in all cases. The 195 nm band, not visible in α-synuclein spectra above, is present in all except the highly-scattering BTLE sample. Bands at 208 and 222 nm are clear in all cases, with similar magnitudes (slightly lower for soybean PC).

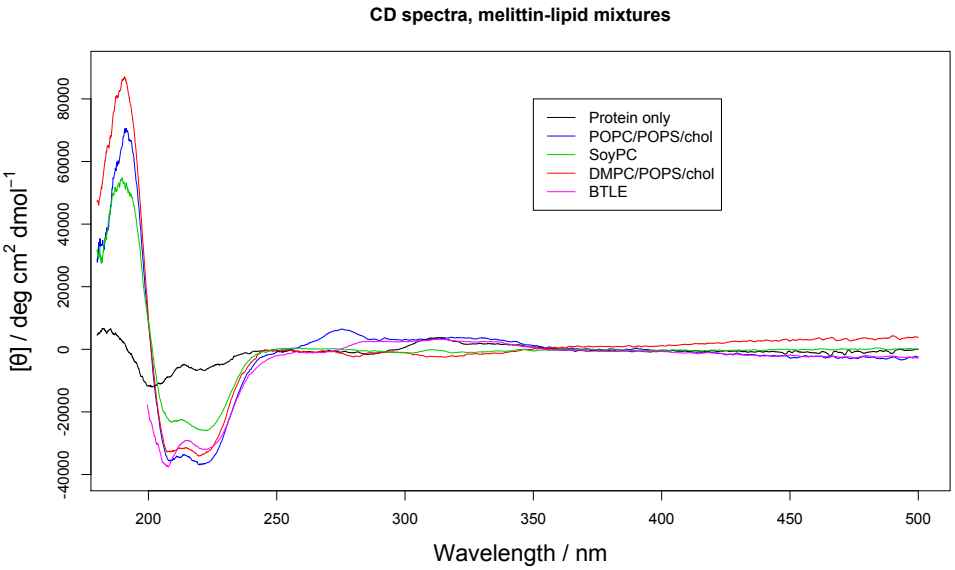

Figure 5.10: *CD* spectra gathered for melittin mixed with lipid vesicles. Black line represents melittin without lipid. In other cases, melittin was mixed with lipid vesicles at molar ratio of 1 mole protein:100 moles lipid. Path length was 500 μm in total, and protein concentration was 0.1 mg/mL.

Some discrepancies at higher wavelengths may be observed, for example around 270 nm. These are attributed to some slight aberration of the *LD* capillary – a scratch or some birefringence effect altering the baseline (Nordén *et al.*, 2010). In general, however, this

experiment gave very promising results indicating the suitability of the *LD* cell for *CD* measurements. The *CD* spectra measured here are representative of those reported in the literature (Damianoglou *et al.*, 2010).

5.3.4 Amyloid oligomers studied by circular dichroism

The technique in Section 5.3.3 of measuring *CD* in apparatus designed for *LD* was applied to α-synuclein. Spectra gathered for the monomeric Y39W protein in the absence of lipid are shown in Figure 5.11.

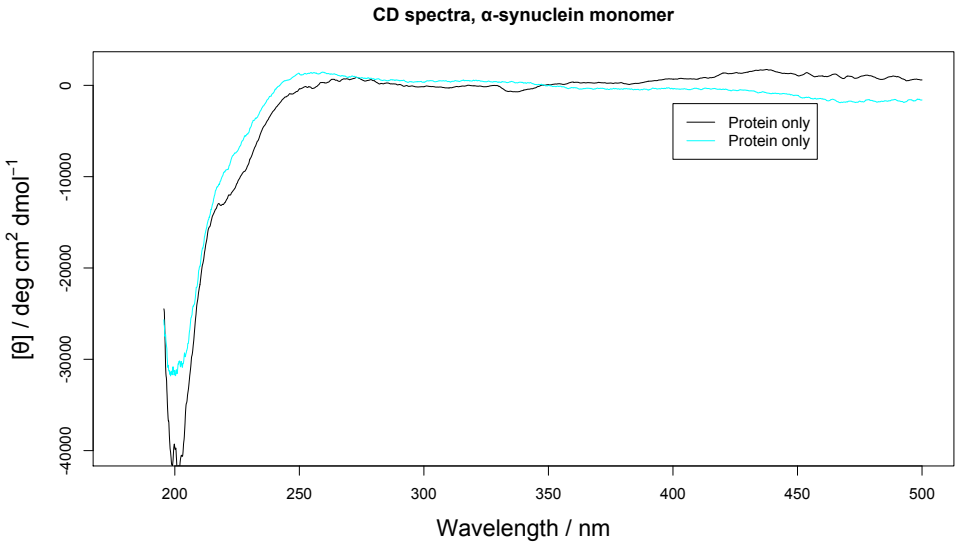

Figure 5.11: *CD* spectra gathered for α-synuclein monomer in absence of lipid. Two replicates shown. Path length was 500 μm in total, and protein concentration was 0.1 mg/mL.

The data shown in Figure 5.11 demonstrate that although lower signal:noise is achieved than in either the melittin case or the previous α-synuclein case described above, the key random coil signal at 200 nm is observable in these conditions. At wavelengths lower than around 195 nm these spectra are not useful: the signal is lost in some kind of scattering or other aberration.

Oligomeric α-synuclein was also measured by this method, and generated *CD* spectra shown in Figure 5.12.

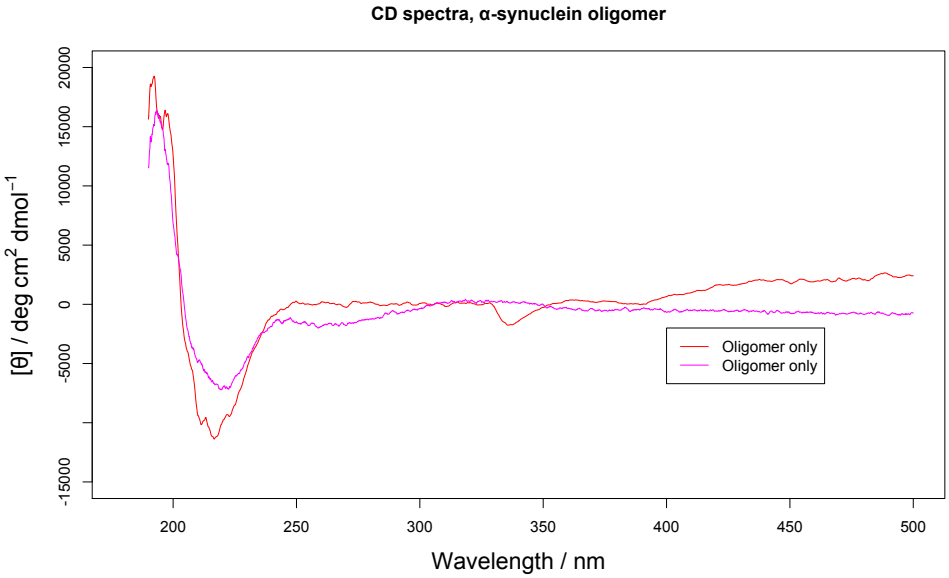

Figure 5.12: *CD* spectra gathered for α-synuclein oligomer in absence of lipid. Two replicates shown. Path length was 500 μm in total, and protein concentration was 0.1 mg/mL.

Here we observed characteristic β-sheet *CD* spectra, with a positive band at 195 nm and a smaller, negative band at 219 nm. This is good evidence that the oligomer production and purification method refined in the Pinheiro laboratory is effective, as the signal is not dwarfed by random coil signals. The data also conform to those sections of the literature that describe amyloid oligomers as having β-sheet structure, though data has also supported the existence of α-helical oligomers (Apetri *et al.*, 2006; Rochet *et al.*, 2000; Stöckl *et al.*, 2012b). The signal is not high enough to overcome all the noise present for this variation of the *CD* technique, but for initial estimation of secondary structure this may be sufficient in many cases. The red trace does display two unusual abnormalities: one small band at around 340 nm, and a non-flat baseline above 400 nm. These both may be due to birefringence or imperfections in the *LD* capillary. The capillaries have not been optimised for *CD*, which may represent the next crucial step to developing this experiment

further.

Figure 5.13 shows the *CD* spectra collected for monomeric α-synuclein in the presence of the two different lipid mixtures of most interest: POPC/POPS/cholesterol, and BTLE. As expected from the earlier monomer-lipid interaction experiments, the random coil signal of Figure 5.11 is replaced by α-helix to some extent. The conversion is not complete, as the molar ratios involved are smaller than those required for complete conversion, as demonstrated in Section 5.3.1, but bands are visible at approximetely 208 and 222 nm.

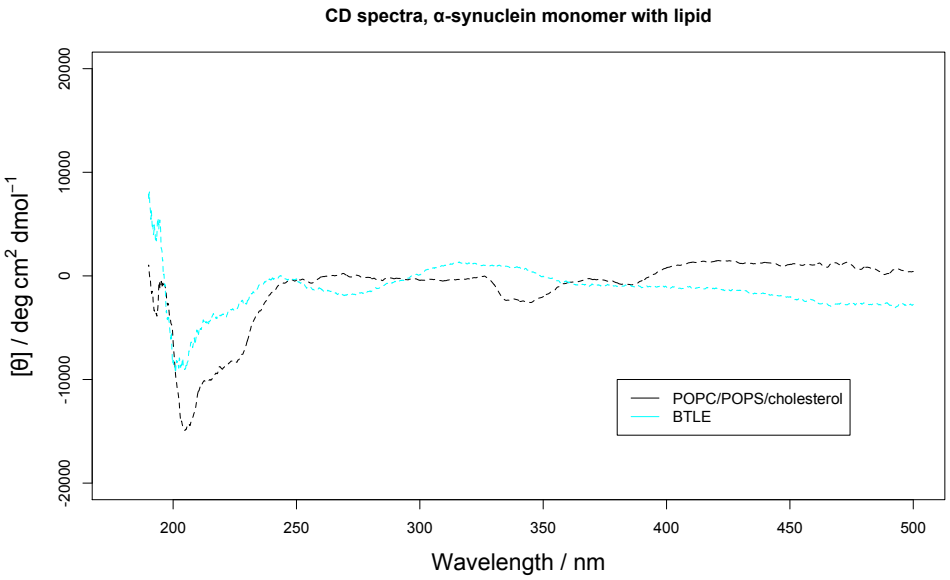

Figure 5.13: *CD* spectra gathered for α-synuclein monomer in presence of lipids. Black dashed trace for the POPC/POPS/cholesterol case, blue dashed line for BTLE. Path length was 500 μm in total, and protein concentration was 0.1 mg/mL.

Oligomeric α-synuclein was mixed in the same ratio with the same kinds of lipids, and again *CD* spectra were measured. These are shown in Figure 5.14. According to these data, the secondary structure of the oligomers is not affected by the lipid environment. The same shape and magnitude of bands is observed in this Figure as in Figure 5.12 above.

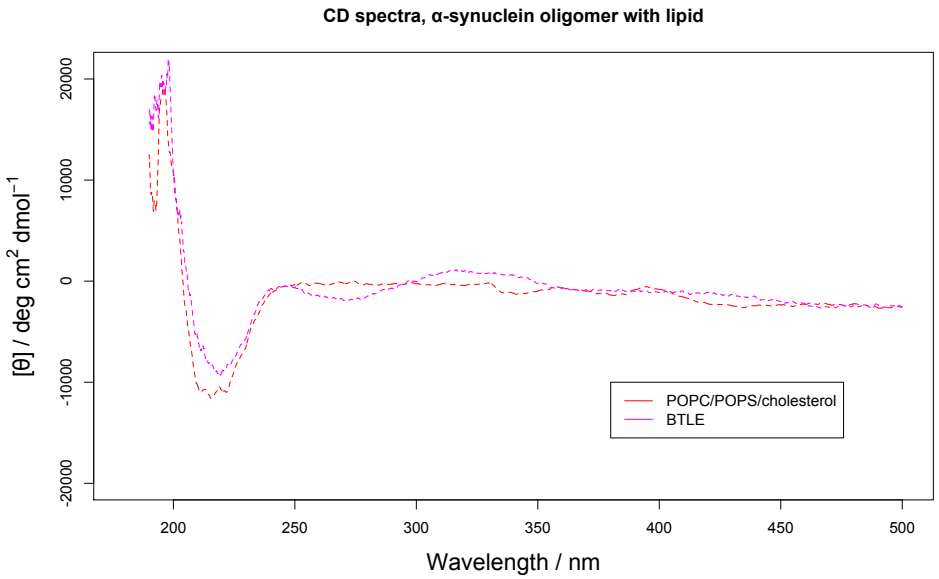

Figure 5.14: *CD* spectra gathered for α-synuclein oligomer in presence of lipids. Black dashed trace for the POPC/POPS/cholesterol case, blue dashed line for BTLE. Path length was 500 μm in total, and protein concentration was 0.1 mg/mL.

5.4 Conclusions

In this chapter, three series of experiments have been conducted. First, *CD* was measured for α-synuclein monomers mixed with lipid vesicles. These data demonstrate the propensity of the protein to fold to α-helix when it encountered lipid. Significantly, it was possible to determine the affinity of the protein for the lipid vesicles used by monitoring its *CD* signal at the characteristic α-helix bands. The secondary structure of the protein changed in a lipid ratio-dependent manner, with more α-helix developing as more lipid was present. Greater proportions of POPS in the vesicle composition give much smaller dissociation constants, *i.e.* the proportion of protein folded to α-helix is much greater, for a much lower ratio of lipid:protein.

Binding coefficients generated in this way corroborate those generated from the fluorescence blue shift data discussed earlier, and therefore demonstrate that the insertion of the W39

residue into the membrane happens at the same protein:lipid ratio as the folding of the protein. In other words, the chance that the two traits are involved in the binding process is high, rather than insertion leading the way and folding following later, for example.

The second experiment series, to use a model protein to assess the quality of *CD* generated in an *LD* instrument gave some significant results. Melittin appears to interact strongly with all types of membrane used in this work. It ready adopts its α-helix configuration on exposure to vesicles with mixed charges, mixed acyl chains, and diverse head groups. The spectra gathered agree with those previously reported in the literature. More pertinently, the quality of the spectra, while not perfect, is clear and usable. The *LD* cell is therefore a suitable sample holder for *CD*. There may be technical aspects that can be improved over time, reducing imperfections in capillaries for example, that will improve this use of the apparatus further.

It is possible to draw several conclusions from the final experimental series. First, the *LD* cell can be a useful tool for measuring *CD*. Second, α-synuclein monomers are dynamic in structure, and change easily in response to their environment. This might represent pathways to formation of oligomers, fibrils, tetramers, or some other structure, but evidence of this was not observed here. Additionally, oligomers are stable when exposed to membranes of varying charge and complexity, at least in the short term. *CD* does not indicate any change of structure, and therefore does not indicate the nature of any interaction between oligomer and membrane, *i.e.* whether the oligomers insert into the membrane. Other techniques must be employed to make conclusions about these specific questions. These experiments do not answer the question of how the oligomers could kill cells, but it is reasonable to conclude that the annular structure of these oligomers would not be immediately altered by interaction with lipids.

Chapter 6

Linear dichroism spectroscopy studies of protein-lipid interaction

6.1 Introduction

Using circular dichroism data from Chapter 5, it has been possible to test the use of the *LD* cell as a chamber in which to observe secondary structural changes of melittin and α-synuclein as they interact with lipids. This change in secondary structure can give clues to the strength the protein-lipid interaction. Linear dichroism gives similar clues to binding strength in a different way: the lipids are aligned in the shear flow, and the proteins align only if they interact with the lipids. *LD*, importantly, also gives clues to the *mode* of protein-lipid interaction, where the sign of the *LD* signal indicates whether the protein has inserted across the membrane. The quality of *CD* data obtainable in the *LD* cell was demonstrated in Chapter 5. This success gave confidence that it was possible to prepare a single sample, for a single instrument, and make both measurements in the same experimental session, without even the need to change cuvette.

In this chapter, results are presented from *LD* experiments on the same protein-lipid

systems as in Chapter 5: the model protein melittin, monomeric α-synuclein, and oligomeric α-synuclein. The first set of results presented demonstrate the difficulties encountered in both lipid system experiments and *LD* experiments. Different lipid mixtures respond to the Couette flow in unpredictable ways, and these effects are discussed. Once near-optimal conditions were determined, the proteins were used.

Melittin has been studied by *LD* previously, so it was of interest whether technique and instrument development has altered the results obtained since then (Damianoglou *et al.*, 2010). Once these data were in place, it was necessary to compare the *LD* spectra of monomeric α-synuclein, to determine if its binding mode is the same as, or distinct from, that of melittin. And finally the question of oligomer lipid-binding was addressed, to gather data on whether these oligomers insert across the membrane, or contact in a different way.

6.2 Materials and methods

The linear dichroism spectrum of DPH was measured after drying onto stretched polyethylene film, in order to assess its potential as an *LD* probe, following modifications made to the established stretched film approach to *LD* of Razmkhah *et al.* (Nordén *et al.*, 2010; Razmkhah *et al.*, 2014). *LD* was measured of stretched polyethylene film as a baseline, then a 50 mg/mL solution of DPH in chloroform was deposited onto the film surface and allowed to dry. 8 spectra were accumulated and averaged. Couette flow *LD* was carried out for vesicles with DPH incorporated into the lipid mixture at 1 % w/w.

Linear dichroism spectra were measured for melittin mixed with different types of lipid vesicle. The two sample components were mixed to a molar ratio of 1:100 (protein:lipid), with protein at 0.1 mg/mL (approximately 35 μM). α-synuclein was mixed to a molar ratio of 1:100 (protein:lipid), with protein at 0.1 mg/mL (approximately 10 μM). Monomeric

and oligomeric forms of α-synuclein were used; the oligomeric form was prepared as described in Section 2.2.6. Lipid vesicles used contained 1 % w/w diphenylhexatriene (DPH), and four different mixtures of lipids: brain total lipid extract, soybean PC, POPC/POPS/cholesterol (molar ratio 75:10:15), and DMPC/POPS/cholesterol (molar ratio 75:10:15). Lipids were prepared by the extrusion method described in Section 2.2.4, and mixed with protein shortly before use. In preliminary work, the lipid vesicles were prepared by sonication until the suspension was clear, as with the *CD* data gathered in Section 5.3.1.

Couette flow *LD* data were gathered in Jasco J-1500 and J-815 spectropolarimeters, and all data were collected for 80–100 μL of sample in a 0.5 mm path length capillary, in the *LD* cell. Rotation speed was 3000 rpm, with baselines measured at 0 rpm. Measurement speed was 200 nm/min, integration time was 0.5 seconds, and each spectrum was the average of 8 measurements. Spectra were gathered from 180 nm to 500 nm.

The orientation parameter S was calculated by solving Equation 3.6, obtaining the degree of orientation of DPH. This calculation was carried out in MATLAB by correcting for the scattering effect of the lipid sample, then extracting the region of the spectrum where DPH gave *LD* signal. S of this region was then calculated. This process is shown in Appendix C.

6.3 Results and Discussion

6.3.1 DPH acts as a probe for orientation of vesicles

The *LD* spectrum of DPH was measured on PE film in order to confirm it was capable of generating a signal in this technique. This spectrum is shown in Figure 6.1. The figure revealed several important details, validating DPH as a useful *LD* probe: first, peaks are well defined at around 200, 340, 355, and 380 nm. While the 200 nm band might

be masked by any protein signal in an experiment, the other peaks are well clear of the protein region, and should allow interpretation of vesicle orientation.

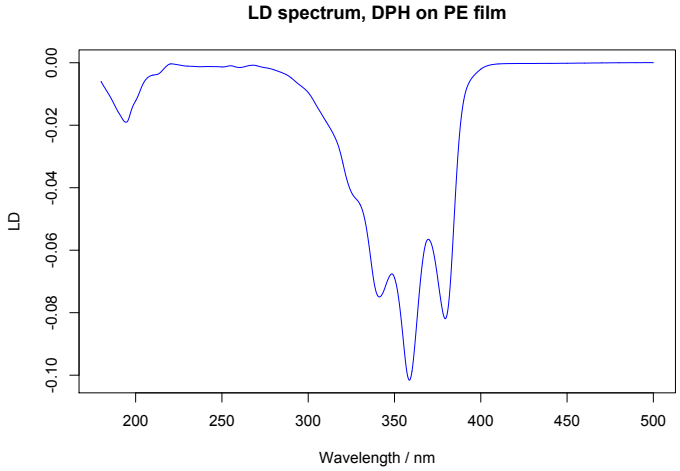

Figure 6.1: *LD* spectrum of DPH deposited on polyethylene film.

The *LD* spectra of vesicles containing DPH were measured at various concentrations in order to demonstrate the effectiveness of DPH as a probe for *LD*. The orientation method was Couette flow. Representative spectra are shown in Figures 6.2 and 6.3.

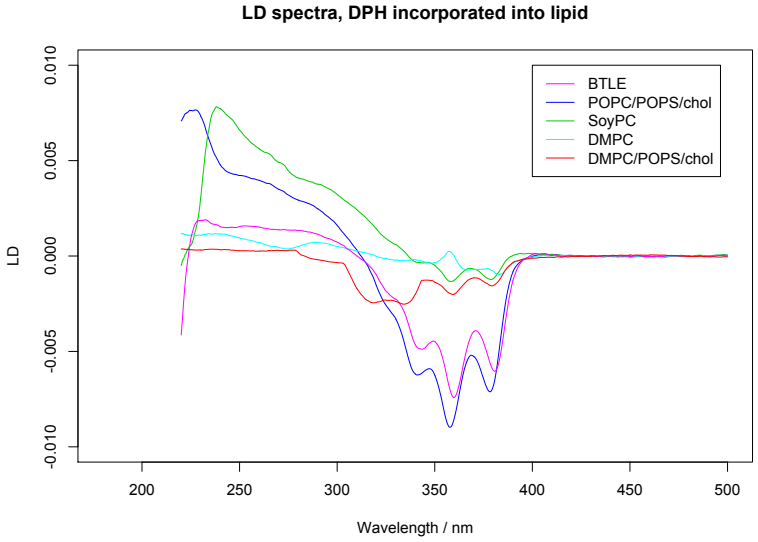

Figure 6.2: *LD* spectrum of DPH in lipid vesicles at approximately 50 mg/mL in aqueous buffer.

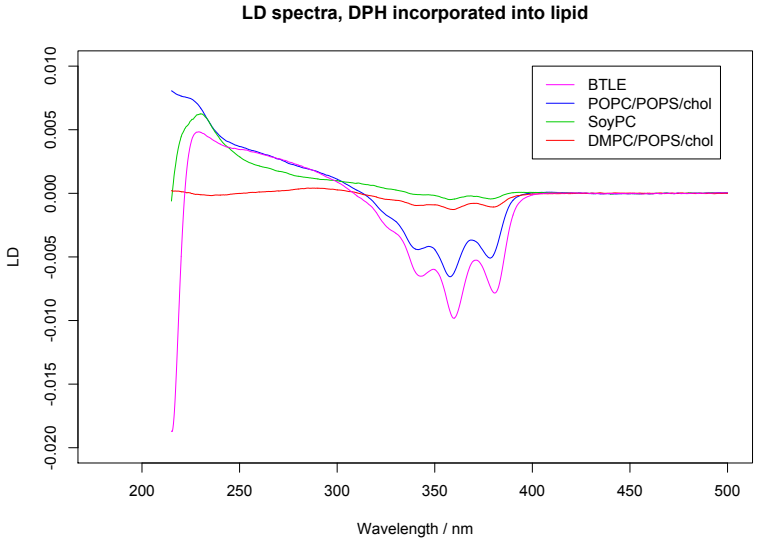

Figure 6.3: *LD* spectrum of DPH in lipid vesicles at approximately 25 mg/mL in aqueous buffer.

It was apparent from Figures 6.2 and 6.3 that DPH did not orient to the same extent in all cases, and that clear trends, or reproducibility, have not been achieved. However, the bands associated with DPH from Figure 6.1 are present to some extent in all case, and in some cases are extremely strong. Spectra gathered with BTLE and POPC/POPS/cholesterol, for example, are dominated by the DPH bands. In other cases, soybean PC for example, the bands are visible but not strong, and could be overwhelmed by introductions of other compounds. The bands for DPH have negative sign, indicating that the DPH orients as if it were another lipid in the membrane, *i.e.* it is parallel to the normal to the lipid surface.

The data shown in Figures 6.2 and 6.3 posed a problem, as it was necessary to determine standardised, optimised, methods for utilising DPH as an *LD* probe, and results from different lipid systems contradicted each other. The optimal bands for *LD* probes would be present and clear, but minimal, so as not to be confused with other analytes. It was, therefore, essential to reduce the strength of DPH *LD* bands, and also to reduce the amount of lipid required for the sample, so as to be comparable with the experiments presented in Chapters 4 and 5: *i.e.* 1 mM, or around that order of magnitude.

DPH was incorporated into revised vesicle systems, and the *LD* measured. These samples contained lipid at around 5 mg/mL. Figures 6.4, 6.5, 6.6 and 6.7 show *LD* spectra gathered for the lipid systems with DPH present. Figure 6.4 includes a spectrum without DPH to verify that DPH does not influence the position of the lipid band observed.

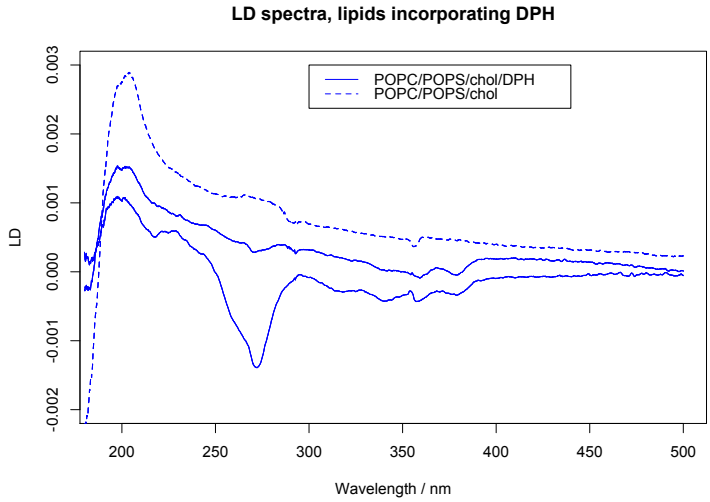

Figure 6.4: *LD* spectra of vesicles comprising POPC, POPS, cholesterol. Solid lines represent data gathered for vesicles also containing DPH, dotted line for vesicles without. Lipids at approximately 5 mg/mL. Path length of capillary was 500 μm.

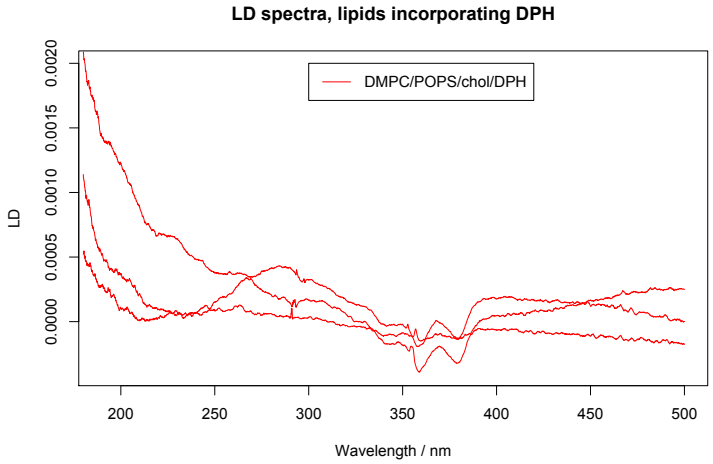

Figure 6.5: *LD* spectra of vesicles comprising DMPC, POPS, cholesterol and DPH. Lipids at approximately 5 mg/mL. Path length of capillary was 500 μm.

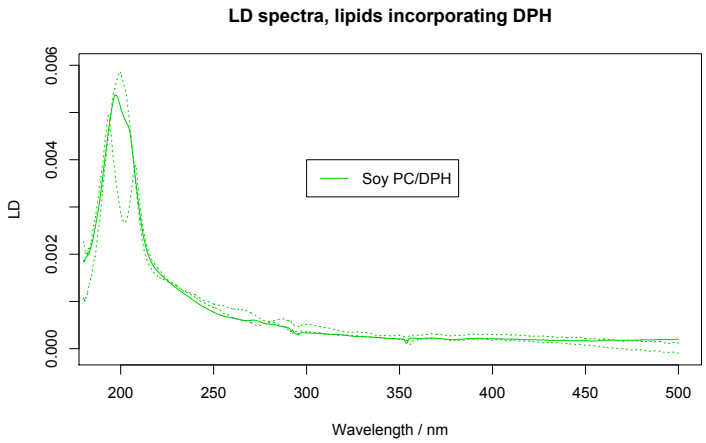

Figure 6.6: *LD* spectra of vesicles comprising soybean PC and DPH. Lipids at approximately 5 mg/mL. Path length of capillary was 500 μm.

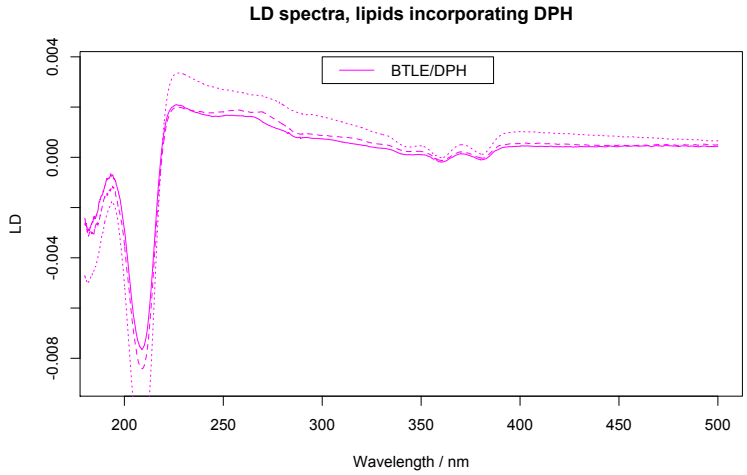

Figure 6.7: *LD* spectra of vesicles comprising brain total lipid extract and DPH. Lipids at approximately 5 mg/mL. Path length of capillary was 500 μm.

Some of the spectra presented in Figures 6.4, 6.5, 6.6 and 6.7 show that DPH gives still gives discernible bands under these revised conditions. The proportion of DPH used was optimised such that minimal bands would be observed in the POPC/POPS/cholesterol sample, thereby reducing any potential impact on a signal from protein. However, it is clear that the soybean PC vesicles do not display DPH *LD* signal at this concentration. DPH may not be able to incorporate into the soybean lipids, or may have its *LD* signal quenched by other vesicle components. The work presented in this thesis does not answer why this is the case. Extensive work may be required to determine why soybean PC prevents DPH giving strong *LD*. Unpublished data from the Rodger laboratory does appear to show that if the concentration of DPH is very high (around 10 % w/w), or if the lipid concentration is very high (over 50 mg/mL) it will generate an *LD* signal, however, this was not compatible with the experimental aims in this case.

Another interesting result from this set of data is the strikingly different shape of the spectrum for BTLE (Figure 6.7). While the other three systems have strongly positive signals around 200 nm, BTLE has a very sharp negative band here. This is not easily explained by usual factors such as scattering of light by vesicles, however there is no evidence of an absorption band at this wavelength for BTLE. Some combination of factors, including some scattering, may be responsible for this *LD* band. It is believed that the BTLE is such a complex extract the some components of the lipid mixture are able to give very strong negative *LD* signal when oriented in Couette flow, with their head groups oriented perpendicular to the direction of the flow. There *must* be some other chromophore, as yes unidentified.

The orientation parameter S was calculated for the DPH bands observed in these lipid/DPH *LD* spectra. The spectra were first corrected for sloping between 500 and 400 nm, so that the region around the DPH bands was as uniform as possible. Table 6.1 shows the values for S calculated here. An example of the method used for this calculation is given in Appendix C.

Table 6.1: Values for S calculated from DPH *LD* signal in lipid/DPH *LD* spectra (1 significant figure). An implementation of the method used for this calculation is given in Appendix C.

Lipid components	S
POPC/POPS/cholesterol	0.01
DMPC/POPS/cholesterol	0.001
Soybean PC	0.0003
BTLE	0.01

It may be noted that these values are lower than those reported in Chapter 3. This may indicate that the model should be reformulated, or that more data is needed before calculating S.

6.3.2 Lipid selection influences linear dichroism spectra

The *LD* spectrum of melittin was measured in the presence of different lipid vesicles. The lipids selected were the same as those used for melittin *CD* in Chapter 5, and melittin had adopted an α-helical structure when interacting with each lipid preparation.The *LD* spectrum of melittin in lipid has a shape characterised previously in the Rodger laboratory (Damianoglou *et al.*, 2010). The data in Figure 6.8 demonstrate that despite instrumental change, a similar spectrum is still observed. There is a strong band around 200 nm, and a weaker band, a shoulder, around 250 nm. Unfortunately there is interference in this band from some instrument-induced artefact around 270 nm, but the overall shape of the spectrum remains consistent. Importantly, the DPH bands are still clearly visible, confirming that the lipid vesicles themselves are oriented.

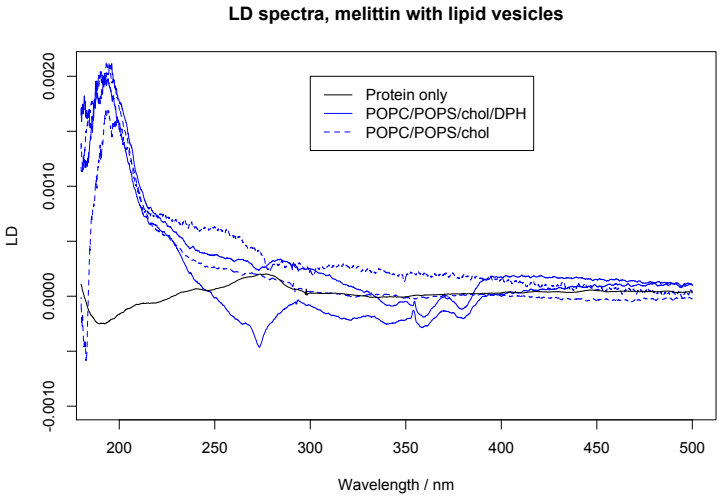

Figure 6.8: *LD* spectrum of melittin with POPC/POPS/cholesterol/DPH vesicles (solid blue traces), and POPC/POPS/cholesterol vesicles (dotted blue trace). Solid black trace is protein in solution in the absence of lipid.

Figure 6.9 shows the effect of using DMPC in the lipid mixture rather than POPC. It was demonstrated in Chapter 3 that despite its common use, this shorter chain lipid is not necessarily the most appropriate. Here we observe that the *LD* spectra generated are not consistent with each other, While the DPH signals are reasonably reproducible, the baseline shifts, and there is unpredictable peak broadening in some cases. In other cases, the band at 200 nm fails to develop at all. The conclusion here is that when DMPC is a major component of the vesicles used, an *LD* experiment carried out in this way may well fail.

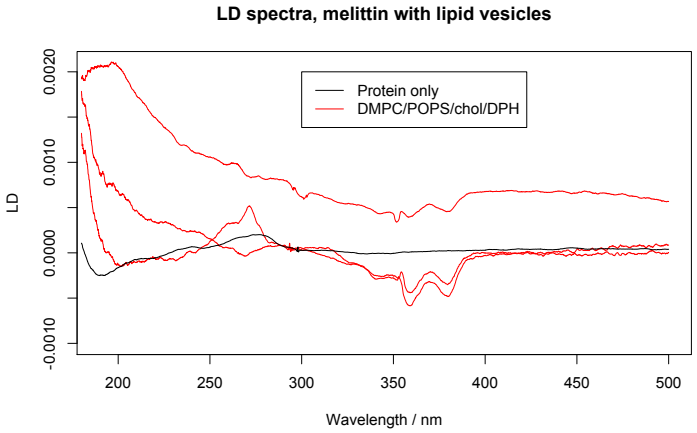

Figure 6.9: *LD* spectrum of melittin with DMPC/POPS/cholesterol/DPH vesicles (red traces). Solid black trace is protein in solution in the absence of lipid.

In the soybean PC case, Figure 6.10, the 200 nm band is not reliably reproduced. It is present in some repeats, absent in others. The lack of clear DPH peaks discussed above makes it impossible to say whether this is due to lipids failing to orient, or protein failing to insert into the lipid. Again, the conclusion is that although this lipid extract is easily obtained, cost-effective, and easy to handle, it is not appropriate for this style of experiment.

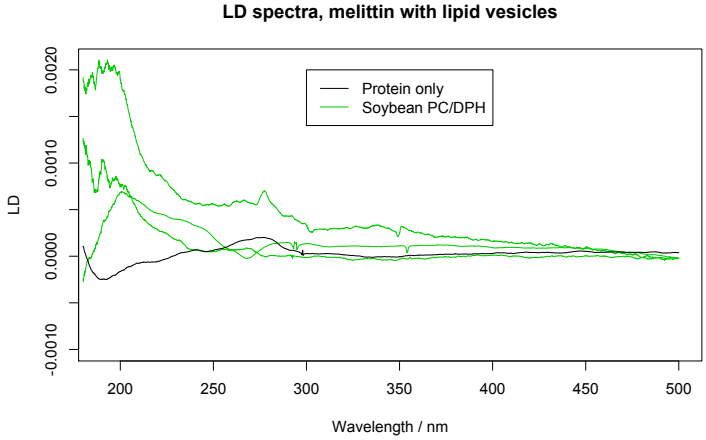

Figure 6.10: *LD* spectrum of melittin with soybean PC/DPH vesicles (green traces). Solid black trace is protein in solution in the absence of lipid.

Figure 6.11 shows that the melittin plus BTLE *LD* spectra are consistent and clear. We observe the DPH bands, as well as the characteristic negative BTLE band. It is also striking that the positive band at 200 nm is present in this case, whereas it was absent in the lipid/DPH spectra shown earlier. BTLE is a lipid extract of interest because of the neurodegeneration aspect to this work. The fact that promising *LD* spectra are generated in this context makes it a very promising candidate for further work.

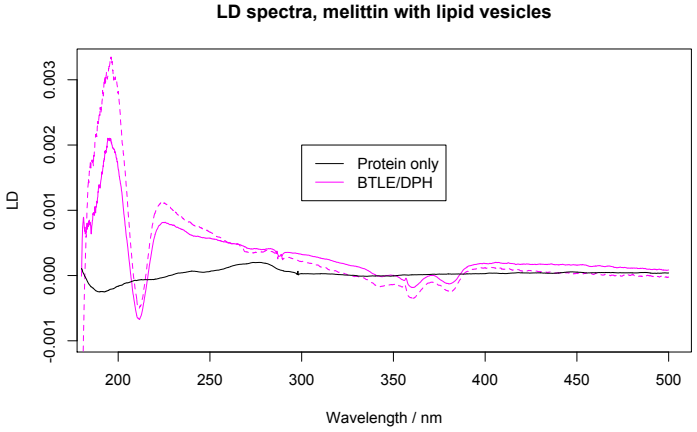

Figure 6.11: *LD* spectrum of melittin with BTLE/DPH vesicles (pink traces). Solid black trace is protein in solution in the absence of lipid.

6.3.3 Linear dichroism measurements of α-synuclein with lipid vesicles

Monomeric α-synuclein was mixed with lipid vesicles, and its *LD* spectrum measured. Initially, the lipid preparation was by the simpler method of sonication rather than extrusion, *i.e.* the method used in Sections 4.3.1 and 5.3.1. This produced the data shown in Figure 6.12. These data show no *LD* bands, and no effect of lipid concentration on the spectra. It was deduced that this sample preparation is not appropriate for these experiments.

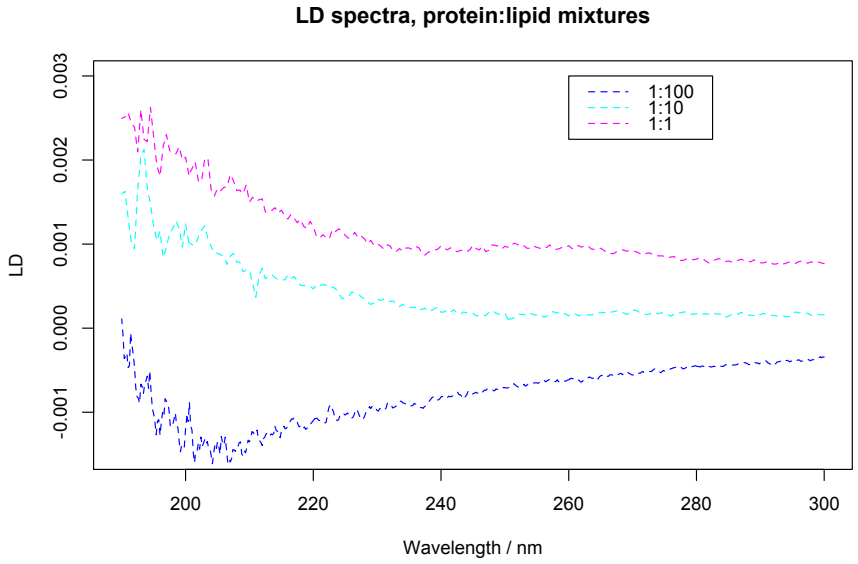

Figure 6.12: *LD* spectra of α-synuclein with POPC/POPS/cholesterol vesicles at different molar ratios of protein:lipid.

The effect of sonication on a lipid suspension is to generate unilamellar vesicles, as required in these experiments, however this process will lead to other consequences. The length of time sonication is performed will affect the average particle size, and will usually result in a sample with a large dispersity of particle size. Such a sample would be expected to scatter light unpredictably, thereby reducing data quality. Extrusion, on the other hand, usually results in a narrow distribution of particle sizes. Due to the poor quality of the data shown

in Figure 6.12, the lipid preparation method was altered to use the same method as for the results gathered in Sections 6.3.1 and 6.3.2. The vesicles chosen were the same as those selected as for the *LD* cell experiment in Chapter 5: POPC/POPS/cholesterol, and brain total lipid extract. Figures 6.13 and 6.14 show the *LD* spectra gathered for α-synuclein mixed with POPC/POPS/ cholesterol/DPH vesicles. A band is clearly visible at 200 nm, as are the bands for DPH discussed above. An artefact is present in some spectra at 270 nm due to an instrumental issue.

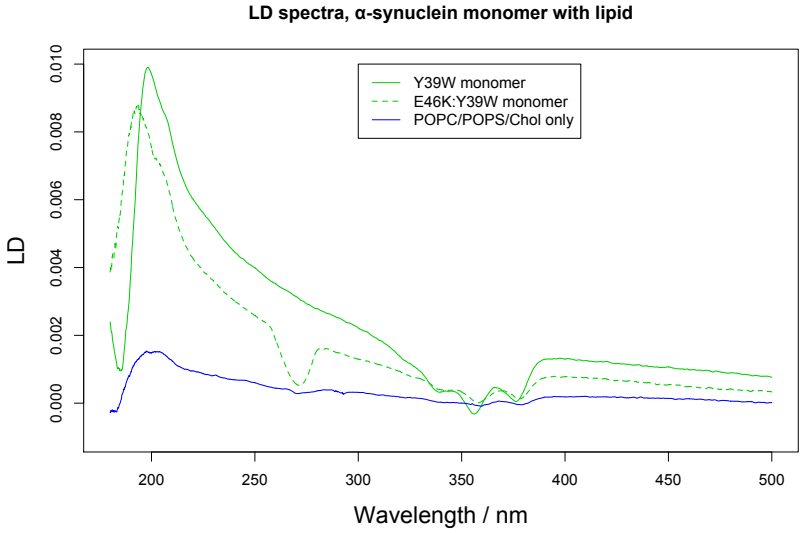

Figure 6.13: *LD* spectra of α-synuclein with POPC/POPS/cholesterol/DPH vesicles. Green traces are for monomeric protein samples with lipid, blue for lipid only. Solid line for Y39W, dashed line for E46K:Y39W. An aberration is observed at around 270 nm due to an instrumental fault, however the rest of the curve is believed to be sound.

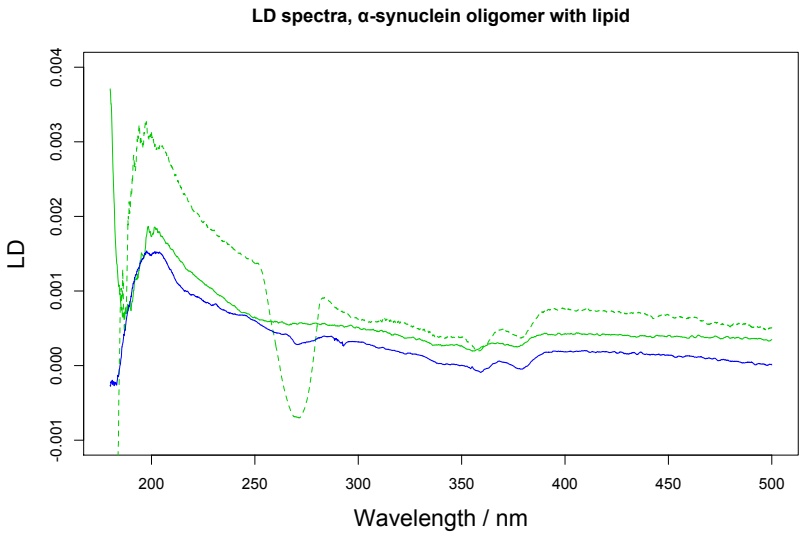

Figure 6.14: *LD* spectra of α-synuclein with POPC/POPS/cholesterol/DPH vesicles. Green traces are for oligomeric protein samples with lipid, blue for lipid only. Solid line for Y39W, dashed line for E46K:Y39W. An aberration is observed at around 270 nm due to an instrumental fault, however the rest of the curve is believed to be sound.

Figures 6.15 and 6.16 show *LD* spectra gathered for α-synuclein with BTLE/DPH vesicles. Similarly to Figures 6.7 and 6.11, a negative band was present at around 210 nm. One spectrum has a disrupted baseline but the DPH bands and protein band are as expected.

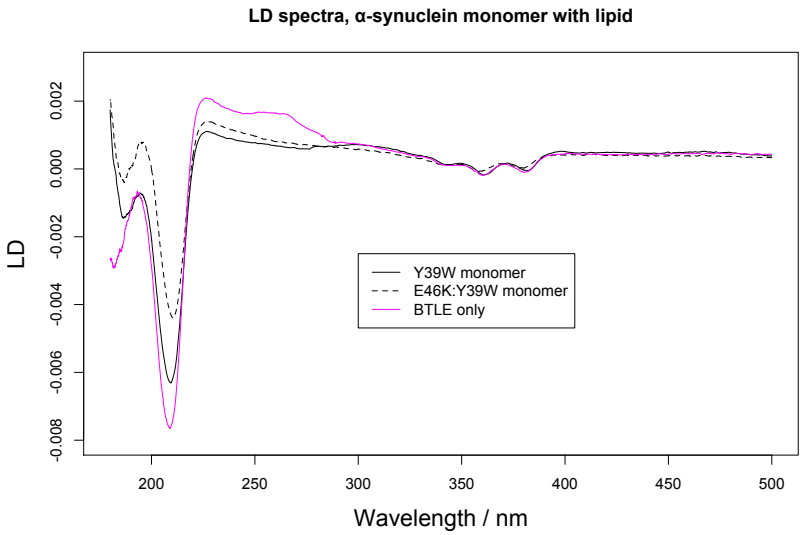

Figure 6.15: *LD* spectra of α-synuclein with BTLE/DPH vesicles. Black traces are for monomeric protein samples with lipid, pink for lipid only. Solid line for Y39W, dashed line for E46K:Y39W.

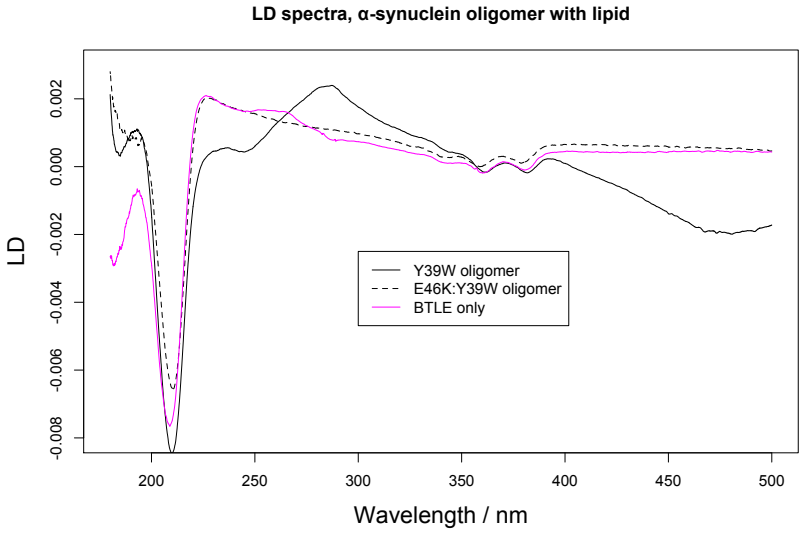

Figure 6.16: *LD* spectra of α-synuclein with BTLE/DPH vesicles. Black traces are for monomeric protein samples with lipid, pink for lipid only. Solid line for Y39W, dashed line for E46K:Y39W. An aberrant baseline is observed in the Y39W spectrum, however the bands at the lowest wavelengths are believed to be sound.

While Figures 6.13, 6.14, 6.15 and 6.16 do show bands of *LD* signal, it is not clear by eye whether this is due to the protein or the lipid present, and if there is a difference between the monomer and oligomer cases, or between the Y39W and E46K:Y39W cases. Hence difference spectra were created. These were generated by subtracting the spectra for lipid with DPH from the spectra for protein with lipid and DPH. This process has the effect of increasing noise and enhancing aberrations in the spectra, but does present the *LD* signal for the oriented protein alone. These difference spectra are shown in Figures 6.17, 6.18, 6.19 and 6.20.

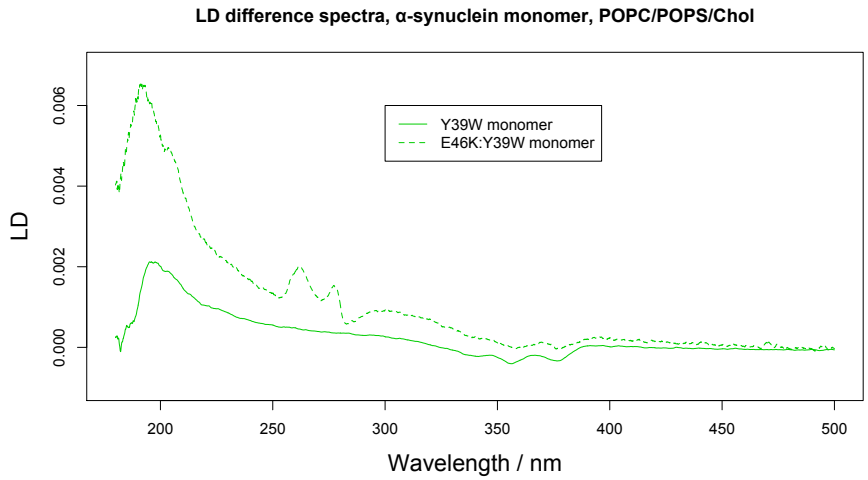

Figure 6.17: *LD* difference spectra for α-synuclein monomer mixed with POPC/POPS/ cholesterol/DPH vesicles, where lipid spectra have been subtracted from protein + lipid spectra. Aberrations at around 270 nm have been exacerbated by this process.

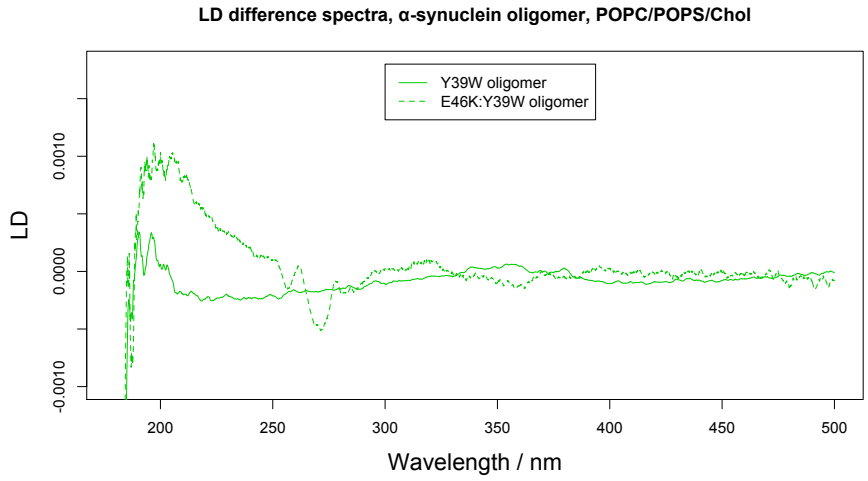

Figure 6.18: *LD* difference spectra for α-synuclein oligomer mixed with POPC/POPS/ cholesterol/DPH vesicles, where lipid spectra have been subtracted from protein + lipid spectra. Aberrations at around 270 nm have been exacerbated by this process.

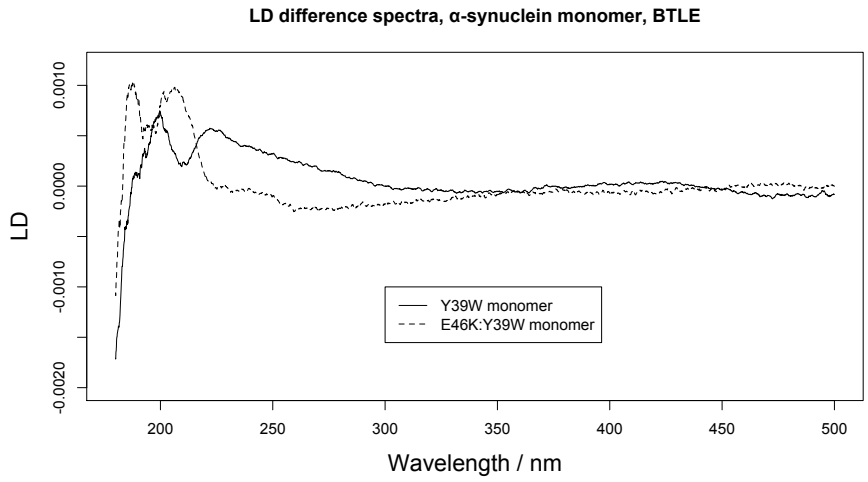

Figure 6.19: *LD* difference spectra for α-synuclein monomer mixed with BTLE/DPH vesicles, where lipid spectra have been subtracted from protein + lipid spectra. Aberrations at around 270 nm have been exacerbated by this process.

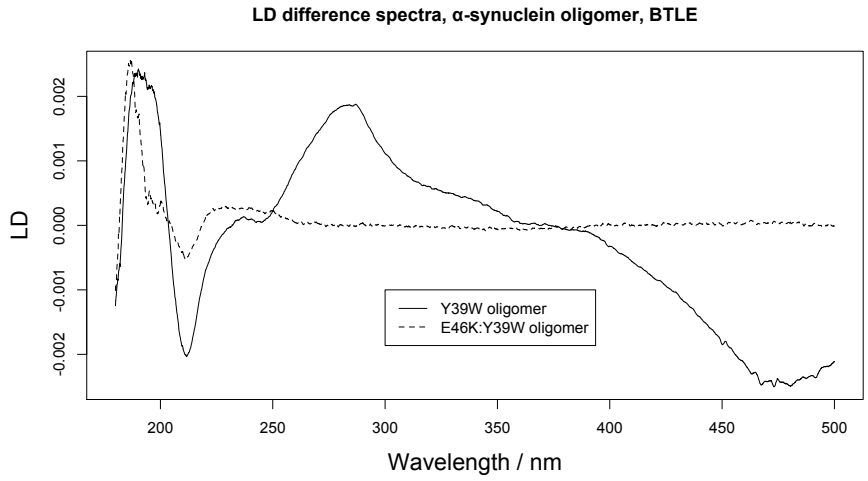

Figure 6.20: *LD* difference spectra for α-synuclein oligomer mixed with BTLE/DPH vesicles, where lipid spectra have been subtracted from protein + lipid spectra. Aberrations have been exacerbated by this process.

There is one important problem with combining two *LD* spectra in this manner: since spectra are combined linearly, the range of error is doubled, reducing the significance of conclusions drawn from the data. However, the difference spectra provide good data here. From the green traces in Figure 6.17 and the black traces in Figure 6.19, we observe that the monomeric α-synuclein has a positive band, similar to that for melittin, around 200 nm. This indicates that the protein is oriented in the same direction as the Couette flow – along the surface of the long side of compressed vesicles. This confirms the NMR data cited above in an entirely different experimental setup.

In POPC/POPS/cholesterol vesicles (Figure 6.18), the oligomer does not have this 200 nm band at anything near the same magnitude. It could be said that something of a band remains here, but not reproducibly so. In short, the oligomer has not oriented parallel to, or perpendicular to, the Couette flow, and therefore there is no data in this Figure to suggest the oligomer has interacted with the lipids. In BTLE (Figure 6.20), the oligomer samples give a negative band at 205 nm, the same position as the negative band for BTLE alone. In this case, therefore, the protein has generated even greater negative signal, implying that the protein oligomer has inserted into the membrane, as discussed in Section 1.8.3 and Figure 1.19. The oligomer is oriented perpendicular to the Couette flow, suggesting that in this case the oligomer has inserted across the membrane. This potentially validates the hypothesis that oligomers act as pores through the membrane, and is the first time *LD* has been used to show this result.

However, the signals and bands obtained are weak, and therefore do not represent a strong argument at this point. It is recommended that further study be carried out into other improvements to technique or sample preparation, in order to obtain higher quality data.

6.4 Conclusions

The results presented in this chapter give promising scope for the use of DPH as an *LD* probe. This easily-handled compound is incorporated into some types of vesicles readily, and gives good, reproducible *LD* signal. In some cases, however, insertion is not observed at low concentrations, so some screening before proceeding with a lipid choice is necessary. This is unfortunately true of soybean PC, which is a good lipid system in many other experimental types.

Instrumental technology has evolved over the last decade or so, and at times *LD* data has not been reproducible between generations. The data on *LD* of melittin shows that the latest instruments (namely the Jasco J-1500) reproduce features of melittin spectra generated in the past. This allows us to proceed with confidence, and use the technique to probe more deeply into protein-lipid interactions.

This chapter also shows that *LD* has the potential to be a powerful tool in understanding amyloid oligomers. These experiments have shown that it is possible to detect whether or not an amyloid oligomer preparation with interact with a lipid vesicle preparation, opening routes to straightforward screening assays - several oligomer preparations could be presented with several lipid preparations and then pairs that gave *LD* signal taken forward for more detailed study. There is also the intriguing prospect of measuring the formation of oligomers. The positive *LD* signal observed for monomeric α-synuclein would be reduced and replaced with the negative oligomeric signal. Conditions obviously need to be improved to observe this process, and potentially need incubation over long periods of time. No indication of oligomerisation was observed in the experiments reported here.

The quality of *LD* difference spectra was low in the experiments presented here. Some further refinement of the technique and sample preparation will be necessary to fully

understand the LD obtained from α-synuclein–lipid experiments.

Chapter 7

Discussion

There were two major interlinking themes to the work described above: the ability of two constructs of α-synuclein to interact with lipids, and the understanding and manipulation of vesicles in Couette flow. The link between these themes was in using linear dichroism to study the protein-lipid interaction, generating results giving clues to the method of toxicity of the protein: a cause of Parkinson's Disease. The interdisciplinary approach taken to the work has led to a collection of studies giving insights into amyloid-lipid interaction, lipid vesicle behaviour, and good practice for *LD* experimentation.

7.1 Amyloid-lipid interaction

It has been emphasised many times in this thesis that key to the function and disfunction of α-synuclein is its interactions with lipids. Whether its true role is in vesicle transport or not, its interactions with lipids are the major focus of the field (Lotharius & Brundin, 2002; Auluck *et al.*, 2010; Pfefferkorn & Lee, 2010; Fantini & Yahi, 2011). The combination of intrinsic tryptophan fluorescence and circular dichroism presented in this work, has allowed investigation into a protein-lipid interaction in more detail than before – that of α-synuclein and POPS. Two constructs of the protein were used, one with the Parkinson's Disease mutation E46K, and both with the mutation Y39W. The *CD* and fluorescence data gathered demonstrated two aspects of the lipid interaction very clearly – the change

in secondary structure of the protein, and the change in environment of the aromatic tryptophan.

As the environment of the tryptophan residue changed, as it became buried in the lipid membrane, a shift in λ_{max} was observed. This shift was recorded, and plotted against the ratio of lipid:protein in the samples, thereby giving binding curves. Binding curves were also obtained by plotting the same lipid:protein molar ratio against the *CD* signal at 208 nm and 222 nm (the positions of α-helix bands in *CD*). Apparent dissociation constants were obtained from these measurements that indicated both processes were occurring at roughly similar lipid:protein ratios. While the data may be improved by further work, this result implies that when the protein encounters the lipid vesicle and interacts, it adopts its folded structure. There would likely not be a population of unfolded protein anchored by the tryptophan to the membrane, though there could be some bound, aggregated protein.

It was believed that the interaction between POPS and α-synuclein was non-specific, and due to the charge on the lipid head group. Several other lipids were used in combination, in order to determine if binding by different methods was possible. Cholesterol, SM1, and GM1 did not influence binding. This was of some concern, as GM1 has been shown to bind α-synuclein in other studies. It is believed that the Y39W mutation removed this binding ability, despite the similarity in size and structure of tyrosine and tryptophan, shown in Figure 7.1.

From the work presented here, and that of Fantini and Yahi, we may conclude that Y39 is crucial for interaction with GM1, and not simply because of its hydrophobicity (Fantini & Yahi, 2011). However, in their simulations, it was shown that Y39F still retains its ability to bind the ganglioside GM3, and only a substitution for a small group, like the methyl obtained by the Y39A mutation, will remove the binding. In their study, the flanking lysine residues, K34 and K45, play just as important a role as Y39 in the interaction.

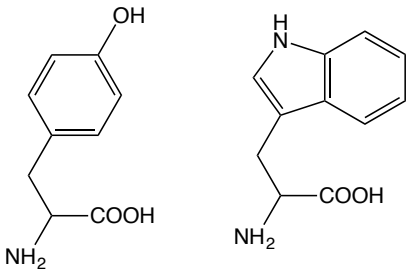

Figure 7.1: *(left)* Tyrosine and *(right)* Tryptophan.

The mutated proteins in this thesis still retain these lysine residues, so why the binding ability is lost by Y39W remains unclear. This warrants deeper study, as GM1 or other gangliosides, enriched in brain lipids, could be key to the PD-causing ability of α-synuclein, as they may be for prion protein diseases (Sanghera *et al.*, 2011).

The lipid binding experiments represent a more thorough study of the ability of these two constructs of α-synuclein to interact with carefully selected model membranes than has gone before. This data should be complemented with data for wild type protein in order to more fully understand the implications for Parkinson's Disease mechanisms, but it has value as a standalone study in its own right. The possible loss of ability to interact with GM1 may explain why there are no very dramatic differences between the constructs examined here, or perhaps we should not expect such differences as PD is clearly a very subtle disease that takes many decades to become apparent. In any case, these data are relevant and useful for any researcher aiming to carry out similar studies considering using Y39W constructs. They would have to prepare to use WT much more extensively.

7.2 Lipid vesicle behaviour

A combination of classic dye-leakage assay and Couette flow revealed that vesicles formed from some lipids can withstand the forces involved in *LD* much better than others. This

was an important result for lipid biophysics, as lipid selection may heavily influence the quality of data obtained if any shear flow was required by an experiment. Certain lipids, such as the DMPC commonly used in NMR experiments, did not seem to have any integrity once formed into vesicles. It was shown, however, that combining DMPC with the longer POPS, and cholesterol, enabled it to be stable in *LD*, although it still failed to generate completely reproducible data. Other lipids were much more reliable, and would make vesicles capable of enduring *LD*, POPC for example.

The calcein leakage in flow assay also gave rise to a new experimental design. While not employed here, it was determined that the relationship between calcein concentration and the position of its $\lambda_{\max}$ was robust enough to use as a calibration curve. A suitable experimental design would be able to determine the concentration of calcein from $\lambda_{\max}$, rather than in the relative terms as presented in this thesis. The fact that calcein fluorescence exhibits this property, of concentration-dependent shift may be useful to several lipid-using fields. Lipid preparation methods are varied in protocol and in results, and it may be difficult to accurately determine the concentration of lipid or other sample components. Often, the leakage of the vesicle is the important result, for example when studying pore-forming proteins from infectious agents, hence the use of calcein. This result allows concentration of calcein to be accurately measured, therefore reducing some uncertainty in such an experiment.

Theoretical work was carried out to understand further vesicles in flow. It was possible to obtain a range of possible length and radius parameters, and then implement the method of McLachlan *et al.* to calculate the orientation parameter S of vesicles with those dimensions. It was determined that a vesicle would be stretched to be around three times as long as they were wide in the flow, if it was to generate the observed values for S. This validated experimental data from other work (Mader *et al.*, 2006).

7.3 Good practice in linear dichroism

As demonstrated by Figure 6.12, samples that would be expected to give *CD* signals and fluorescence signals do not necessarily give *LD* signals. This may be due to chromophores in the samples not orienting, or may be due to poor sample preparation. Lipids are notoriously light-scattering in spectroscopy, and the data shown in Figure 6.12 demonstrate that overcoming this characteristic in one technique does not solve the issue in another. The sonication method of vesicle preparation used in Chapter 4, was not suitable for generating good *LD* data. Once the extrusion method was adopted, as used in Chapter 3, good *LD* spectra were generated, shown in Figures 6.4 and 6.7, for example. Data were generated for lipids with and without DPH, for lipids and melittin together, and for lipids and α-synuclein together. While the quality for α-synuclein spectra was low, this was the first time such data has been gathered for either the monomeric or oligomeric forms of the protein. Work that further optimised the technique could answer questions about the toxicity of the protein: if we knew that oligomers inserted across the membrane and the resulting pore was responsible for cell death, a drug target could be the pore itself. If the oligomer does not cross the membrane but lies on the surface, then this interaction may represent a target for intervening in Parkinson's Disease.

It was apparent from the data gathered for lipid behaviour that only certain lipids can endure the Couette flow aspect of *LD* experiments. Vesicles made from POPC/POPS/ cholesterol, and extruded rather than sonicated, have the most optimal characteristics of those studied in this work. However, vesicles prepared from brain total lipid extract were also well suited to *LD*. These provided a novel lipid mixture for studies of this kind, and did give some data, but the lipids themselves require additional study. The very strong negative *LD* band they generate has been shown to be characteristic of this mixture, but has not been attributed to any specific component as yet. It would be desirable to delve more deeply into why this characteristic spectrum is generated, before using BTLE for

further *LD* of proteins.

Chapter 8

Conclusions and future work

8.1 Conclusions

It has been shown in this thesis that in order to achieve experimentally feasible values for the orientation parameter S, vesicles of around 100 nm diameter should be compressed, and stretched to around 180 nm in length. This causes their volume to decrease by 25 %, and the shape to change from sphere to capsule around three times longer than the width. When dye-leakage assays were carried out, however, it was determined that this is not true for different types of vesicles. Vesicles of different compositions behave differently in flow, with some compositions (*e.g.* pure DMPC) leaking vastly more of their contents even without flow. Only two of the vesicle types tested here compared favourably to the theoretical data: POPC/POPS/cholesterol, and DMPC/POPS/cholesterol. Vesicle choice, therefore, may be considered crucial to any lipid shear flow experimental design.

By measuring the shift in tryptophan fluorescence emission, the ability of two Y39W-containing α-synuclein constructs to interact with lipid vesicles was measured. In the data presented here, only POPS was found to bind the protein, with POPC, cholesterol, GM1 and SM1 not showing any increase on the binding affinity. Indeed, the more complex the SUVs used in this experiment, the lower the binding affinity seemed to be. It was shown that the predicted ability of the protein to interact with GM1 is not detected here. One explanation for this is that the Y39 residue is key for this interaction, and Y39W is not

sufficiently similar to retain binding ability. Similar binding data to those obtained from fluorescence were obtained from circular dichroism experiments. Since the dissociation constants observed were fairly similar in both cases, it may be concluded that the folding of the protein to α-helix occurs at similar lipid:protein ratios as the insertion of W39 into the lipid bilayer. Differences between E46K and WT protein that may be apparent in a future experiment using GM1 could have been obscured here due to the Y39W mutation, so the main conclusion from this work is that E46K:Y39W and Y39W interact with lipids with similar affinity.

CD data presented in this thesis also demonstrated that viable spectra may be obtained even when using the *LD* cell. Small volumes of sample (50 – 100 μL) generated strong spectra even with lipids present, and despite the non-optimal shape of the *LD* capillary. Spectroscopists may use this system with confidence if they wish to quickly determine the secondary structure of protein samples before gathering *LD* spectra. The system is not perfect, however, and some aberrations still exist. These were revealed in measuring the *CD* spectrum of α-synuclein in various forms, so further optimisation would be needed to get the most out of the technique. It has been shown here that the α-synuclein monomers used in this work fold to α-helix from random coil as expected, and this is observable in data gathered in the *LD* cell. The α-synuclein oligomers used here maintain their β-sheet folding in the presence and absence of lipid, indicating their stability. Since they seem not to be altered by the vesicles, they may form viable pores in the membrane, or they may not to interact with the membrane at all.

DPH has been validated in this work as a good probe for *LD* of vesicles. It has clear bands on the *LD* spectra, and appears to incorporate into most of the lipids tested here. In some cases, such as soybean PC, it does not perform as well, however, and different probes may be more suitable. It was shown that *LD* of melittin in different sorts of lipids than those tested previously can be measured and gives data comparable to that in the literature, with the interesting exception that vesicles of DMPC/POPS/cholesterol seem to not be

reliable, only giving usable data on some occasions. When the *LD* of α-synuclein was measured, it was found that the signals were difficult to interpret by eye, and difference spectra were required to remove the *LD* of the lipids used. These showed that in general the protein oriented on the vesicle surface, but in one case (oligomeric α-synuclein with brain total lipid extract) appears to insert across the membrane, supporting the hypothesis that amyloid oligomers act as membrane pores. However, more data and a more reliable quality of data would be needed to make this case strongly. The data gathered were not of convincing quality, and only hint at underlying mechanisms.

8.2 Suggestions for future work

- ***LD* of α-synuclein to be strengthened**

  Difference spectra were required here to observe the weak signals generated by the protein. It might be beneficial to take conditions and concentrations that are less representative of biology to get improved *LD* here. Stronger signal:background would improve the data. Some technical problems were encountered following adoption of new instruments. Correcting these errors should improve the data gathered.

- **Understanding the effect of the Y39W mutation**

  The choice of Y39W constructs of α-synuclein was justified by its proximity to the residues associated with Parkinson's Disease, but may be flawed if Y39 is essential for the interaction with GM1. Were it to be proved that interaction with GM1 is critical to development of PD, it would be vital to understand both this interaction, and why Y39W damages it. A preliminary attempt at solving this problem is shown in Appendix A.

- **Understanding the poor *LD* signal of DPH in soybean PC**

  The *LD* signal of DPH appears suppressed in soybean PC, especially when compared

to its signal in the other lipid systems. Soybean PC is usually an ideal lipid mixture to work with – a natural extract, cheap, easy to handle, and with reasonable solubility in chloroform – so ruling it out for this sort of lipid work is not desirable. While DPH *LD* signal can be achieved in soybean PC, the concentration of DPH or of lipid in the sample must be much higher than required for the experiments presented here. Some work solving why this should be the case might go a long way to improving insertion of compounds into membranes generally, and may improve the quality of *LD* overall.

- **Understanding BTLE**

  While BTLE has provided interesting data in this thesis, a question remains over what causes its characteristic negative *LD* band. The lipid mixture itself is poorly characterised, but a thorough attempt at this, perhaps by FTICR mass spectrometry, might shed some light on which components would be oriented perpendicular to membrane normal.

Bibliography

Allen, T M & Cleland, L G. 1980. Serum-induced leakage of liposome contents. *Biochimica et Biophysica Acta (BBA) - Biomembranes*, **597**(2), 418–426.

Apetri, Mihaela M; Maiti, Nakul C; Zagorski, Michael G; Carey, Paul R & Anderson, Vernon E. 2006. Secondary Structure of α-Synuclein Oligomers: Characterization by Raman and Atomic Force Microscopy. *Journal of Molecular Biology*, **355**(1), 63–71.

Appel-Cresswell, Silke; Vilarino-Guell, Carles; Encarnacion, Mary; Sherman, Holly; Yu, Irene; Shah, Brinda; Weir, David; Thompson, Christina; Szu-Tu, Chelsea; Trinh, Joanne *et al.* 2013. Alpha-synuclein p.H50Q, a novel pathogenic mutation for Parkinson's disease. *Movement Disorders*, **29**(Mar.), 811–813.

Ardhammar, Malin; Mikati, Nabil & Nordén, Bengt. 1998. Chromophore Orientation in Liposome Membranes Probed with Flow Dichroism. *Journal of the American Chemical Society*, **120**(38), 9957–9958.

Auluck, Pavan K; Caraveo, Gabriela & Lindquist, Susan. 2010. α-Synuclein: Membrane interactions and toxicity in Parkinson's Disease. *Annual review of cell and developmental biology*, **26**, 211–233.

Bagchi, Prosenjit & Kalluri, R. 2009. Dynamics of nonspherical capsules in shear flow. *Physical Review E*, **80**(1), 016307.

Bartels, Tim; Choi, Joanna G & Selkoe, Dennis J. 2011. α-Synuclein occurs physiologically as a helically folded tetramer that resists aggregation. *Nature*, **477**, 107–111.

Bellucci, Arianna; Navarria, Laura; Zaltieri, Michela; Missale, Cristina & Spano, Pierfranco. 2012. Alpha-synuclein synaptic pathology and its implications in the development of novel therapeutic approaches to cure Parkinson's disease. *Brain research*, **1432**(Jan.), 95–113.

Biben, Thierry; Farutin, Alexander & Misbah, Chaouqi. 2011. Three-dimensional vesicles under shear flow: Numerical study of dynamics and phase diagram. *Physical Review E*, **83**(3), 031921.

Bradford, M M. 1976. A rapid and sensitive method for the quantitation of microgram quantities of protein utilizing the principle of protein-dye binding. *Analytical biochemistry*, **72**(May), 248–254.

Breckenridge, W C; Gombos, G & Morgan, I G. 1972. The lipid composition of adult rat brain synaptosomal plasma membranes. *Biochimica et biophysica acta*, **266**(3), 695–707.

Burke, Kathleen A; Yates, Elizabeth A & Legleiter, Justin. 2013. Amyloid-Forming Proteins Alter the Local Mechanical Properties of Lipid Membranes. *Biochemistry*, **52**(5), 808–817.

Bussell, Jr, Robert & Eliezer, David. 2003. A Structural and Functional Role for 11-mer Repeats in α-Synuclein and Other Exchangeable Lipid Binding Proteins. *Journal of Molecular Biology*, **329**(4), 763–778.

Bussell, Jr, Robert & Eliezer, David. 2004. Effects of Parkinson's disease-linked mutations on the structure of lipid-associated α-synuclein. *Biochemistry*, **43**, 4810–4818.

Bussell, Jr, Robert; Ramlall, Trudy F & Eliezer, David. 2005. Helix periodicity, topology, and dynamics of membraneassociated αSynuclein. *Protein science*, **14**, 862–872.

Calissano, Pietro; Alemà, Stefano & Rusca, Graziella. 1972. Effect of haemoglobin on liposome permeability to Rb^+ and other solutes. *Biochimica et Biophysica Acta (BBA) - Biomembranes*, **255**(3), 1009–1013.

Carafa, M; Santucci, E; Alhaique, F; Coviello, T; Murtas, E; Riccieri, F M; Lucania, G & Torrisi, M R. 1998. Preparation and properties of new unilamellar non-ionic/ionic surfactant vesicles. *International journal of pharmaceutics*, **160**(1), 51–59.

Chandra, Sreeganga S; Chen, Xiaocheng; Rizo, Josep; Jahn, Reinhard & Südhof, Thomas C. 2003. A broken a-helix in folded a-synuclein. *Journal of Biological Chemistry*, **278**(17), 15313–15318.

Choi, Woong; Zibaee, Shahin; Jakes, Ross; Serpell, Louise C; Daveltov, Bazbek; Crowther, R Anthony & Goedert, Michel. 2004. Mutation E46K increases phospholipid binding and assembly into filaments of human α-synuclein. *FEBS letters*, **576**, 363–368.

Conway, K A; Harper, J D & Lansbury, P.T. 1998. Accelerated in vitro fibril formation by a mutant α-synuclein linked to early-onset Parkinson disease. *Nature Medicine*, **4**(11), 1318–1320.

Cotman, Carl; Blank, M L; Moehl, Anita & Snyder, Fred. 1969. Lipid composition of synaptic plasma membranes isolated from rat brain by zonal centrifugation. *Biochemistry*, **8**(11), 4606–4612.

D M Michaelson, G Barkai Y Barenholz. 1983. Asymmetry of lipid organization in cholinergic synaptic vesicle membranes. *Biochemical Journal*, **211**(1), 155.

Damianoglou, Angeliki; Rodger, Alison; Pridmore, Catherine J; Dafforn, Timothy R; Mosely, Jackie A; Sanderson, John M & Hicks, Matthew R. 2010. The synergistic action of melittin and phospholipase A2 with lipid membranes: development of linear dichroism for membrane-insertion kinetics. *Protein and peptide letters*, **17**(11), 1351–1362.

Danzer, Karin M; Haasen, Dorothea; Karow, Anne R; Moussaud, Simon; Habeck, Matthias; Giese, Armin; Kretzschmar, Hans; Hengerer, Bastian & Kostka, Marcus. 2007. Different Species of α-Synuclein Oligomers Induce Calcium Influx and Seeding. *The Journal of Neuroscience*, **27**, 9220–9232.

Davidson, W Sean; Jonas, Ana; Clayton, David F & George, Julia M. 1998. Stabilization of α-Synuclein Secondary Structure upon Binding to Synthetic Membranes. *The Journal of biological chemistry*, **273**(16), 9443–9449.

de Haas, K H; Blom, C; van den Ende, D; Duits, M H G & Mellema, J. 1997. Deformation of giant lipid bilayer vesicles in shear flow. *Physical Review E*, **56**(6), 7132–7137.

de Jongh, Harmen HJ; Goormaghtigh, Erik & Killian, J Antoinette. 1994. Analysis of circular dichroism spectra of oriented protein-lipid complexes: toward a general application. *Biochemistry*, **33**(48), 14521–14528.

Deschamps, J; Kantsler, V & Steinberg, V. 2009. Phase Diagram of Single Vesicle Dynamical States in Shear Flow. *Physical review letters*, **102**(11), 118105.

Di Pasquale, Eric; Fantini, Jacques; Chahinian, Henri; Maresca, Marc; Taïeb, Nadira & Yahi, Nouara. 2010. Altered ion channel formation by the Parkinson's-Disease-linked E46K mutant of α-Synuclein is corrected by GM3 but not by GM1 gangliosides. *Journal of Molecular Biology*, **397**, 202–218.

Dietrich, C; Bagatolli, L A; Volovyk, Z N; Thompson, N L; Levi, M; Jacobson, K & Gratton, E. 2001a. Lipid rafts reconstituted in model membranes. *Biophysical Journal*, **80**(3), 1417–1428.

Dietrich, C; Volovyk, Z N; Levi, M; Thompson, N L & Jacobson, K. 2001b. Partitioning of Thy-1, GM1, and cross-linked phospholipid analogs into lipid rafts reconstituted in supported model membrane monolayers. *Proceedings of the National Academy of Sciences of the United States of America*, **98**(19), 10642–10647.

Dikiy, Igor & Eliezer, David. 2012. Folding and misfolding of α-synuclein on membranes. *Biochimica et Biophysica Acta (BBA) - Biomembranes*, **1818**(4), 1013–1018.

Dusa, Alexandra; Kaylor, Joanna; Edridge, Shauna; Bodner, Nika; Hong, Dong-Pyo & Fink, Anthony L. 2006. Characterization of oligomers during alpha-synuclein aggregation using intrinsic tryptophan fluorescence. *Biochemistry*, **45**(8), 2752–2760.

Eliezer, David; Kutluay, Esin; Bussell, Jr, Robert & Browne, Gillian. 2001. Conformational properties of α-synuclein in its free and lipid-associated states. *Journal of Molecular Biology*, **307**(4), 1061–1073.

Fantini, Jacques & Yahi, Nouara. 2010. Molecular insights into amyloid regulation by membrane cholesterol and sphingolipids: common mechanisms in neurodegenerative diseases. *Expert reviews in molecular medicine*, **12**, e27.

Fantini, Jacques & Yahi, Nouara. 2011. Molecular basis for the glycosphingolipid-binding specificity of α-Synuclein: key role of tyrosine 39 in membrane insertion. *Journal of Molecular Biology*, **408**(4), 654–669.

Fantini, Jacques; Garmy, Nicolas; Mahfoud, Radhia & Yahi, Nouara. 2002. Lipid rafts: structure, function and role in HIV, Alzheimer's and prion diseases. *Expert reviews in molecular medicine*, **4**(1), 1–22.

Fares, Mohamed-Bilal; Ait-Bouziad, Nadine; Dikiy, Igor; Mbefo, Martial K; Jovičić, Ana; Kiely, Aoife; Holton, Janice L; Lee, Seung-Jae; Gitler, Aaron D; Eliezer, David *et al.* 2014. The novel Parkinson's disease linked mutation G51D attenuates in vitro aggregation and membrane binding of α-synuclein, and enhances its secretion and nuclear localization in cells. *Human Molecular Genetics*, **23**(17), 4491–4509.

Fauvet, Bruno; Mbefo, Martial K; Fares, Mohamed-Bilal; Desobry, Carole; Michael, Sarah; Ardah, Mustafa T; Tsika, Elpida; Coune, Philippe; Prudent, Michel; Lion, Niels *et al.* 2012. α-Synuclein in central nervous system and from erythrocytes, mammalian cells, and Escherichia coli exists predominantly as disordered monomer. *Journal of Biological Chemistry*, **287**(19), 15345–15364.

Feany, Mel B & Bender, Welcome W. 2000. A *Drosophila* model of Parkinson's Disease. *Nature*, **404**, 394–398.

Ferreon, Allan Chris M; Gambin, Yann; Lemke, Edward A & Deniz, Ashok A. 2009. Interplay of alpha-synuclein binding and conformational switching probed by single-molecule fluorescence. *Proceedings of the National Academy of Sciences*, **106**(14), 5645–5650.

Georgieva, Elka R; Ramlall, Trudy F; Borbat, Peter P; Freed, Jack H & Eliezer, David. 2008. Membrane-Bound α-Synuclein Forms an Extended Helix: Long-Distance Pulsed ESR Measurements Using Vesicles, Bicelles, and Rodlike Micelles. *Journal of the American Chemical Society*, **130**(39), 12856–12857.

Gitler, Aaron D; Bevis, Brooke J; Shorter, James; Strathearn, Katherine E; Hamamichi, Shusei; Su, Linhui J; Caldwell, Kim A; Caldwell, Guy A; Rochet, Jean-Christophe; McCaffery, J Michael *et al.* 2008. The Parkinson's disease protein α-synuclein disrupts cellular Rab homeostasis. *Proceeding of the National Academy of Science*, **105**, 145–150.

Gitler, Aaron D; Chesi, Alessandra; Geddie, Melissa L; Strathearn, Katherine E; Hamamichi, Shusei; Hill, Kathryn J; Caldwell, Kim A; Caldwell, Guy A; Cooper, Anthony A; Rochet, Jean-Christophe *et al.* 2009. α-Synuclein is part of a diverse and highly conserved interaction network that includes PARK9 and manganese toxicity. *Nature Genetics*, **41**, 308–315.

Gliozzi, Alessandra; Relini, Annalisa & Chong, Parkson Lee-Gau. 2002. Structure and permeability properties of biomimetic membranes of bolaform archaeal tetraether lipids. *Journal of Membrane Science*, **206**(1-2), 131–147.

Greenfield, Norma J & Fasman, Gerald D. 1969. Computed circular dichroism spectra for the evaluation of protein conformation. *Biochemistry*, **8**(10), 4108–4116.

Haque, Farzin; Pandey, Anjan P; Cambrea, Lee R; Rochet, Jean-Christophe & Hovis, Jennifer S. 2010. Adsorption of alpha-synuclein on lipid bilayers: modulating the structure and stability of protein assemblies. *The journal of physical chemistry B*, **114**(11), 4070–4081.

Hardy, John & Selkoe, Dennis J. 2002. The Amyloid Hypothesis of Alzheimer's Disease: Progress and Problems on the Road to Therapeutics. *Science*, **297**(5580), 353–356.

Jellinger, Kurt A. 2012. The role of α-synuclein in neurodegeneration — An update. *Translational Neuroscience*, **3**(2), 75–122.

Jesorka, Aldo & Orwar, Owe. 2008. Liposomes: Technologies and Analytical Applications. *Annual Review of Analytical Chemistry*, **1**(1), 801–832.

Johnson, W. Curtis. 1999. Analyzing protein circular dichroism spectra for accurate secondary structures. *Proteins: Structure, Function, and Bioinformatics*, **35**(3), 307–312.

Kaiser, Robert D & London, Erwin. 1998. Location of diphenylhexatriene (DPH) and its derivatives within membranes: comparison of different fluorescence quenching analyses of membrane depth. *Biochemistry*, **37**(22), 8180–8190.

Kaoui, Badr; Farutin, Alexander & Misbah, Chaouqi. 2009. Vesicles under simple shear flow: Elucidating the role of relevant control parameters. *Physical Review E*, **80**(6), 061905.

Kayed, Rakez; Pensalfini, Anna; Margol, Larry; Sokolov, Yuri; Sarsoza, Floyd; Head, Elizabeth; Hall, James & Glabe, Charles G. 2008. Annular Protofibrils Are a Structurally and Functionally Distinct Type of Amyloid Oligomer. *Journal of Biological Chemistry*, **284**(7), 4230–4237.

Kelly, Sharon M & Price, Nicholas C. 1997. The application of circular dichroism to studies of protein folding and unfolding. *Biochimica et biophysica acta*, **1338**(2), 161–185.

Khalaf, Ossama; Fauvet, Bruno; Oueslati, Abid; Dikiy, Igor; Mahul-Mellier, Anne-Laure; Ruggeri, Francesco Simone; Mbefo, Martial K; Vercruysse, Filip; Dietler, Giovanni; Lee, Seung-Jae *et al.* 2014. The H50Q Mutation Enhances α-Synuclein Aggregation, Secretion, and Toxicity. *Journal of Biological Chemistry*, **289**(32), 21856–21876.

Kim, Hai-Young; Cho, Min-Kyu; Kumar, Ashutosh; Maier, Elke; Siebenhaar, Carsten; Becker, Stefan; Fernandez, Claudio O; Lashuel, Hilal A; Benz, Roland; Lange, Adam *et al.* 2009. Structural properties of pore-forming oligomers of α-Synuclein. *Journal of the American Chemical Society*, **131**, 17482–17489.

Kolesnick, Richard & Golde, David W. 1994. The sphingomyelin pathway in tumor necrosis factor and interleukin-1 signaling. *Cell*, **77**(3), 325–328.

Kurz, Alexander; Rabbani, Naila; Walter, Michael; Bonin, Michael; Thornalley, Paul; Auburger, Georg & Gispert, Suzana. 2010. Alpha-synuclein deficiency leads to increased glyoxalase I expression and glycation stress. *Cellular and molecular life sciences*, **68**(4), 721–733.

Ladokhin, Alexey S; Jayasinghe, Sajith & White, Stephen H. 2000. How to measure and analyze tryptophan fluorescence in membranes properly, and why bother? *Analytical biochemistry*, **285**(2), 235–245.

Lashuel, H; Eliezer, D & Lansbury Jr, P. 2007. The impact of the E46K mutation on the properties of α-synuclein in its monomeric and oligomeric states. *Biochemistry*.

Lashuel, Hilal A; Petre, Benjamin M; Wall, Joseph; Simon, Martha; Nowak, Richard J; Walz, Thomas & Lansbury Jr, Peter T. 2002a. α-Synuclein, Especially the Parkinson's Disease-associated Mutants, Forms Pore-like Annular and Tubular Protofibrils. *Journal of Molecular Biology*, **322**(5), 1089–1102.

Lashuel, Hilal A; Hartly, Dean; Petre, Benjamin M; Walz, Thomas & Lansbury, Peter T. 2002b. Neurodegenerative disease: amyloid pores from pathogenic mutations. *Nature*, **418**, 291.

Lasko, Merja; Vartiainen, Suvi; Moilanen, Anu-Maarit; Sirvio, Jouni; Thomas, James H; Nass, Richard; Blakely, Randy D & Wong, Garry. 2003. Dopaminergic neuron loss and motor deficits in Caenorhabditis elegans overexpressing human α-synuclein. *Journal of Neurochemistry*, **86**, 165–172.

Lee, Jennifer C; Langen, Ralf; Hummel, Patrick A; Gray, Harry B & Winkler, Jay R. 2004. Alpha-synuclein structures from fluorescence energy-transfer kinetics: implications for the role of the protein in Parkinson's disease. *Proceedings of the National Academy of Sciences of the United States of America*, **101**(47), 16466–16471.

Lesné, S; Koh, M; Kotilinek, L; Kayed, R & Glabe, C. 2006. A specific amyloid-b protein assembly in the brain impairs memory. *Nature*.

Lingwood, Daniel & Simons, Kai. 2010. Lipid rafts as a membrane-organising principle. *Science*, **327**(5961), 46–50.

Lloyd, Katherine. 2012. *Stability of Lipid Vesicles in Flow at High Shear Rates*. Project Dissertation, University of Warwick.

Lorenzen, Nikolai; Nielsen, Søren Bang; Buell, Alexander K; Kaspersen, Jørn Døvling; Arosio, Paolo; Vad, Brian Stougaard; Paslawski, Wojciech; Christiansen, Gunna; Valnickova-Hansen, Zuzana; Andreasen, Maria *et al.* 2014. The Role of Stable α-Synuclein Oligomers in the Molecular Events Underlying Amyloid Formation. *Journal of the American Chemical Society*, **136**(10), 3859–3868.

Lotharius, Julie & Brundin, Patrik. 2002. Pathogenesis of Parkinson's Disease: dopamine, vesicles and α-Synuclein. *Nature Reviews Neuroscience*, **3**, 1–11.

Mader, M A; Vitkova, V; Abkarian, M; Viallat, A & Podgorski, T. 2006. Dynamics of viscous vesicles in shear flow. *The European physical journal. E, Soft matter*, **19**(4), 389–397.

Marrington, Rachel; Dafforn, Timothy R; Halsall, David J & Rodger, Alison. 2004. Micro-Volume Couette Flow Sample Orientation for Absorbance and Fluorescence Linear Dichroism. *Biophysical Journal*, **87**(3), 2002–2012.

Martinez, Z; Zhu, M; Han, S & Fink, Anthony L. 2007. GM1 specifically interacts with α-synuclein and inhibits fibrillation. *Biochemistry*, **46**, 1868–1877.

MATLAB. 2013. *version 8.1.0.604 (R2013a)*. Natick, Massachusetts: The Mathworks Inc.

Matsuzaki, K; Kato, K & Yanagisawa, K. 2010. Aβ Polymerization though interaction with membrane gangliosides. *Biochimica et biophysica acta*, **1801**, 868–877.

McLachlan, James R A; Smith, David J; Chmel, Nikola P & Rodger, Alison. 2013. Calculations of flow-induced orientation distributions for analysis of linear dichroism spectroscopy. *Soft Matter*, **9**(20), 4977–4984.

Mocchetti, I. 2005. Exogenous gangliosides, neuronal plasticity and repair, and the neurotrophins. *Cellular and molecular life sciences*, **62**(19-20), 2283–2294.

Munishkina, Larissa A; Phelan, Cassandra; Uversky, Vladimir N & Fink, Anthony L. 2003. Conformational Behavior and Aggregation of α-Synuclein in Organic Solvents: Modeling the Effects of Membranes. *Biochemistry*, **42**(9), 2720–2730.

Noguchi, Hiroshi & Gompper, Gerhard. 2005. Shape transitions of fluid vesicles and red blood cells in capillary flows. *Proceedings of the National Academy of Sciences of the United States of America*, **102**(40), 14159–14164.

Nordén, Bengt; Kubista, Mikael & Kurucsev, Tomas. 1992. Linear dichroism spectroscopy of nucleic acids. *Quarterly review of Biophysics*, **25**(01), 51–170.

Nordén, Bengt; Rodger, Alison & Dafforn, Timothy R. 2010. *Linear dichroism and circular dichroism: A textbook on polarized-light spectroscopy.* Cambridge, UK: RSC Publishing.

Ohvo-Rekilä, Henna; Ramstedt, Bodil; Leppimäki, Petra & Slotte, J Peter. 2002. Cholesterol interactions with phospholipids in membranes. *Progress in Lipid Research*, **41**(1), 66–97.

Outeiro, Tiago F & Lindquist, Susan. 2003. Yeast cells provide insight into α-Synuclein biology and pathobiology. *Science*, **302**, 1772–1775.

Papahadjopoulos, D; Jacobson, K; Nir, S & Isac, I. 1973. Phase transitions in phospholipid vesicles Fluorescence polarization and permeability measurements concerning the effect of temperature and cholesterol. *Biochimica et Biophysica Acta (BBA) - Biomembranes*, **311**(3), 330–348.

Pettersen, Eric F; Goddard, Thomas D; Huang, Conrad C; Couch, Gregory S; Greenblatt, Daniel M; Meng, Elaine C & Ferrin, Thomas E. 2004. UCSF Chimera – A visualization system for exploratory research and analysis. *Journal of Computational Chemistry*, **25**(13), 1605–1612.

Pfefferkorn, Candace M & Lee, Jennifer C. 2010. Tryptophan probes at the α-synuclein and membrane interface. *The journal of physical chemistry B*, **114**(13), 4615–4622.

Pfefferkorn, Candace M; Jiang, Zhiping & Lee, Jennifer C. 2012. Biophysics of α-synuclein membrane interactions. *Biochimica et Biophysica Acta (BBA) - Biomembranes*, **1818**(2), 162–171.

Pinheiro, T. 2006. The role of rafts in the fibrillization and aggregation of prions. *Chemistry and physics of lipids*.

Prendergast, F G. 1978. Quantitation of hindered rotations of diphenylhexatriene in lipid bilayers by differential polarized phase fluorometry. *Science*, **200**(4348), 1399–1401.

Prism. 2015. *version 6.0*. GraphPad Software, Inc.

Prusiner, S B. 1982. Novel proteinaceous infection particles cause scrapie. *Science*, **216**, 136–144.

Rajendra, Jascindra; Baxendale, Mark; Dit Rap, Laurence Georges & Rodger, Alison. 2004. Flow linear dichroism to probe binding of aromatic molecules and DNA to single-walled carbon nanotubes. *Journal of the American Chemical Society*, **126**(36), 11182–11188.

Rajendra, Jascindra; Damianoglou, Angeliki; Hicks, Matthew; Booth, Paula; Rodger, P Mark & Rodger, Alison. 2006. Quantitation of protein orientation in flow-oriented unilamellar liposomes by linear dichroism. *Chemical Physics*, **326**(1), 210–220.

Razmkhah, Kasra; Little, Haydn; Sandhu, Sandeep; Dafforn, Timothy R & Rodger, Alison. 2014. RSC Advances. *RSC Advances*, **4**(Aug.), 37510–37515.

Reynolds, Nicholas P; Soragni, Alice; Rabe, Michael; Verdes, Dorinel; Liverani, Ennio; Handschin, Stephan; Riek, Roland & Seeger, Stefan. 2011. Mechanism of Membrane Interaction and Disruption by α-Synuclein. *Journal of the American Chemical Society*, **133**(48), 19366–19375.

Rhoades, Elizabeth; Ramlall, Trudy F; Webb, Watt W & Eliezer, David. 2006. Quantification of α-synuclein binding to lipid vesicles using fluorescence correlation spectroscopy. *Biophysical Journal*.

Rochet, J-C; Conway, K A & Lansbury, P.T. 2000. Inhibition of fibrillization and accumulation of prefibrillar oligomers in mixtures of human and mouse alpha-synuclein. *Biochemistry*, **39**(35), 10619–10626.

Rodger, Alison & Nordén, Bengt. 1997. *Circular dichroism and linear dichroism*. Oxford, UK: Oxford University Press.

Rodger, Alison; Rajendra, Jascindra; Marrington, Rachel; Ardhammar, Malin; Nord n, Bengt; Hirst, Jonathan D; Gilbert, Andrew T B; Dafforn, Timothy R; Halsall, David J; Woolhead, Cheryl A *et al.* 2002. Flow oriented linear dichroism to probe protein orientation in membrane environments. *Physical Chemistry Chemical Physics*, **4**(16), 4051–4057.

Roucou, Xavier; Gains, Malcolm & LeBlanc, Andréa C. 2004. Neuroprotective functions of prion protein. *Journal of Neuroscience Research*, **75**(2), 153–161.

Sanghera, Narinder & Pinheiro, Teresa J T. 2002. Binding of prion protein to lipid membranes and implications for prion conversion. *Journal of Molecular Biology*, **315**(5), 1241–1256.

Sanghera, Narinder; Correia, Bruno E F S; Correia, Joana R S; Ludwig, Christian; Agarwal, Sonya; Nakamura, Hironori K; Kuwata, Kazuo; Samain, Eric; Gill, Andrew C; Bonev, Boyan B *et al.* 2011. Deciphering the Molecular Details for the Binding of the Prion Protein to Main Ganglioside GM1 of Neuronal Membranes. *Chemistry & biology*, **18**(11), 1422–1431.

Scherzer, Clemens R; Jensen, Roderick V; Gullans, Steven R & Feany, Mel B. 2003. Gene expresson changes presage neurodegeneration in a *Drosophila* model of Parkinson's Disease. *Human Molecular Genetics*, **12**, 2457–2466.

Selkoe, D J. 1994. Cell biology of the Amyloid β-protein precursor and the mechanism of Alzheimer's Disease. *Annual Review of Cell Biology*, **10**, 373–403.

Selkoe, D J. 2008. Soluble oligomers of the amyloid β-protein impair synaptic plasticity and behaviour. *Behavioural Brain Research*, **192**, 106–113.

Selkoe, D J; Ihara, Y & Salazar, F J. 1982. Alzheimer's disease: insolubility of partially purified paired helical filaments in sodium dodecyl sulphate and urea. *Science*, **215**, 1243–1245.

SigmaPlot. 2013. *version 13*. Systat Software Inc.

Simoneau, Steve; Rezaei, Human; Salès, Nicole; Kaiser-Schulz, Gunnar; Lefebvre-Roque, Maxime; Vidal, Catherine; Fournier, Jean-Guy; Comte, Julien; Wopfner, Franziska;

Grosclaude, Jeanne *et al.* 2007. In Vitro and In Vivo Neurotoxicity of Prion Protein Oligomers. *PLoS Pathogens*, **3**(8), 1175–1186.

Smith, Rachel. 2013. *Oligomerisation of Alpha-Synuclein.* Project Dissertation, University of Warwick.

Solomon, Isaac H; Schepker, Jessie A & Harris, David A. 2010. Prion neurotoxicity: insights from prion protein mutants. *Current issues in molecular biology*, **12**(2), 51–61.

Stöckl, Martin; Claessens, Mireille M A E & Subramaniam, Vinod. 2012a. Kinetic measurements give new insights into lipid membrane permeabilization by α-synuclein oligomers. *Molecular BioSystems*, **8**(1), 338–345.

Stöckl, Martin T; Zijlstra, Niels & Subramaniam, Vinod. 2012b. α-Synuclein Oligomers: an Amyloid Pore? *Molecular Neurobiology*, **47**(2), 613–621.

Sui, Sen-Fang; Wu, Hua; Guo, Yong & Chen, Kai-Sheng. 1994. Conformational changes of melittin upon insertion into phospholipid monolayer and vesicle. *Journal of biochemistry*, **116**(3), 482–487.

Svensson, Frida R; Lincoln, Per; Nordén, Bengt & Esbjörner, Elin K. 2011. Tryptophan orientations in membrane-bound gramicidin and melittin—a comparative linear dichroism study on transmembrane and surface-bound peptides. *Biochimica et Biophysica Acta (BBA) - Biomembranes*, **1808**(1), 219–228.

Sweers, Kim K M; Segers-Nolten, Ine M J; Bennink, Martin L & Subramaniam, Vinod. 2012. Structural model for α-synuclein fibrils derived from high resolution imaging and nanomechanical studies using atomic force microscopy. *Soft Matter*, **8**(27), 3215–3222.

Terwilliger, Thomas C & Eisenberg, David. 1982a. The structure of melittin. I. Structure determination and partial refinement. *The Journal of biological chemistry*, **257**(11), 6010–6015.

Terwilliger, Thomas C & Eisenberg, David. 1982b. The structure of melittin. II. Interpretation of the structure. *The Journal of biological chemistry*, **257**(11), 6016–6022.

Ulmer, Tobias S; Bax, Ad; Cole, Nelson B & Nussbaum, Robert L. 2005. Structure and Dynamics of Micelle-bound Human -Synuclein. *Journal of Biological Chemistry*, **280**(10), 9595–9603.

van Rooijen, B & van Leijenhorst-Groener, K. 2009. Tryptophan Fluorescence Reveals Structural Features of α-Synuclein Oligomers. *Journal of Molecular Biology*, **394**, 826–833.

van Rooijen, Bart D; Claessens, Mireille M A E & Subramaniam, Vinod. 2008. Membrane binding of oligomeric α-synuclein depends on bilayer charge and packing. *FEBS letters.*

Varadarajan, S; Yatin, S; Aksenova, M & Butterfield, D A. 2000. Review: Alzheimer's amyloid β-peptide-associated free radical oxidative stress and neurotoxicity. *Journal of Structural Biology*, **130**, 184–208.

Varkey, Jobin; Mizuno, Naoko; Hegde, Balachandra G; Cheng, Naiqian; Steven, Alasdair C & Langen, Ralf. 2013. α-Synuclein oligomers with broken helical conformation form lipoprotein nanoparticles. *The Journal of biological chemistry*, **288**(24), 17620–17630.

Wang, Wei; Perovic, Iva; Chittuluru, Johnathan; Kaganovich, Alice; Nguyen, Linh T T; Liao, Jingling; Auclair, Jared R; Johnson, Derrick; Landeru, Anuradha; Simorellis, Alana K *et al.* 2011. A soluble α-synuclein construct forms as dynamic tetramer. *Proceedings of the National Academy of Sciences of the United States of America*, **108**(43), 17797–17802.

Warner, Thomas T & Schapira, Anthony H V. 2003. Genetic and environmental factors in the cause of Parkinson's disease. *Annals of Neurology*, **53**(S3), S16–S25.

Yanagisawa, Katsuhiko; Odaka, Asano; Suzuki, Nobuhiro & Ihara, Yasuo. 1995. GM1 ganglioside-bound amyloid β-protein (Aβ): a possible form of preamyloid in Alzheimer's Disease. *Nature Medicine*, **1**, 1062–1066.

Yoshiike, Y; Kayed, R; Milton, S C; Takashima, A & Glabe, C G. 2007. Pore-forming proteins share structural and functional homology with amyloid oligomers. *Neuromolecular Medicine*, **9**, 270–275.

Yu, Seonghyun; Cho, Kun; Kim, Young Hwan; Park, Soojin; Kim, Jaedong & Oh, Han Bin. 2006. Identification of phospholipid molecular species in porcine brain extracts using high mass accuracy of 4.7 Tesla Fourier transform ion cyclotron resonance mass spectrometry. *BULLETIN-KOREAN CHEMICAL SOCIETY*, **27**(5), 793.

Zarranz, Juan J; Alegre, Javier; Gómez-Esteban, Juan C; Lezcano, Elena; Ros, Raquel; Ampuero, Israel; Vidal, Lídice; Hoenicka, Janet; Rodriguez, Olga; Begoña, Atarés *et al.* 2004. The new mutation, E46K, of alpha-synuclein causes Parkinson and Lewy body dementia. *Annals of Neurology*, **55**(2), 164–173.

Zhang, P; Liu, B; Jenkins, G M; Hannun, Y A & Obeid, L M. 1997. Expression of neutral sphingomyelinase identifies a distinct pool of sphingomyelin involved in apoptosis. *The Journal of biological chemistry*, **272**(15), 9609–9612.

Zhu, Min; Li, Jie & Fink, Anthony L. 2003. The Association of α-Synuclein with Membranes Affects Bilayer Structure, Stability, and Fibril Formation. *The Journal of biological chemistry*, **278**(41), 40186–40197.

Appendix A

Ultracentrifugation assay

A.1 Introduction

In Chapters 4 and 5, it was noted that α-synuclein does not seem to have specific binding affinity for GM1 in these studies – a somewhat surprising result. The α-synuclein constructs used here contain the Y39W mutation, however, and Y39 has the putative crucial role in the ability of the protein to bind to the gangliosides (Fantini & Yahi, 2011). Y39W was selected for the experiments discussed in Chapters 4 and 5 because intrinsic tryptophan fluorescence is a sensitive and straightforward technique. However, it was believed that a technique that did not rely on changing the native Y39 residue, in order to deduce if the Y39W mutation damaged the ability of the protein to bind ganglioside. The following experiment was carried out in order to assess the ability of wild type, E46K, and E46K:Y39W α-synuclein to bind vesicles containing GM1.

The Bradford assay for determining protein concentration, is long-established, and known to biochemists as a matter of course, updated by the availability of the necessary reagent and refined method from Bio-Rad (Hercules, CA, USA) (Bradford, 1976). This assay was used to determine the concentration of protein in solution *after* incubation of the protein with lipid, and separation using ultracentrifugation. Protein remaining after separation is unbound, and can be compared to the amount unbound from other constructs of the protein.

A.2 Materials and methods

Lipid vesicles were prepared as described in Section 2.2.3. Lipids used were 50 % GM1 and 50 % POPC.

Bradford assay reagent was obtained from Bio-Rad (Hercules, CA, USA). Lipid and protein were mixed and incubated for 10 minutes, then ultracentrifugation was carried out for 10 minutes at 100,000 g to separate lipids from unbound protein. The Bradford assay was then carried out according to Bio-Rad instructions, using a Jenway 6300 spectrophotometer, and concentrations recorded. The Bradford assay was calibrated by the curve shown in Figure A.1.

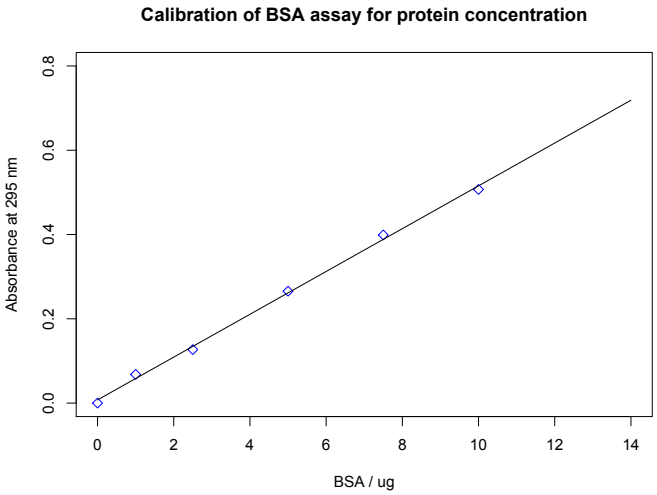

Figure A.1: Calibration curve for the Bradford protein concentration assay in the relevant range. Each data point is the average of three replicates.

A.3 Results and discussion

Concentration of unbound protein was recorded as a percentage of the initial concentration, for the three protein constructs. These data are shown in Figure A.2. This experiment

was not replicated, and so this may only be treated as qualitative data.

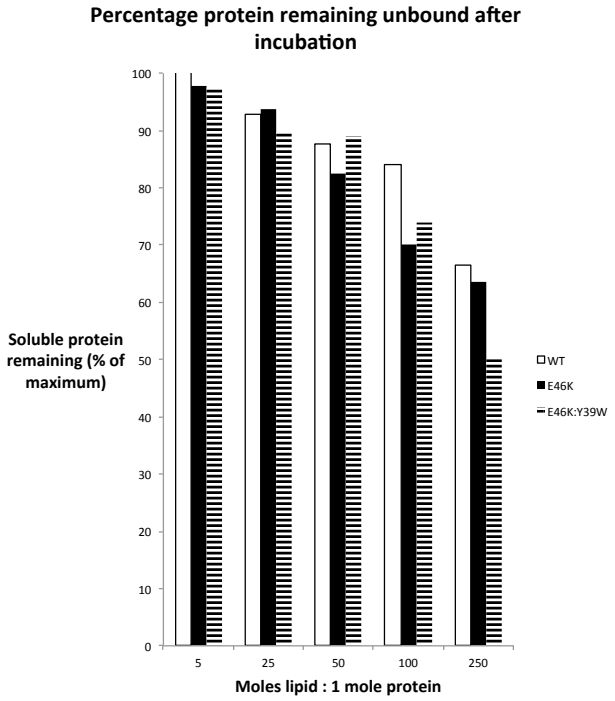

Figure A.2: Percentage of free protein remaining in solution after incubation with lipid vesicles and ultracentrifugation. Lipid vesicles used were sonicated SUVs containing 50 % POPC and 50 % GM1. Data is drawn from one replicate only.

As shown in Figure A.2, in most cases less protein remains in solution for samples containing a higher ratio of lipid to protein, *i.e.* with more lipid present, more protein is bound. However, this is the only clear trend in the data. Wild type shows the lowest binding (highest unbound percentage) in the 5:1, 100:1, and 250:1 moles samples, but not in the other two cases. E46K shows stronger binding than E46K:Y39W in two cases, but not in the other three. From the literature, it was expected that E46K would bind most strongly, but this is not shown in the data presented here.

A.4 Conclusions

The data presented in this appendix do not suggest any clear conclusions. In some cases E46K bound most strongly, in others E46K:Y39W. Wild type bound least strongly in some cases, not in others. This experiment was not repeated. With more sensitive equipment this technique might be a useful alternative to the *CD* and fluorescence work discussed above, but in this case the data were inconclusive.

Appendix B

Binding curve fitting report

B.1 Report generated by Prism during curve fitting

The following tables were generated by Prism when fitting the one site ligand binding curves shown in Chapter 4 and Chapter 5. It includes the statistical tests employed in the fitting process. Fitting data are shown for fluorescence experiments with POPC/POPS lipids, with complex lipids, and for *CD* experiments with the POPC/POPS SUVs.

Equation: Ligand Binding, one site saturation

$$f = B_{\max} * \frac{abs(x)}{K_d + abs(x)}$$

Table B.1: Fitting report generated in Prism for fluorescence data gathered for Y39W and E46K:Y39W α-synuclein interacting with lipid SUVs composed of POPC and POPS. '—' indicates ambiguity or unfeasibly wide ranges.

	Y39W				E46K:Y39W			
	100 % POPC	10 % POPS	25 %POPS	50 %POPS	100 % POPC	10 % POPS	25 %POPS	50 %POPS
Best-fit values								
Bmax	0.7486	14.44	11.37	11.52	—	14.63	11.97	10.91
Kd	-0.2362	138.7	20.36	7.258	—	259.9	81.96	34.43
Std Error								
Bmax	0.2224	0.7486	0.6587	0.3880	—	0.3919	0.5055	0.5672
Kd	0.4157	23.02	5.540	1.370	—	18.89	12.37	7.630
95 % c.i.								
Bmax	0.1312-1.366	12.80-16.09	9.918-12.82	10.67-12.38	—	13.77-15.50	10.86-13.09	9.663-12.16
Kd	-1.391-0.9181	88.03-189.4	8.167-32.55	4.243-10.27	—	218.3-301.4	54.74-109.3	17.64-51.23
Goodness of fit								
D.f.	4	11	11	11	4	11	11	11
R square	0.4286	0.9796	0.9130	0.9569	0.9424	0.9972	0.9817	0.9565
Abs s.s.	0.7619	5.815	16.58	8.468	0.01200	0.6550	4.363	9.471
Sy.x	0.4364	0.7271	1.228	0.8774	0.05476	0.2440	0.6398	0.9279

Table B.2: Fitting report generated in Prism for fluorescence data gathered for Y39W and E46K:Y39W α-synuclein interacting with lipid SUVs composed of POPC/POPS/ Cholesterol (3 component), POPC/POPS/ Cholesterol/SM1 (4 component), and POPC/POPS/ Cholesterol/SM1/GM1 (5 component).

	Y39W			E46K:Y39W		
	3 component	4 component	5 component	3 component	4 component	5 component
Best-fit values						
Bmax	25.67	34.69	32.82	21.49	43.79	119.0
Kd	782.4	1518	1654	590.6	2703	8358
Std Error						
Bmax	2.610	10.41	8.607	1.917	23.46	161.9
Kd	146.0	674.3	626.9	107.2	1860	12466
95 % c.i.						
Bmax	19.86-31.49	11.49-57.89	13.64-51.99	17.22-25.76	-8.485-96.07	-241.7-479.6
Kd	456.1-1107	15.67-3020	257.5-3051	351.6-829.5	-1441-6847	-19419-36135
Goodness of fit						
D.f.	10	10	10	10	10	10
R square	0.9925	0.9800	0.9866	0.9904	0.9777	0.9830
Abs s.s.	2.381	5.731	3.006	2.598	4.545	3.782
Sy.x	0.4879	0.7570	0.5482	0.5097	0.6742	0.6150

Table B.3: Fitting report generated in Prism for *CD* data gathered at 222 nm for Y39W and E46K:Y39W α-synuclein interacting with lipid SUVs composed of POPC and POPS. Data was also gathered at 208 nm, not shown here as it was judged to be less accurate. '—' indicates ambiguity or unfeasibly wide ranges.

	Y39W				E46K:Y39W			
	100 % POPC	10 % POPS	25 %POPS	50 %POPS	100 % POPC	10 % POPS	25 %POPS	50 %POPS
Best-fit values								
Bmax	—	102.4	115.2	72.50	—	58.71	103.5	69.40
Kd	—	386.3	185.8	36.75	—	109.7	163.9	20.13
Std Error								
Bmax	—	8.324	8.565	5.042	—	3.960	4.554	3.629
Kd	—	74.64	41.25	10.75	—	24.93	22.22	4.954
95 % c.i.								
Bmax	—	83.89-121.0	96.10-134.3	61.26-83.73	—	49.89-67.54	93.37-113.7	61.31-77.49
Kd	—	220.0-552.6	93.90-277.7	12.79-60.71	—	54.18-165.3	114.4-213.4	9.098-31.17
Goodness of fit								
D.f.	3	10	10	10	3	10	10	10
R square	0.8811	0.9852	0.9694	0.9260	0.9811	0.9643	0.9879	0.9327
Abs s.s.	7.300	127.0	478.3	657.0	4.273	189.0	159.9	460.0
Sy.x	1.560	3.563	6.916	8.106	1.194	4.347	3.999	6.782

Appendix C

Solving for orientation parameter

C.1 Method for calculating *S*

Having generated *LD* spectra of DPH in lipid, the parameter S (as in Equation 3.6) was calculated, in order to quantify the *LD* signal observed. The code given below demonstrates the approach taken to this calculation for one example. This was implemented in MATLAB. The figure generated by this code is shown in Figure C.1. The *LD* spectrum is partially corrected for slope caused by scattering by subtracting a straight line fitted to the high wavelength region of the spectrum. LD^r is calculated from *LD* and absorbance spectra, then S calculated for the whole spectrum. The region around the DPH peaks is extracted such that no other peak is considered, and then the highest value taken as the value for S for DPH in that sample.

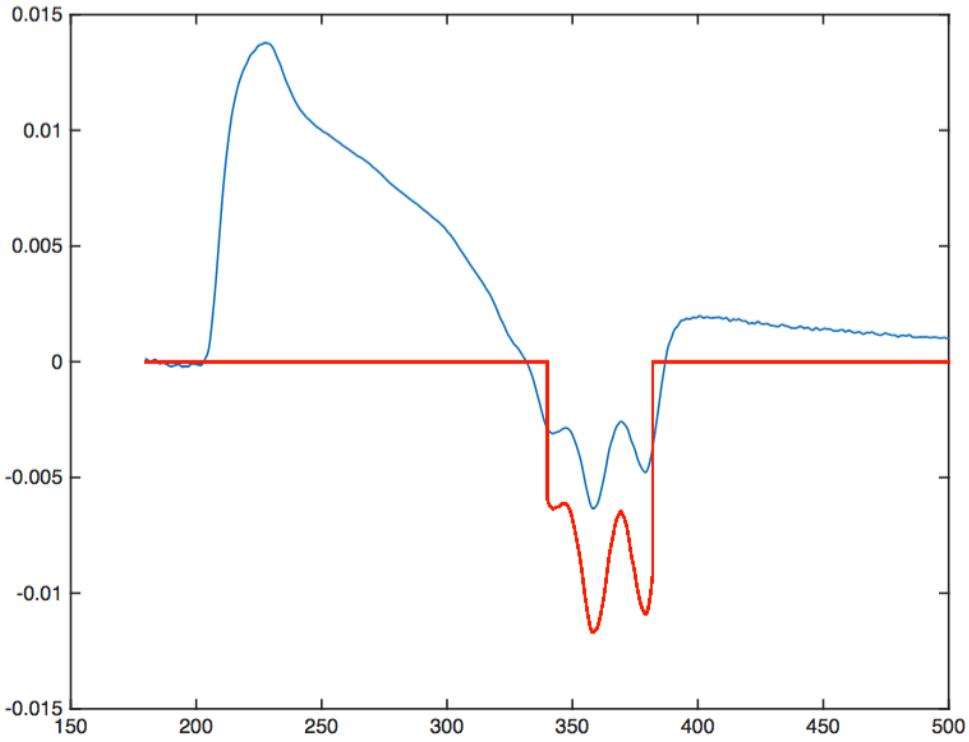

Figure C.1: Figure generated in MATLAB showing LD spectrum of DPH in POPC/POPS/ cholesterol vesicles (blue trace) and isolated region of LD^r spectrum (red trace) around DPH peaks. The LD^r trace outside of the region around the DPH peaks has been set to zero.

```
%Extracting data for POPC/POPS/cholesterol, 25 mg\mL

pop25_WL=dlmread('./DPH_expts1/POPC_POPS_CHOL/25mgmL_abs.txt','\t',[19 0 3219 0]);
%wavelength vector
pop25_LD=dlmread('./DPH_expts1/POPC_POPS_CHOL/25mgmL_abs.txt','\t',[19 1 3219 1]);
%LD
pop25_HT=dlmread('./DPH_expts1/POPC_POPS_CHOL/25mgmL_abs.txt','\t',[19 2 3219 2]);
% HT (V)
%pop25_Abs=dlmread('./DPH_expts1/POPC_POPS_CHOL/25mgmL_abs.txt','\t',[19 3
%3219 3]);
%absorbance (if needed)
waterabs=dlmread('./DPH_expts1/waterblank_abs_corr.txt','\t',[19 2 3219 2]);
%absorbace of water
pop25_Abs=pop25_HT-waterabs;
%different way to achieve absorbance spectrum


pop25_AbsIso=pop25_Abs+(pop25_LD./3)+log10(1+10.^(pop25_LD))-log10(2);
```

```
%isotropic absorbance

pop25_S=(4.*pop25_LD)./(3.*pop25_AbsIso.*(1-3.*(cos(0).^2)));
%calculating S for whole spectrum

pop25_LDr=pop25_LD./pop25_AbsIso;
%reduced LD

pop25_peaks=pop25_LDr(1180:1600,:);
%capturing region around DPH peaks
[pop25max,pop25maxpos]=max(pop25_peaks);
%Finding max peak

pop25maxpos
pop25_S=pop25_S(pop25maxpos)
%output the position of the max peak and find the value of S there

Vp25=zeros(3201);
%empty vector
```

```
for i = 1:421
    Vp25(i+1180,:) = pop25_peaks(i);
end
% filling vector with the region around the peaks

figure
%plotting
plot(pop25_WL, pop25_LD)
hold on
plot(pop25_WL, Vp25, 'r')
```